Bioactive Materials 24 (2023) 263–312

Contents lists available at ScienceDirect

Bioactive Materials

journal homepage: www.keaipublishing.com/en/journals/bioactive-materials

Review article

Nanomaterial-assisted theranosis of bone diseases

Kai Zheng [a], Jiaxiang Bai [a,**], Huilin Yang [a], Yaozeng Xu [a], Guoqing Pan [c], Huaiyu Wang [b,*], Dechun Geng [a,***]

[a] Department of Orthopedics, The First Affiliated Hospital of Soochow University, 188 Shizi Road, Suzhou, 215006, Jiangsu, China
[b] Center for Human Tissues and Organs Degeneration, Shenzhen Institute of Advanced Technology, Chinese Academy of Sciences, Shenzhen, 518055, China
[c] Institute for Advanced Materials, School of Materials Science and Engineering, Jiangsu University, Zhenjiang, 212013, Jiangsu, China

ARTICLE INFO

Keywords:
Nanomaterials
Delivery
Diagnosis
Therapy
Bone-related diseases

ABSTRACT

Bone-related diseases refer to a group of skeletal disorders that are characterized by bone and cartilage destruction. Conventional approaches can regulate bone homeostasis to a certain extent. However, these therapies are still associated with some undesirable problems. Fortunately, recent advances in nanomaterials have provided unprecedented opportunities for diagnosis and therapy of bone-related diseases. This review provides a comprehensive and up-to-date overview of current advanced theranostic nanomaterials in bone-related diseases. First, the potential utility of nanomaterials for biological imaging and biomarker detection is illustrated. Second, nanomaterials serve as therapeutic delivery platforms with special functions for bone homeostasis regulation and cellular modulation are highlighted. Finally, perspectives in this field are offered, including current key bottlenecks and future directions, which may be helpful for exploiting nanomaterials with novel properties and unique functions. This review will provide scientific guidance to enhance the development of advanced nanomaterials for the diagnosis and therapy of bone-related diseases.

1. Introduction

1.1. Bone-related diseases

Bone-related diseases refer to a group of skeletal disorders that manifest as homeostasis imbalance, increased inflammation levels and osteoimmunology dysregulation, thus resulting in bone erosion and joint deformity [1]. The most common bone-related diseases include (1) osteoporosis (OP), characterized by low bone mineral density, disrupted bone microstructure, increased bone fragility and fracture risk [2]; (2) osteoarthritis (OA), characterized by degenerated articular cartilage, serious joint stiffness and deformity [3]; (3) rheumatoid arthritis (RA), characterized by aggressive synovial hyperplasia, joint inflammation, cartilage damage and joint deformity [4]; (4) bone fracture, characterized by destroyed structural integrity, interrupted bone contiguity, limited movement and deformity [5]; (5) bone cancer, characterized by weakened bone, disrupted bone microstructure, persistent bone pain and limited mobility [6]; and (6) bone infection, characterized by inflammation and bone destruction caused by bacteria or fungi [7]. With the aggravation of the aging population, bone-related diseases have become a growing public health problem worldwide.

The prevalence of bone-related diseases has increased dramatically in recent years. OP is estimated to affect over 200 million individuals worldwide, and an osteoporotic fracture occurs every 3 s [8]. The prevalence of OA exceeds 20% of the middle-aged and elderly population in China [9]. In addition, the prevalence of RA has risen to 2.5% of the global population [10]. Although the incidence of bone cancer is relatively rare, approximately half of patients die of the disease [11]. In addition, bone infection is a difficult-to-treat disease with high failure rates of up to 20%–30% [12]. Overall, the increased prevalence of bone-related diseases imposes a tremendous clinical and socioeconomic burden on a global level.

1.2. Conventional diagnosis approaches for bone-related diseases

Early diagnosis is a prerequisite for improvement in therapeutic

Peer review under responsibility of KeAi Communications Co., Ltd.
* Corresponding author.
** Corresponding author.Department of Orthopedics, The First Affiliated Hospital of Soochow University, Suzhou, 215006, Jiangsu, China.
*** Corresponding author. Department of Orthopedics, The First Affiliated Hospital of Soochow University, Suzhou, 215006, Jiangsu, China.
E-mail addresses: jxbai1995@163.com (J. Bai), hy.wang1@siat.ac.cn (H. Wang), szgengdc@suda.edu.cn (D. Geng).

https://doi.org/10.1016/j.bioactmat.2022.12.014
Received 18 September 2022; Received in revised form 16 December 2022; Accepted 18 December 2022

efficacy and survival. The identification of patients with early-stage bone-related diseases would be of great importance to avoid unnecessary surgical intervention, considering only lifestyle management or pharmacological treatments. Conventional diagnosis approaches for bone-related diseases mainly depend on radiologic imaging and laboratory tests. Current clinical diagnositic methods for arthritis are traditionally based on clinical symptoms, radiographic observation and biomarker examination. However, when narrowed joint space and osteophytes are observed by X-rays, late-stage arthritis is already reached [13]. Fortunately, magnetic resonance imaging (MRI) is a useful tool for the detection of changed joint signals in the early stage of arthritis. For the diagnosis of bone cancer, different approaches are widely used, including X-ray, computed tomography (CT), MRI, positron emission tomography (PET)-CT scan and biopsy [14]. The diagnosis of OP is mainly based on BMD measured by dual-energy X-ray absorptiometry (DXA) [15], and the diagnosis of bone fracture is mainly based on X-rays and CT scans.

However, there is substantial room for improvement. Although MRI allows early visualization of structural changes and tumor determination, developing novel contrast agents with more precise visualization, higher biocompatibility and lower toxicity is still needed. In addition, invasive measurement of biomarkers in human biofluids may provide a better understanding of the dynamic events that occur in the joints [16]. Moreover, conventional technological methods are time-consuming, relatively costly and poorly predictive. To overcome the aforementioned limitations and drawbacks associated with conventional diagnostic methods, biological imaging and biosensors based on novel advanced nanomaterials, which enable more accurate, timely and safer diagnosis for bone-related diseases are crucially needed.

1.3. Conventional therapies for bone-related diseases

Bone-related diseases are notoriously difficult to treat due to varying pathogenesis, management and treatment for these diseases, which have become a major medical challenge. Since OP is associated with an imbalance in bone homeostasis, antiresorptive drugs such as bisphosphonates, RANKL inhibitors, estrogen and the anabolic drug such as teriparatide are the main therapeutic options [17,18]. The current management of RA is to suppress disease progression and alleviate symptoms using disease-modifying anti-rheumatic drugs (DMARDs), biological agents, non-steroidal anti-inflammatory drugs (NSAIDs) and glucocorticoids [19]. In contrast to RA, there is no effective disease modification for OA, and pharmacological therapies largely depend on symptom relief using NSAIDs, glucosamine and chondroitin sulfate [20]. Current bone fracture therapies are mainly based on titanium alloy materials and autologous or allogeneic bone grafts combined with anabolic drug administration [21]. For bone cancer, the most common treatments are neoadjuvant/adjuvant chemotherapy, surgery and radiation therapy [22]. With rapid advances in anticancer drug discovery, targeted therapy drugs such as cabozantinib (Cabometyx), regorafenib (Stivarga) and sorafenib (Nexavar) are commercially available [23–25]. Current treatment for bone infection mainly depends on long-term high-dose antibiotic administration together with aggressive debridement [26].

However, there are still some inevitable problems in current therapeutic approaches. First, the retention time of drugs is short in vivo due to decomposition before reaching the zone of action [27]. Additionally, the protection of drugs is limited. The drug structure and function in response to a complex physiological environment may be destroyed, thus leading to insufficient accumulation of drugs in the lesion site and poor clinical efficacy [28]. The targeting ability of drugs is also limited, and most drugs can hardly accumulate at bone lesion predilection sites, which decreases the therapeutic efficacy of drugs to a large extent [29]. In addition, drug overuse easily drives drug resistance to infection, which has reached alarming proportions [30]. Moreover, conventional orthopaedic implant materials without antibacterial activity may easily lead to an inflammatory response and even infection [31], and should be concerned for the insufficient biocompatibility and non-degradability [32] (Fig. 1). Hence, novel drugs as well as effective drug delivery strategies against bone-related diseases with more precise therapeutic benefits and fewer adverse side effects are in urgent demand. In this context, nanomaterials have emerged as promising candidates for bone-related diseases due to their potential versatility, strengthened flexibility and diversity.

1.4. Nanomaterials in bone-related diseases

The family of nanomaterials has enriched numerous applications in the biomedical field due to their diverse structures and compositions. Nanomaterials can be classified into inorganic and organic nanomaterials depending on their chemical composition. Organic nanomaterials are a class of emerging materials at the nanoscale composed of organic compounds obtained from the extraction of natural products or through chemical synthesis. They can be primarily divided into lipid-based (e.g., liposomes), polymeric (e.g., solid spheres, micelles, vesicles, and dendrimers), protein and nucleic acid-based nanomaterials. Advances in the development of functional organic nanomaterials have facilitated their applications in many fields [33]. Relatively, inorganic nanomaterials are nanosized materials without carbon-hydrogen bonds in their chemical structures. Compared with organic nanomaterials, inorganic nanomaterials are generally more chemically and mechanically stable. They can be categorized into metal, ceramic (e.g., metal oxide), magnetic, quantum dots, carbon and silica nanomaterials. These nanomaterials play a crucial role in energy, chemical industries, environment and medicine [34].

During the last decade, nanomaterials have been introduced in the field of bone-related diseases. Various emerging applications of nanomedicine for the diagnosis and therapy of bone-related diseases have been proposed, including biological tumor imaging, microcrack detection, arthritis biomarker sensors, targeted delivery and complication prevention. In this review, we first described quantum dots, gold, rare earth and metal oxide nanomaterials, which provide biological imaging for the early diagnosis of bone microfractures, bone tumors and metastases. Additionally, the potential of nanomaterials as biosensors for arthritis biomarkers in synovial fluids and peripheral blood is illustrated. Then, we focused on current nano-based therapies for bone-related diseases. Nanomaterials serve as therapeutic carriers or multifunctional platforms for bone homeostasis regulation and cellular modulation are highlighted. Finally, perspectives in this field are offered, including current key bottlenecks and future directions of nanomaterials for bone-related diseases. This review provides a comprehensive and up-to-date overview of advanced theranostic nanomaterials in bone-related diseases and shows promise for exploiting nanomaterials with novel properties and unique functions for better therapeutic efficacy (Fig. 2).

2. Nanomaterials for bone-related disease diagnosis

2.1. Nanomaterials for biomedical imaging

In most cases, radiographic imaging is still considered to be the first choice to diagnose and monitor bone-related diseases. X-rays reveal changes in the damaged bone structure and joint space. Computed tomography (CT) reconstructs the area of impaired bone and joints in multiple planes. MRI evaluates the pathologic conditions of cartilage, ligaments, muscles and tendons. Ultrasound can be used to assess the variations of bone structures and density. Photoacoustic imaging reveals lesion location based on the photoacoustic effect. However, there are still some limitations of the current imaging methods. With the development of nanomaterials, quantum dots, superparamagnetic iron oxide, metal and other nanomaterials have been broadly used in biological imaging with higher precision and sensitivity (Table 1).

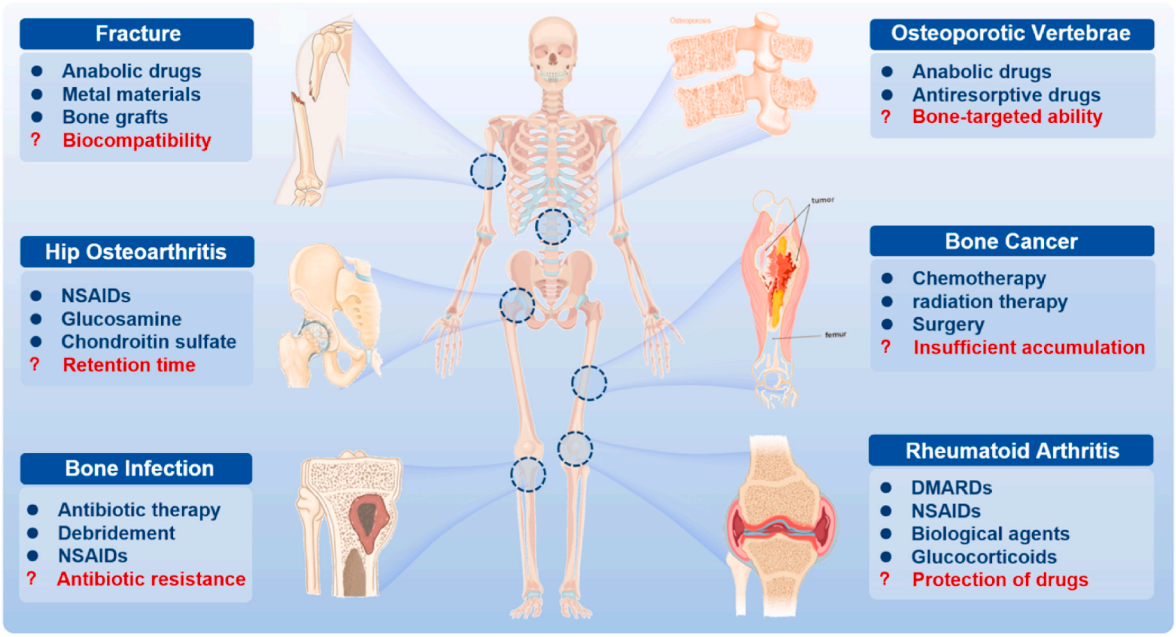

Fig. 1. Typical bone-related diseases and conventional approaches (blue) for management with inevitable problems (red). NSAIDs, non-steroidal anti-inflammatory drugs; DMARDs, disease-modifying anti-rheumatic drugs.

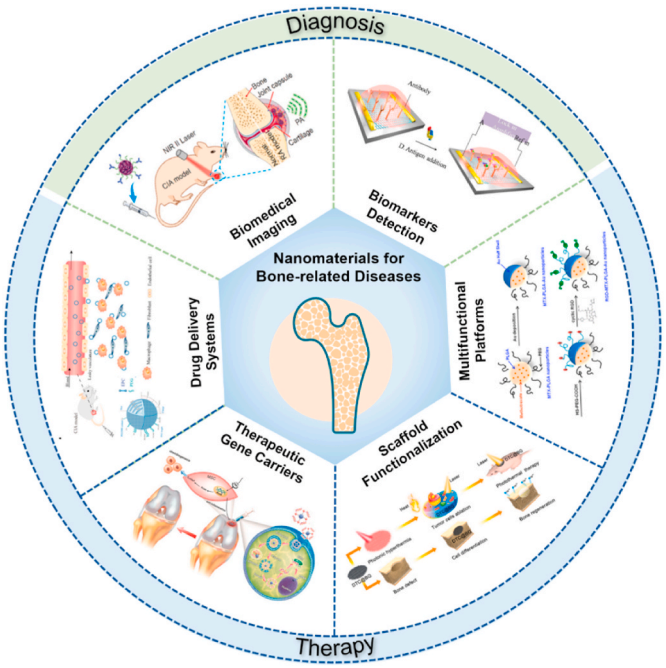

Fig. 2. General overview of current nanomaterials for bone-related disease diagnosis and therapy. Novel nanomaterials provide biomedical imaging [35] and biomarker detection [36] for the early diagnosis of bone-related diseases. The images reproduced with the permission from Wiley-VCH GmbH and Elsevier B.V. Moreover, nanomaterials serve as drug delivery systems [37], gene carriers [38], multifunctional scaffolds [39] or platforms [40] for treatment of bone-related diseases. The images reproduced with the permission from Oxford University Press, American Chemical Society and WILEY-VCH.

2.1.1. *Quantum dots*

Carbon nanodots (C-dots) are attracting considerable attention as a nascent candidate for biological imaging [50]. The carboxylic acid moieties on the surface of C-dots endowed them with excellent water solubility and suitability for subsequent functionalization. Krishana et al. showed a modified C-dots nanoprobe to detect calcium deposits in bone through fluorescence imaging [41]. Glutamic acid (GA) along with amino-functionalized C-dots were conjugated onto hyaluronic acid (HA) on the basis of *N*-(3-dimethylaminopropyl)-N′-ethylcarbodiimide (EDC) chemistry. This probe reflected its potential to detect microcracks in bone due to its ability to recognize and bind to calcium ions released from crack sites. The bound areas could be visualized through illumination by UV light (365 nm). Moreover, the existence of other basic ions, such as Na^+ and K^+, has no impact on the fluorescence intensity, thus the fluorescence could be easily and clearly detected in bone, especially in new crack sites. Thereafter, Krishna et al. fabricated another C-dots based probe containing both GA and ciprofloxacin, aiming to detect micro bone crack, as well as control infection at the crack sites simultaneously [51] (Fig. 3A). In addition, Pan et al. synthesized spheroidal C-dots with PEG monophosphates in a one-step carbonization process [42]. This probe indicated affinity to hydroxyapatite minerals with remarkable optophysical properties for imaging after intramuscular administration (Fig. 3B). The strong fluorescence traced by C-dots under UV light (365 nm) in areas of bone microcracks enabled the long-term prediction of more serious bone-related diseases such as occult fractures and osteoporosis.

Apart from bone crack detection, C-dots are also capable of enhancing bone formation. Shao et al. developed citric acid-based C-dots and their derivative 1-ethyl-5-oxo-1,2,3,5-tetrahy-droimidazo-[1,2-a] pyridine-7-carboxylic acid (Et-IPCA) for tracking and promoting osteogenic differentiation of mesenchymal stem cells (MSCs) [52]. When the concentration of this fluorescent probe was lower than 50 μg/ml, it labeled MSCs without affecting cell viability or apoptosis. Importantly, this C-dots probe could facilitate osteogenic transcription and increase matrix mineralization via the ROS-mediated MAPK signaling pathway. Li et al. found that C-dots with low quantum yield lighted up calcified zebrafish bones with high affinity, specificity and stable retention [53] (Fig. 3C). This novel C-dots probe may be a promising vehicle to deliver fluorescein to bones without detectable toxicity. To further address whether the high-affinity binding of C-dots to bone was preserved after surface modification, several C-dots and their conjugates were synthesized by the same research team [54]. No negative effect was observed on binding affinity and selectivity to bone after functionalization of C-dots. These unique optical properties of

Table 1
Summary of example nanomaterials for biomedical imaging.

Types of nanomaterials	Imaging methods	Diagnosis	Advantages	Ref.
Carbon nanodots	Fluorescent microscope	Bone cracks	• clear visualization of new bone crack under UV light illumination (365 nm) • fluorescence intensity is not affected by basic ions	[41]
Carbon nanodots	In vivo imaging system	Bone cracks	• remarkable fluorescence for imaging after intramuscular administration • biodegradable	[42]
Ultrasmall superparamagnetic iron oxide (USPIO)	MRI	Rheumatoid arthritis	• assess early stages of RA before structural changes via significant T1 and T2 effects in synovium and synovial effusion after intravenous administration	[43]
Superparamagnetic iron oxide nanoparticles	MRI	Rheumatoid arthritis	• taken by phagocytic active macrophages of the synovium after intravenous injection • visualized in MRI for accurate early diagnosis of RA	[44]
Superparamagnetic iron oxide nanoparticles	MRI	Osteosarcoma	• significantly detect tumor-associated macrophages response to CD47 mAb in osteosarcoma	[45]
Gold nanorods	Photoacoustic imaging	Osteosarcoma	• bind selectively to UMR-106 xenografts after systemic administration • enhance the contrast of osteosarcoma images by 230% compared with the control group	[46]
Gold nanorods	Photoacoustic imaging	Rheumatoid arthritis	• high targeting affinity to inflamed regions • feature 1.7 times more signal than the control group	[47]
Lutecium-based upconversion nanoparticles	CT	Osteosarcoma	• relative higher spectral CT performance than iohexol for the diagnosis of osteosarcoma • excellent biocompatibility	[48]
PLGA-PEG-Folate nanoparticles	MRI and In vivo imaging system	Rheumatoid arthritis	• more absorbed in activated macrophages • improve the NIR signal in arthritic inflamed tissue at early time point after intravenous administration • high diagnostic specificity for RA • enable the quantification of drug release kinetics.	[49]

C-dots open new venues for bone-specific bioimaging agents and early diagnosis of bone-related diseases.

However, the biosafety of quantum dots (QDs) has been a great concern before the QDs community moves into clinical application owing to their nanosized effect and heavy-metal components. Once exposed to the biological environment, QDs are unlikely to keep their original forms, and the transformation of QDs in cells may lead to cell morphology and structure variation, cell growth inhibition, mitochondrial dysfunction, DNA damage and apoptosis [55]. Therefore, further understanding of the mechanisms of nanomaterial toxicity is necessary.

2.1.2. Metal oxide nanomaterials

Metal oxide nanomaterials could serve as possible magnetic MRI contrast agents in the detection of bone-related diseases. Superparamagnetic iron oxide nanoparticles (SPIONs) reveal a high value of saturation magnetization in the presence of a magnetic field. Active targeting SPIONs can be formed by conjugation with different antibodies, peptides and small molecules, which can also be attached to the polymers [56]. Dai et al. coated SPIONs with glucose and dextran, and subsequently folic acid was conjugated on the surface to form FA glu-dex-SPIONs [57]. The FA glu-dex-SPIONs served as contrast agents to visualize antigen-induced arthritis in rats using 7.0 T MRI (Fig. 4A). Significant differences in T2-weighted MRI images between the synovium and surrounding tissues were observed 24 h post intravenous administration. Besides, FA glu-dex-SPIONs might be useful to quantify the recovery level of inflamed joints after 10 days of cyclooxygenase 2 (COX-2) inhibitor treatment, suggesting that this type of magnetic nanoparticles might be used as novel MRI contrast agents for the diagnosis and therapeutic response of RA.

Additionally, Chen et al. developed targeted SPIONs for in vivo labeling and tracking of T cells in a collagen-induced arthritis model of rheumatoid arthritis [58]. SPIONs were coated with carboxylation of polyethylene glycol through a silane-ligand exchange reaction, and the monoclonal anti-CD3 antibody was subsequently conjugated on the surface via an EDC-NHS reaction to form IOPC-CD3 (Fig. 4B). Serial MRI imaging indicated a clear increase in the signal-to-noise ratio of the femoral growth plates infused with IOPC-CD3, which was consistent with the accumulation of T cells in the corresponding regions. Moreover, IOPC-CD3 exhibited high transverse relaxivity, good selectivity and bioavailability, indicating its potential as a promising MRI probe in clinical applications. Panahifar et al. synthesized a novel bone-seeking contrast agent based on alendronate-conjugated SPIONs (SPION-ALE) for MRI imaging of bone metabolic activity [59]. SPION-ALE exhibited approximately 65% selective affinity binding to HA, which is the principal mineral of bone, and 95% SPION-ALE remained strongly bonded to HA 24 h later (Fig. 4C). The results indicated the potential of SPION-ALE for imaging dynamic bone turnover and diagnosing metabolic bone-related pathology. To detect bone metastases, Pourtau et al. fabricated trastuzumab-functionalized SPION polymersomes against human endothelial receptor 2 (HER2) as novel MRI contrast agents (Fig. 4D) [60]. This approach potentiated the specificity and aggregation of contrast agents to target cancer cells in vivo, indicating that antibody-functionalized magnetic polymersomes might be more powerful diagnostic tools for bone cancer using high-resolution MRI.

2.1.3. Metal nanomaterials

Metal nanomaterials are one of the most extensively studied delivery platforms in numerous fields, such as electronics, chemical catalysis, diagnostics and therapeutics [61]. Gold nanostructures have also been applied in several imaging techniques due to their unique optical properties and broader localized surface plasmon resonance [62]. Fournelle et al. fabricated enlarged gold nanorods conjugated with the antitumor necrosis factor-α (TNF-α)-targeting antibodies infliximab and certolizumab to detect inflammation in arthritis via molecular optoacoustic imaging (OAI) [63]. The OAI platform was equipped with a focused ultrasound transducer and a pulsed neodymium-doped yttrium aluminum garnet (ND: YAG) laser (Fig. 5A). Overexpression of TNF-α in arthritic knees was confirmed by the superb optoacoustic properties of these gold nanorods, suggesting their potential to visualize molecular changes and identify diagnostic markers early over the course of arthritis via OAI. Similarly, Vonnemann et al. designed dendritic polyglycerolsulfate functionalized gold nanorods (AuNR-dPGs) as an optoacoustic signal amplifier for biological imaging of RA (Fig. 5B) [47]. The AuNR-dPGs featured 1.7 times more signal than the control group at 800 nm wavelength illumination. Moreover, AuNR-dPGs demonstrated high targeting affinity to inflamed regions. This finding opens a new avenue for the diagnosis of RA and other inflammation-associated diseases using multispectral optoacoustic tomography.

In addition, Ma et al. synthesized PEGylated gold nanorods (PGNRs) conjugated with two tumor-specific oligopeptides, PT6 and PT7, to target an osteosarcoma cell line (UMR-106) via specific photoacoustic imaging (PAI) (Fig. 5C) [46]. Sequential PAI of the osteosarcoma site

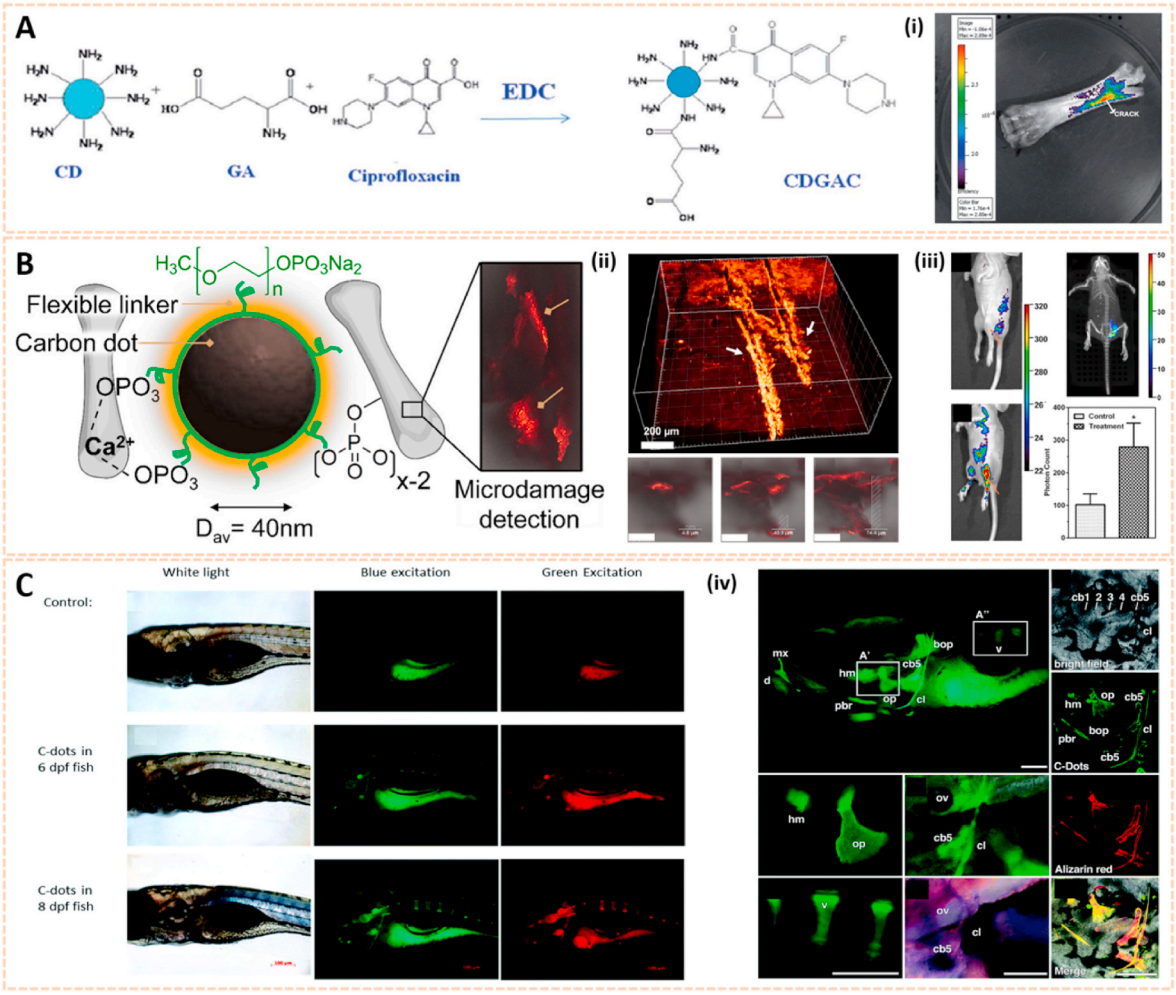

Fig. 3. Quantum dots for biomedical imaging. A) Conjugation of GA and ciprofloxacin onto CDs. (i) Bone crack detection (marked) by CDGAC imaged with the IVIS system [51]. The images reproduced with the permission from The Royal Society of Chemistry. B) Monodentate ligand can come close together on the CD surfaces to chelate $Ca2^{+}$ which gets exposed abundantly at the site of the microcrack. The fluorescence from the CD can be utilized for the detection of bone microcracks. (ii) 3D confocal image of the NPs residing in the bone microcracks (λex = 488 nm). (iii) In vivo fluorescence of monophosphonated CDs in the tibia with distinct site enhancement in the signal to background intensity [42]. The images reproduced with the permission from American Chemical Society. C) Zebrafish images under white light, blue light excitation and green light excitation 6- and 8-days post fertilization (dpf) with 5 nL injection of 1 μg μL-1 C-dots. (iv) C-Dots deposit with high affinity and specificity on ossified bones [53]. The images reproduced with the permission from The Royal Society of Chemistry.

showed clear tumor visualization after intravenous administration of PGNR-PT6 and PGNR-PT7, and PA images of osteosarcoma were contrast enhanced by 170% and 230%, respectively, compared to the control group. The PGNR-based nanoprobe modified with derived oligopeptide-mediated photoacoustic imaging may open an avenue for the tumor type-specific diagnosis of osteosarcoma. Besides, the state of bone-related diseases can be monitored by abnormal endogenous substances. Lee et al. fabricated gold nanoparticles conjugated with near-infrared fluorescence (NIRF) dye-labeled hyaluronic acid (HA) as nanoprobes (HHAuNPs) for the detection of reactive oxygen species (ROS) and hyaluronidase (HAdase) [64]. Local inflammation of rheumatoid arthritis and metastatic tumor sites was identified by strong fluorescence signals after systemic administration of HHAuNPs (Fig. 5D). These results pave the way for the diagnosis of local HA-degrading diseases via optical imaging.

2.1.4. Other nanomaterials

Rare earth (RE) smart materials are emerging as a promising class of biomaterials for bone tissue engineering and implantology [65]. RE nanomaterials such as europium (Eu), ytterbium (Yb), gadolinium (Gd) and lutetium (Lu) are gaining attention in biological imaging due to their unique fluorescence upconversion and penetrating properties in tissues [66]. McMahon et al. synthesized a lanthanide luminescent contrast agent based on a supramolecular Eu^{3+} complex for damaged bone imaging (Fig. 6A) [67]. This contrast agent possessed high affinity binding to Ca^{2+} sites due to the iminodiacetate moieties, which enabled the selective and effective visualization of bone damage for the early diagnosis of microcracks. Ytterbium is another RE material used in biological imaging with different X-ray attenuation characteristics from Ca. Wang et al. synthesized Yb-based nanoparticles conjugated with the bone targeting ligand N-nitrilotriacetic acid (NTA) to form YbNP@SiO2−NTA as a novel contrast agent for gemstone spectral computed tomography (GSCT) scanning (Fig. 6B) [68]. The targeting and accumulation of YbNP@SiO2-NTA toward the bone crack site could be visualized in real time by GSCT, indicating a promising approach for the diagnosis of micro bone fractures in the future.

In addition, Nejadnik et al. developed a caspase-3-sensitive gadolinium-based MRI probe (C-SNAM) for the noninvasive detection of stem cell apoptosis in arthritic joints [69]. The C-SNAM was converted into Gd nanoparticles cleaved by caspase-3, and the ^{1}H MR signal was enhanced by 90% in matrix-associated stem cell implants, thus prolonging retention in vivo (Fig. 6C). This novel approach may be useful for the diagnosis of stem cell transplant failures at an early stage and the development of cartilage regeneration techniques. Additionally, Wang

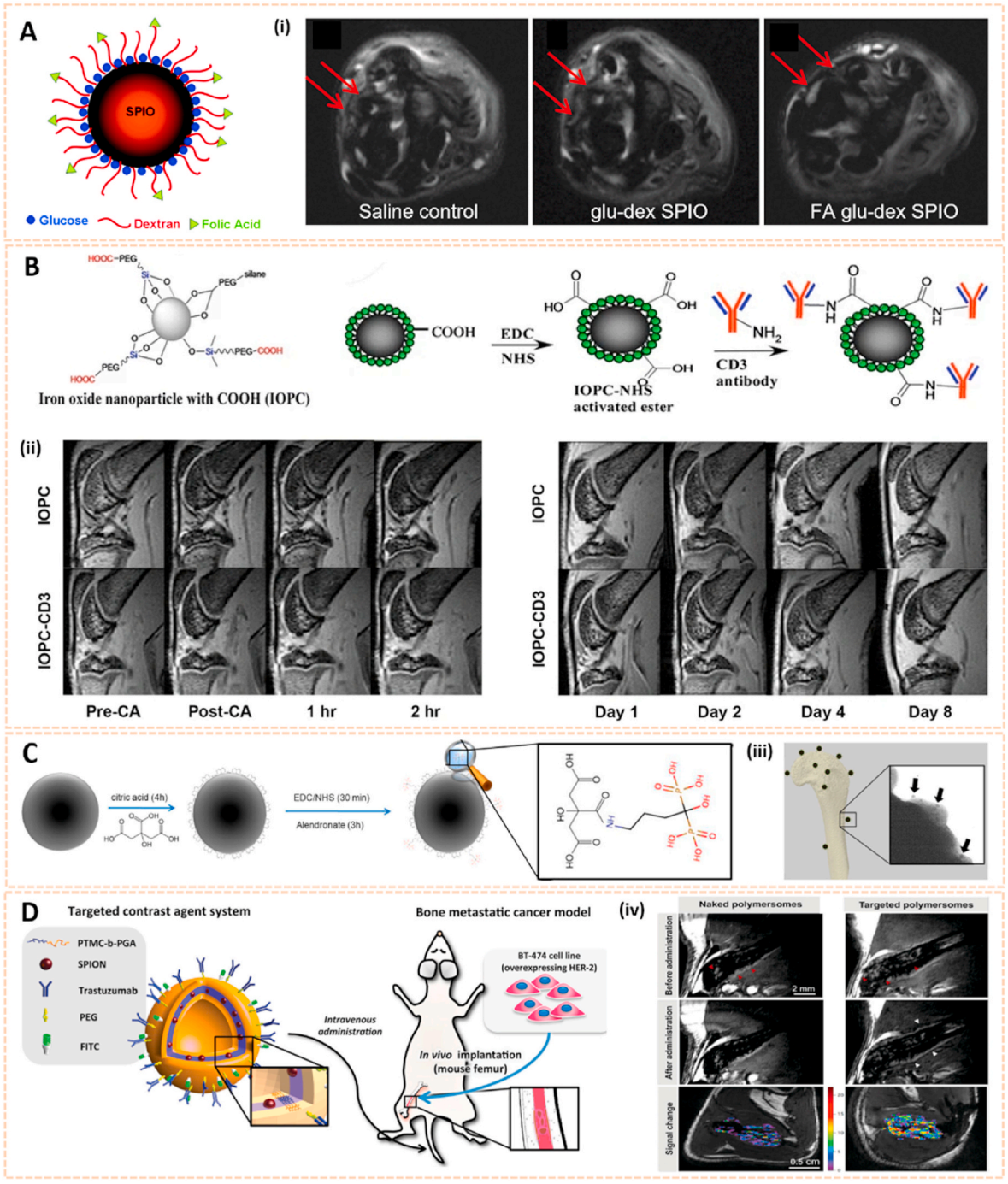

Fig. 4. Metal oxide nanomaterials for biomedical imaging. A) A sketch of a glucose and dextran coated SPIO nanoparticle. (i) T2-weighted MR image of AIA rats 24 h post-injection of SPIO in different groups. The arrow shows the synovium [57]. The images reproduced with the permission from The Royal Society of Chemistry. B) Schematic illustration of the stepwise synthesis of IOPC-CD3. (ii) The defined ROIs. And serial T2*WIs (sagittal view) of CIA rat knees infused with IOPC or IOPC-CD3 [58]. The images reproduced with the permission from World Molecular Imaging Society. C) Schematic picture indicating the preservation of ALN phosphonate moieties during conjugation to SPIONs, for subsequent targeting of bone. (iii) TEM image representing numerous bone-targeting SPION-ALN targeted to a HA crystal after incubation for 2 h [59]. The images reproduced with the permission from American Chemical Society. D) Multifunctional polymersomes loaded with maghemite nanoparticles and grafted with fluorescein and targeting antibodies, directed against HER2, were developed as novel MRI contrast agents for bone metastasis imaging in NOD/SCID mice. (iv) Bone BT-474 tumor targeting as assessed from high resolution 3D TrueFisp MRI. Red arrows denote tumor tissue. White arrows denote contrast variations on tumor boundaries [60]. The images reproduced with the permission from WILEY-VCH.

et al. modified gadolinium nanoparticles (GdNPs) with bovine serum albumin (BSA) and subsequently iodinated them by a chloramine-T procedure to form I-BSA-GdNPs [70]. The I-BSA-GdNPs exhibited good chemical stability, biocompatibility, an intense coefficient of X-ray attenuation and a great drive for MRI. Therefore, the long-circulating accumulation and retention of I-BSA-GdNPs in the tumor matrix after intravenous administration enhanced dual-model MRI and CT visualization of osteosarcoma in rats (Fig. 6D). This multimodal imaging probe highlighted its potential application for the diagnosis and therapy of bone cancer.

Conjugated polymer nanoparticles are emerging as superior imaging substances due to their excellent light trapping nature, tunable

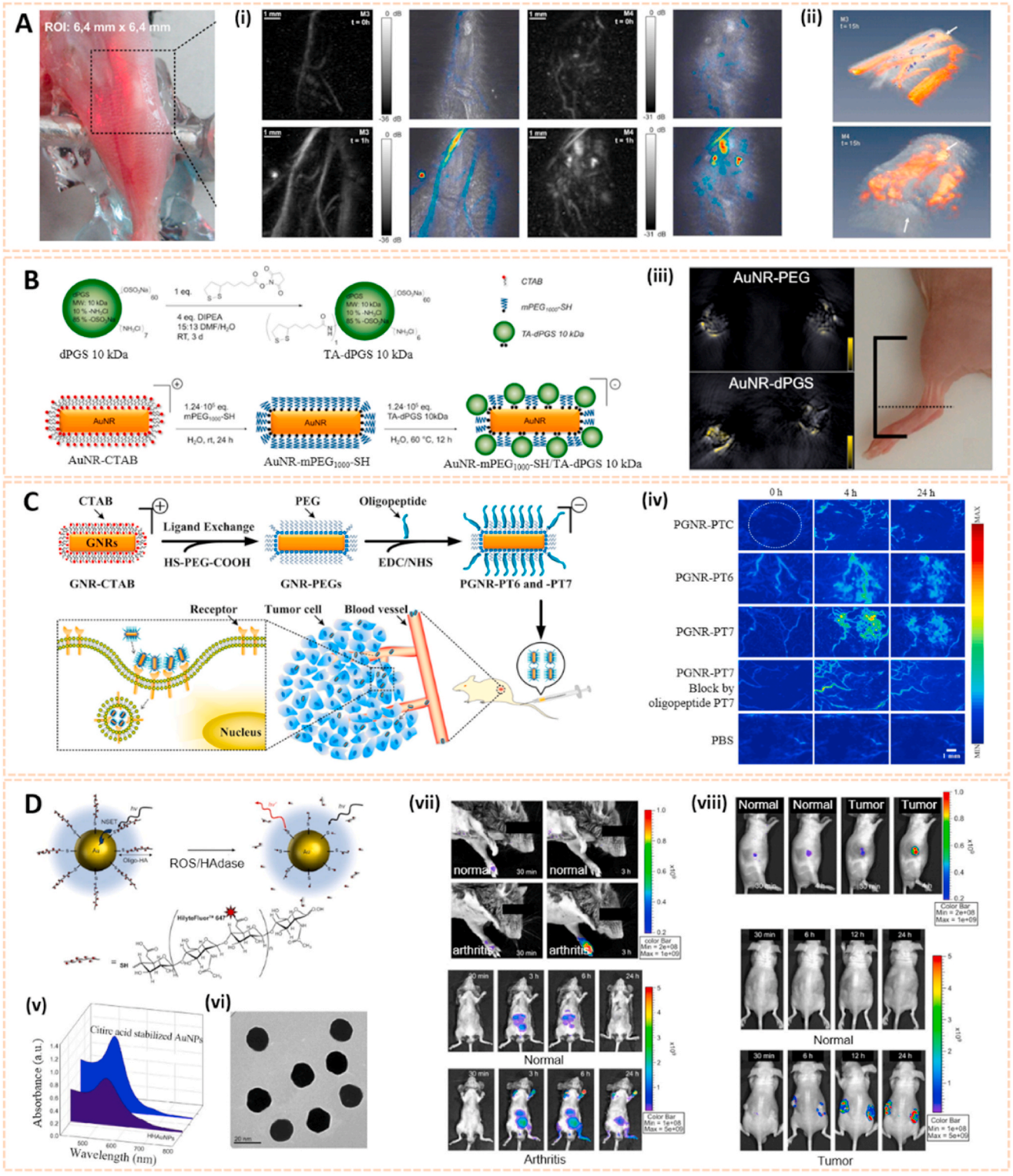

Fig. 5. Gold nanomaterials for biomedical imaging. A) Optical photograph of the region of interest. (i) Images acquired on two mice affected by arthritis before and 1 h after injection of control particles (M3) and of nanoprobes (M4). (ii) 3D reconstruction of the signals illustrates that the signals detected M3 correspond to blood vessels, whereas the M4 shows diffuse signal enrichment in the articular area [63]. The images reproduced with the permission from Elsevier Inc. B) Synthesis of thioctic acid functionalized dendritic polyglycerolsulfate via amide coupling and functionalization of CTAB double-layer coated gold nanorods. (iii) Accumulation of gold nanorods in the ankle of an arthritic mouse with the signal coming from AuNR-PEG and AuNR-dPGS [47]. The images reproduced with the permission from Ivyspring International Publisher. C) Chemical synthesis of functionalized nanoprobes (PGNR-PT6 and -PT7) for tumor imaging. (iv) Sequential PA MIP frames of the tumor site before and after intravenous injection [46]. The images reproduced with the permission from Elsevier Inc. D) Schematic illustration of NSET interaction between Hilyte-647 dye labeled oligo-HA and AuNP. (v) UV/Vis absorbance spectra of citric acid stabilized AuNP and HHAuNPs. (vi) TEM image of HHAuNPs. (vii) In vivo fluorescence images of collagen-induced RA mice upon local or systemic injection of HHAuNPs. (viii) In vivo fluorescence images of tumor-bearing nude mice upon local or systemic injection of HHAuNPs [64]. The images reproduced with the permission from Elsevier Ltd.

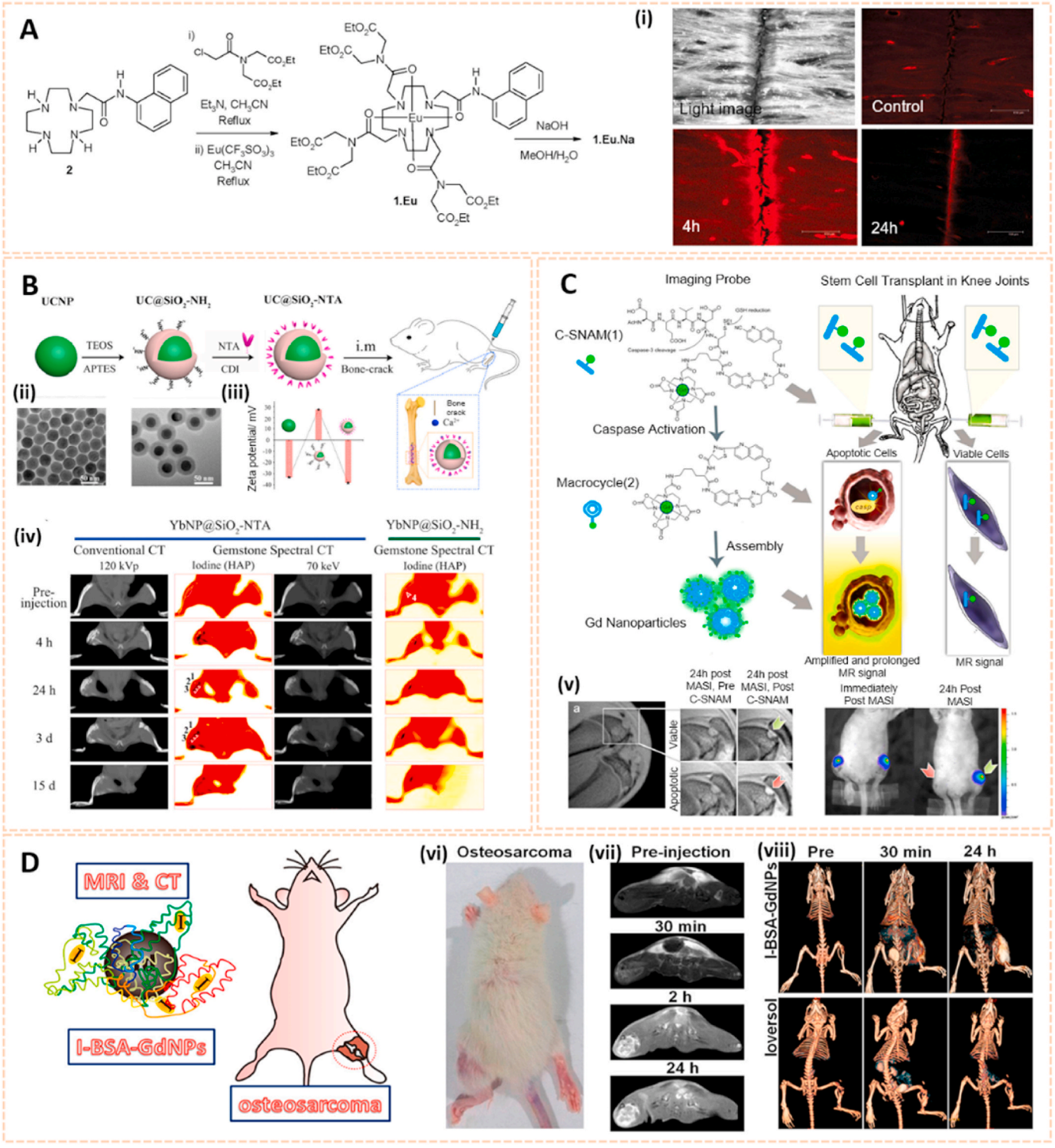

Fig. 6. Rare earth smart nanomaterials for biomedical imaging. A) Synthesis of 1 (Free Ligand) and Corresponding Eu(III) Complexes 1. Eu and 1.Eu.Na. (i) Confocal laser-scanning microscopy images of bone sample immersed in a 1×10^{-3} M solution of 1.Eu.Na [67]. The images reproduced with the permission from American Chemical Society. B) Schematic illustration of the synthesis of YbNP@SiO2-NTA. (ii) TEM images of OA-YbNPs and YbNP@SiO2–NH2. (iii) Zeta potentials of corresponding samples. (iv) Conventional CT image at 120 kVp, iodine (HAP) base image, and 3D image of the bone-cracks in the rat after intramuscular injection of YbNP@SiO2-NTA and YbNP@SiO2–NH2 solution at 4 h, 24 h, 3 d, and 15 d [68]. The images reproduced with the permission from American Chemical Society. C) General design and mechanism of action of the caspase-3-sensitive nanoaggregation MRI probe (C-SNAM). (v) In vivo MRI and BLI of viable and apoptotic rASC implants [69]. The images reproduced with the permission from American Chemical Society. D) Schematic Diagram for the Fabrication of I-BSAGdNPs as a MR/CT Dual Modality Nanoprobe for Osteosarcoma Visualization. (vi) Orthotopic osteosarcoma animal models. (vii) In vivo T1-weighted MRI images of orthotopic osteosarcoma rats. (viii) CT 3D images of orthotopic osteosarcoma rats after Ioversol and I-BSAGdNPs injection [70]. The images reproduced with the permission from American Chemical Society.

adsorption and biocompatibility properties [71]. Chen et al. synthesized polymer nanoparticles (PNPs) conjugated with the antirheumatic targeted drug tocilizumab (TCZ) to form a near infrared (NIR)-responsive nanoplatform (TCZ-PNPs) for the diagnosis and therapy of RA (Fig. 7A) [35]. TCZ-PNPs exhibited high targeted affinity, strong NIR-II extinction and photostability for effective noninvasive monitoring of RA disease progression with a high signal-to-noise ratio of 35.8 dB via photoacoustic imaging. The TCZ-PNPs associated with photoacoustic imaging guided therapeutic monitoring of RA and further clinical translation. To detect articular cartilage degeneration in the early stage, glycosaminoglycan (GAG)-targeted cationic nanoprobes consisting of poly-L-lysine and melanin (PLL-MNPs) were designed for photoacoustic imaging (PAI) enhancement [72,73]. PLL-MNPs exhibited high affinity and sensitivity to GAGs, which decreased stepwise during the progression of OA (Fig. 7B). The cationic nanoprobes enable tracking the changes in GAGs to provide sensitive visualization of the state of OA in living models via PAI, which indicates a novel approach to diagnose OA in the early stage and facilitate OA theranostics.

In addition, Zhou et al. fabricated PCL_{67}-b-P [Glu_6-stat-$(Glu\text{-}ADA)_{16}$] polymer vesicles as a single photon emission computed tomography/computed tomography (SPECT/CT) imaging enhancer to detect bone cancer (Fig. 7C) [74]. The vesicles could be self-assembled into bone-targeted polymer vesicles directly in water. After loading doxorubicin, the polymer vesicles showed an obvious therapeutic effect on malignant bone tumors, and the size of the tumors subsequently decreased from over 2 cm^3 to less than 0.6 cm^3 after 11 days owing to necrosis and apoptosis of the tumor cells. Therefore, this polymer vesicle paves the way for the combination of real-time diagnosis and therapy of bone cancer.

Silica-based nanomaterials are also attractive for bioimaging due to their excellent photostability, multivalent binding capability and biocompatibility. Lu et al. engineered mesoporous silica-coated bismuth sulfide nanoparticles conjugated with arginine-glycine-aspartic acid (RGD) peptide to form RGD-Bi_2S_3@MSN for CT imaging and tumor ablation (Fig. 7D) [75]. The RGD-Bi_2S_3@MSN address the issue of CT imaging owing to the high X-ray attenuation of Bi. The distributed mesoporous pores and large surface areas allowed ultrahigh doxorubicin (DOX) loading and promising drug protection. RGD-Bi_2S_3@MSN/DOX possessed high affinity for tumor cells and enhanced NIR-responsive photothermal therapy and chemotherapy to kill osteosarcoma cells through the mitochondrial apoptosis pathway. The novel silica-based nanomaterial indicated its potential for the diagnosis of malignant bone tumors via CT imaging.

Chemiluminescence (CL) signals activated by chemical reactions have the potential for the early diagnosis of various inflammatory diseases. Singh et al. synthesized a CL nanoprobe (BioNT) with high affinity for endogenous hydrogen peroxide (H_2O_2) for inflammation detection in pathological tissues [76]. The BioNT was engineered by physical integration of 9,10-Bis [4'-[4''-[*N*-methyl-*N*-(2-[4-*tert*-butylbenzoyloxy] ethyl)amino]-styryl]styryl] anthracene (BDSA), bis-[3,4,6-trichloro-2-(pentyloxycarbonyl)phenyl] oxalate (CPPO) and Pluronic F-127 into the ultrafine nanoreactor structure (Fig. 7E). The BioNT generated a strong CL torchlight in the inflamed tissues with dual selectivity after intravenous administration. Even a tumor that requires a long blood circulation duration for targeting could be precisely visualized. The self-lighted nanotorch BioNT might thus be a candidate for further diagnostic biomedical applications.

2.2. Nanosensors for arthritic biomarker detection in human biofluids

Apart from biological imaging, biochemical markers in human biofluids may also serve as an attractive alternative for the assessment and monitoring of bone-related diseases [77]. For instance, glycosaminoglycans (GAGs) released from degrading cartilage, free radical nitric oxide (NO) and proteinases such as ADAMTS, MMP-3 and MMP-13 are essential biomarkers for the early diagnosis of OA [78]. Relatively, rheumatoid factor (RF) and anti-cyclic citrullinated peptide antibody (anti-CCP) are critical biomarkers for RA [79]. Current biomarker detection methods consist of enzyme-linked immunosorbent assay (ELISA), real-time polymerase chain reaction (RT-PCR), spectrometry, etc. These methods still have some disadvantages like insufficient precision, time consumption and high cost. For this reason, several label-free and real-time nanomaterial-based biosensors have been widely adopted in the detection of biomarkers with higher precision and sensitivity (Table 2).

2.2.1. Gold nanomaterials

Recent advances in gold nanomaterials have emerged as novel biosensing tools for the selective detection of biomarkers owing to their excellent chemical stability and convenient visible spectral range. Zhao et al. fabricated an asymmetric heterogeneous dumbbell-like polyaniline-gold (PANI-Au) nanocomposite conjugated with graphite-like carbon nitride (g-C_3N_4) as a label-free chemiluminescence (ECL) immunosensor for the early diagnosis of RA (Fig. 8A) [80]. This biosensor exhibited high selectivity and affinity for anti-CCP. Moreover, the linear range of the biosensor was 0.001 ng/ml to 15 ng/ml with a detection limit of 0.2 pg/ml for the identification of anti-CCP antibody. The good reproducibility and excellent sensing properties may broaden the applications of ECL immunosensors in clinical diagnosis.

To date, the relationship between RA and mycoplasma pneumonia (MP) has been confirmed [86]. Jia et al. synthesized Au@Ag nanoparticles (Au@Ag NPs) conjugated with two layers of the Raman dye 5, 5′-dithiobis-(2-nitrobenzoic acid) (DTNB) as surface-enhanced Raman scattering (SERS) tags for the detection of MP in human serum (Fig. 8B) [81]. The Au/DTNB@Ag/DTNB NPs possessed high sensitivity and affinity to MP-specific IgM with a detection limit of 0.1 ng/ml, which was 100-fold more sensitive than the colorimetric assay. Hence, the Au/DTNB@Ag/DTNB NPs provide potential for the accurate and sensitive detection of RA. In addition, Veigas et al. designed gold nanoparticles conjugated with bifunctional polyethylene glycol (PEG) via a thiol group and subsequently covalently coated them with a human IgG Fc antibody fragment to form AuNP@IgG Fc for the detection of RA using fast colorimetric screening (Fig. 8C) [82]. The aggregation of AuNP@IgG Fc was indicated by the rapid and remarkable change in solution color from red to purple. AuNP@IgG exhibited quick and reliable screening for RF with a detection limit of 4.15 IU/ml, which is obviously lower than the clinical standard threshold of 20 IU/ml. Therefore, AuNP@IgG may be useful for faster and easier molecular screening and diagnosis of inflammatory arthritis.

A disintegrin and metalloproteinase with thrombospondin motif-4 (ADAMTS-4) exerts key functions in early cartilage degeneration, thus screening ADAMTS-4 would be useful for the early diagnosis of cartilage-degrading joint diseases. Peng et al. engineered gold nanoparticles coated with a FITC-modified ADAMTS-4-specific peptide to serve as biosensors to identify the activity of ADAMTS-4 in synovial fluid (Fig. 8D) [83]. The nanoprobe possessed high affinity and sensitivity to ADAMTS-4 with high fluorescence intensity. Moreover, even patients suffered from mild cartilage damage with no obvious pathological changes on T1-and T2-weighted MRI, the nanoprobe could also determine ADAMTS-4 activity in biological samples with strong fluorescence. This probe thus opens an avenue for the detection of biomarkers in human fluids and subsequent diagnosis at an early stage.

2.2.2. Organic nanomaterials

Organic nanomaterials are considered as promising drug delivery platforms due to their good release kinetics and biodegradability. Nitric oxide (NO) is a molecule that plays a key role in the inflammatory and degradative cascade of osteoarthritis. Jin et al. fabricated poly-(lactic-*co*-glycolic acid) (PLGA) nanoparticles encapsulating 4-amino-5-methylamino-2′,7′-difluorofluorescein diaminofluorescein-FM (DAF-FM) as an NO nanosensor for monitoring the progression of OA (Fig. 9A) [87]. This nanosensor tracked NO levels in synovial fluids with strong

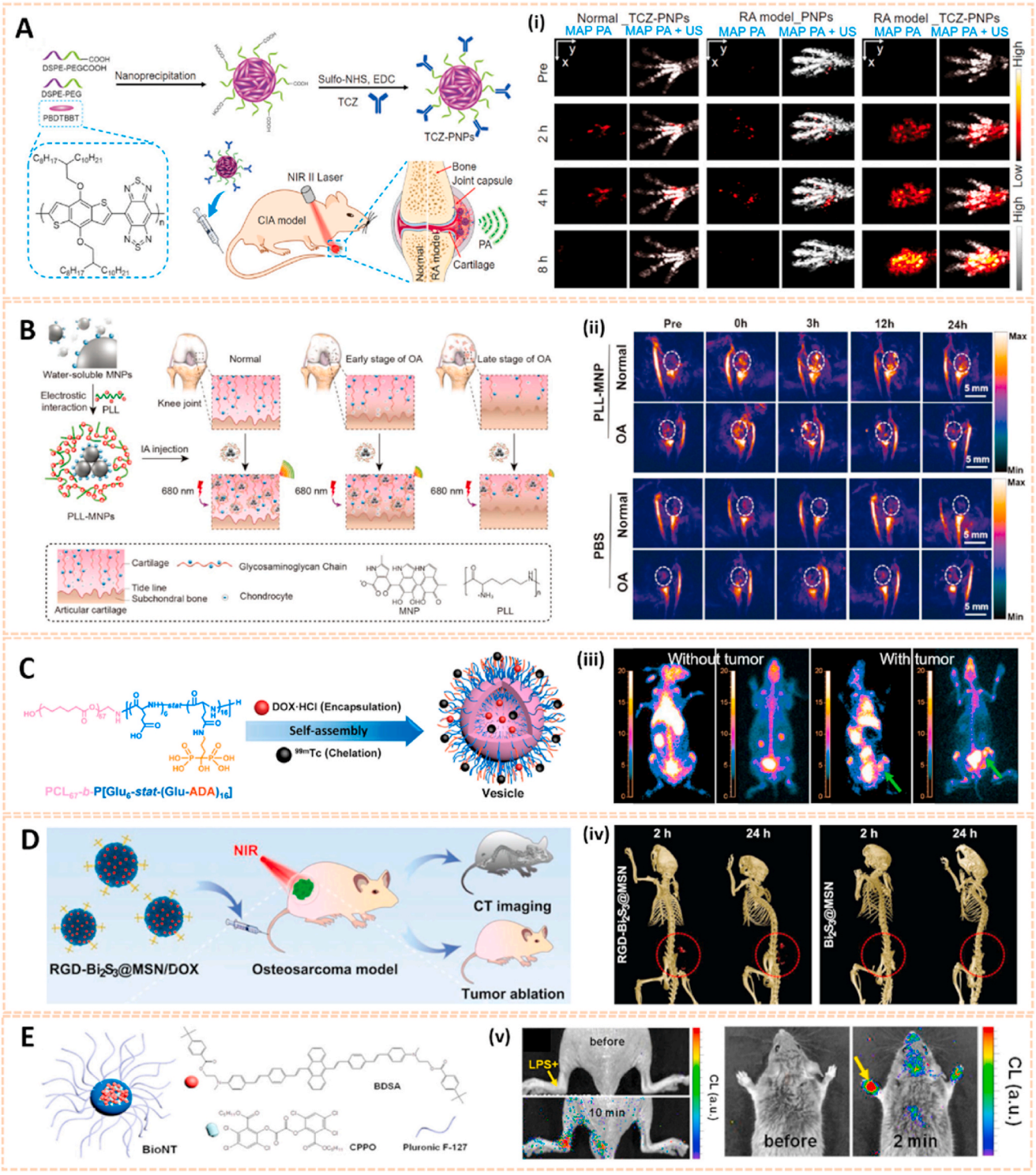

Fig. 7. Other nanomaterials for biomedical imaging. A) Schematic illustration of TCZ-PNPs for NIR-II photoacoustic (PA) imaging and therapy of RA model mouse using a 1064 nm laser (i) MAP PA/US images of forepaws [35]. The images reproduced with the permission from Wiley-VCH GmbH. B). Schematic illustration of the preparation of PLL–MNPs and its mechanism diagnosing OA cartilage degeneration by PAI. (ii) Representative PA images of the knee joints before and after the intraarticular injection of the PLL–MNPs and PBS at different time points [73]. The images reproduced with the permission from The Royal Society of Chemistry. C) Schematic illustration of bone-targeting polymer vesicles for simultaneous diagnosis and treatment of malignant bone tumor. (iii) SPECT/CT imaging of rabbits without and with tumor using 99mTc-labeled vesicles (left) and 99mTc-ADA (right) [74]. The images reproduced with the permission from Elsevier Ltd. D) The smart RGD-Bi_2S_3@MSN/DOX nanoplatform for OS real-time X-ray CT imaging. (iv) In vivo CT images of UMR-106 tumor-bearing nude mice recorded at 2 and 24 h after i. v. injection of the RGD–Bi_2S_3@MSN and Bi_2S_3@MSN. The tumor site is highlighted by the red circle [75]. The images reproduced with the permission from WILEY-VCH. E) Schematic representation of BioNT. (v) Imaging of localized and systemic arthritis with intravenously injected BioNT (n = 4) [76]. The images reproduced with the permission from American Chemical Society.

Table 2
Summary of example nanosensors for arthritic biomarker detection.

Types of nanosensors	Types of biomarkers	Range and limit of detection	Ref.
Polyaniline-gold nanocomposite	Anti-cyclic citrullinated peptide antibody (anti-CCP)	The range of detection was 0.001 ng/ml to 15 ng/ml with a detection limit of 0.2 pg/ml	[80]
Au@Ag nanoparticles	Human IgM	The range of detection was 0.1 ng/ml to 10 μg/ml with a detection limit of 0.1 ng/ml	[81]
Gold nanoparticles	IgM rheumatoid factor (RF)	The range of detection was 1.6 IU/ml to 41.5 IU/ml with a detection limit of 4.15 IU/ml (clinical threshold is 20 IU/ml)	[82]
Gold nanoparticles	A disintegrin and metalloproteinase with thrombospondin motif-4 (ADAMTS-4)	The range of detection was 3.9 pM–250 pM with a detection limit of 1.1 pM	[83]
Gold nanoparticles	Anti-interleukin-1β antibody	The range of detection was 0.05 ng/ml to 10 ng/ml with a detection limit of 21 pg/ml	[84]
Organic–inorganic hybrid nanostructures	Anti-CCP and RF IgM	Multiplexing of anti-CCP and RF IgM was achieved in low concentration ranges, and their detection limits were 0.68 IU/ml and 0.93 IU/ml, respectively	[85]
Graphene	Anti-CCP	The range of detection was 1 fg/ml to 1 μg/ml with a detection limit of 10 fg/ml	[36]

fluorescence and determined the therapeutic effect of $_{L}$-NMMA (a NO inhibitor) and Andro (an anti-inflammatory agent) in a rat OA model. The novel NO biosensor paves the way for predicting the development of OA and therapeutic evaluation.

Recently, organic–inorganic hybrid nanostructures have been widely applied in biological sensing owing to their attractive structural property relationship [88]. Hwang et al. synthesized bimetallic nanoparticle clusters consisting of an Au core and Ag shell and subsequently conjugated them with poly (aniline) to form compartmentalized bimetal cluster-poly (aniline) hybrid nanostructures (CBCPHNs) for the identification of autoantibodies against RA (Fig. 9B) [85]. Anti-CCP and RF IgM were simultaneously detected with a detection limit of 0.68 IU/ml and 0.93 IU/ml, respectively. The CBCPHN biosensor provides potential for the early diagnosis of RA in clinical samples.

2.2.3. Other nanomaterials

Graphene is an allotrope of two-dimensional carbon with high sensitivity, rapid response time and ease-of-operation properties [89]. Based on amine-functionalized graphene (afG) and anti-cyclic citrullinated peptide (anti-CCP) antibody, Islam et al. designed a smart nanosensor for the detection of RA in human fluids [36]. Biosensing was performed by adding specific antigens to the functionalized graphene (Fig. 9C). The nanosensor exhibited high sensitivity and quick response to the specific CCP antigen with a detection limit of 10 fg/ml under optimized conditions. Thus, this probe may be useful for rapid one-site arthritis biomarker detection in clinical samples.

Hyaluronic acid (HA) exerts a critical role in joint lubrication and inflammation. The size distribution and relative abundance of HA in human fluids are considered predictors of the progression of numerous diseases [90]. Rivas et al. synthesized solid-state (SS-) nanopores for the quantitative assessment of HA derived from equine synovial fluids of OA knees [91]. The nanosensor was able to determine the size distribution of as little as 10 ng HA in synovial fluid. In addition, the sensitivity, speed, and small sample volume requirements of this platform provides potential for the quantitative analysis of biochemical markers and further clinical translational applications.

3. Nanomaterials for bone-related disease therapy

Along with bioimaging and biosensor applications for diagnosis with more precision, faster response and higher biocompatibility, nanomaterials offer new insight into the effective prevention and therapy of bone-related diseases [92]. First, nanomaterials provide a new theranostic platform for drug delivery with sufficient retention time and enough systemic concentration at targeted sites, thus achieving the desired pharmacological effect [93]. Moreover, the small size of nanomaterials enables them to enter cells, indicating the potential for intracellular deoxyribonucleic acid (DNA) or small interfering ribonucleic acid (siRNA) delivery, RNA detection and cellular modulation [94]. Additionally, multiple functions can be purposely integrated into nanomaterials, such as photothermal, controlled release, immune system regulation and antioxidation functions, to improve therapeutic effects. Furthermore, the surface nano-topography of the scaffolds is a key factor for cell adhesion, proliferation and differentiation, thus can be tuned for bone tissue regeneration [95]. Finally, some nanomaterials exhibit admirable biocompatibility with reduced adverse effects for medical applications [96]. In this section, recent advances in nanomaterials for the treatment of various bone-related diseases are summarized.

3.1. Nanomaterials in osteoarthritis

3.1.1. Nanomaterials as chondroprotective drug carriers

Nanomaterials are attractive therapeutic tools for osteoarthritis, in view of their outstanding targeted delivery, biocompatibility and sustained release properties (Table 3). Nanocrystal-polymer particles (NNPs) have been adopted as potential carriers for drug delivery, providing a hydrophilic surface and additional bioconjugation capability. Maudens et al. fabricated NNPs with encapsulated KGN (KGN-NNPs) for the treatment of OA (Fig. 10A) [97]. Kartogenin (KGN) serves as a CBFβ-RUNX1 pathway activator to promote chondrogenesis and cartilage protection. The KGN-NPPs exhibited a high drug loading efficiency of 31.5 wt% and a prolonged drug release efficiency of 62% after 3 months. Moreover, this delivery system protected KGN from being eliminated by intra-articular (IA) clearance. The protective effect of KGN-NPPs on cartilage was attributed to the decreased expression of VEGF and Adamts5. Similarly, Fan et al. synthesized polyurethane nanoparticles (PN) embedded KGN through covalent amide bonds between the amine group of PN and the carboxyl group of KGN (PN-KGN) (Fig. 10B) [98]. PN-KGN attenuated cartilage degeneration with less matrix loss and vertical fissures at 12 weeks in the rat OA model, which was established by anterior cruciate ligament transection (ACLT) and medial menisci resection. These novel approaches showed long-term cartilage protection effect for OA treatment.

Chitosan has been widely investigated for drug carriers owing to its polycationic characteristics, good solubility, functionalization and biodegradability. KGN coated with chitosan NPs using EDC/NHS catalysis methods (CHI-KGN) showed a distinct inhibitory effect on cartilage degeneration (Fig. 10C) [111]. CHI-KGN yielded a sustained release in the knee joint for 7 weeks after IA injection. In addition, berberine chloride (BBR) is an isoquinoline alkaloid that serves as a therapeutic agent for ameliorating OA [112]. Zhou et al. fabricated berberine-loaded chitosan NPs (BBR-loaded CNs) using the ionic cross-linking method along with good stability and sustained release properties (Fig. 10D) [113]. The BBR-loaded CNs possessed high

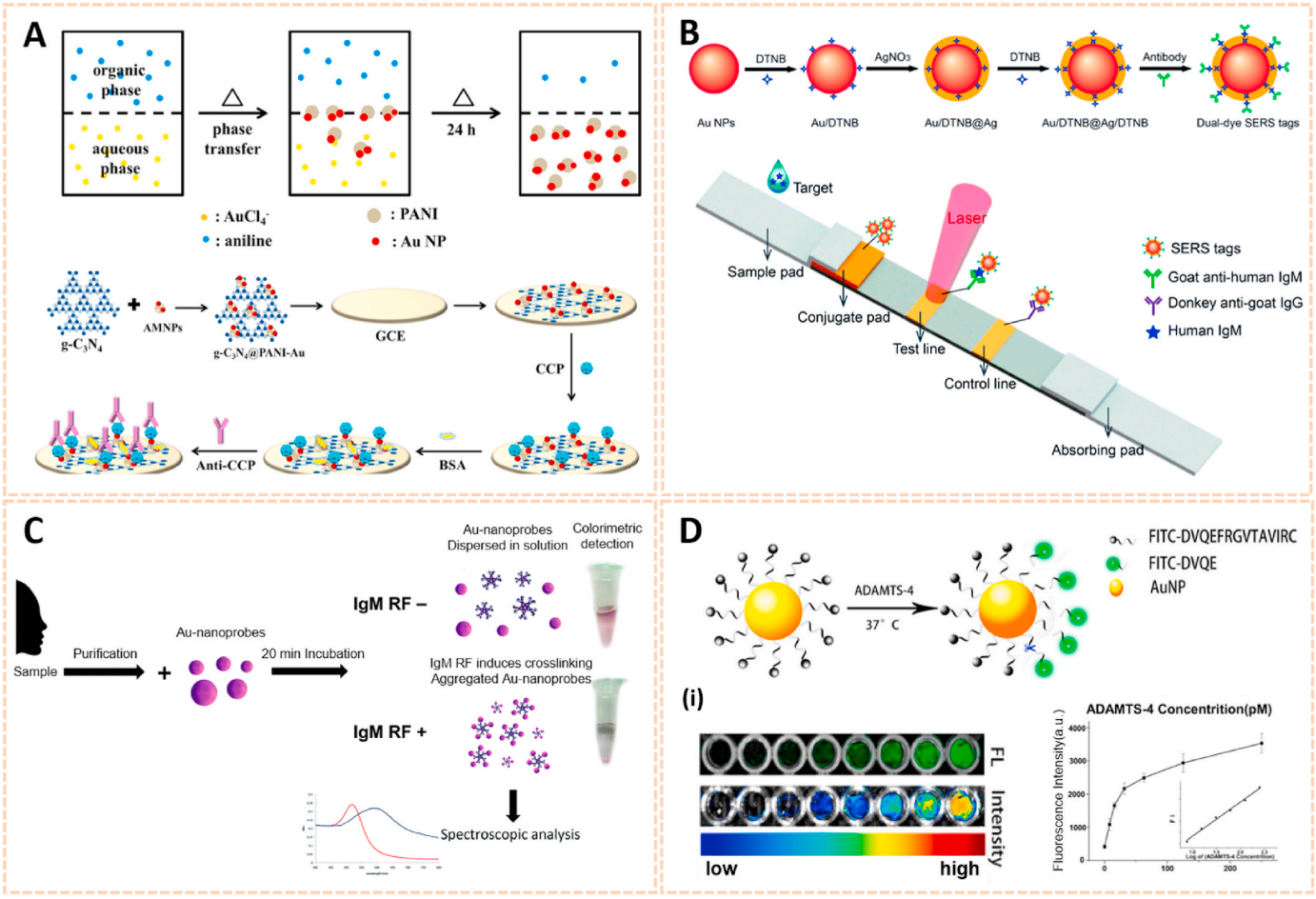

Fig. 8. Gold nanomaterials for biomarkers detection in human biofluids. A) The preparation method of PANI-Au asymmetric composites and the fabrication process of the ECL immunosensor [80]. The image reproduced with the permission from Elsevier B.V. B) Synthetic route for dual dye-loaded SERS tags and schematic illustration of quantitative detection of human IgM using SERS-based lateral flow immunoassay [81]. The images reproduced with the permission from The Royal Society of Chemistry. C) Schematic representation of the Au-nanoprobe detection of the early RA biomarker-IgM RF, whose colorimetric output provides for the readout. On the right: actual photos of real detection samples to illustrate color discrimination by the naked eye [82]. The image reproduced with the permission from The Royal Society of Chemistry. D) Illustration of ADAMTS-4 detective fluorescent turn-on peptide-conjugated AuNP probe (ADAMTS-4-D-Au probe) for the Detection of ADAMTS-4. (i) Fluorescence images and intensity of the ADAMTS-4-D-Au probe in the presence of various concentrations of ADAMTS-4 to test sensitivity [83]. The images reproduced with the permission from American Chemical Society.

anti-apoptosis effects by decreasing the expression of Bax and caspase-3 and increasing the level of Bcl-2. Oral delivery is the most convenient and common route for drug administration, however, gastrointestinal (GI) clearance can suppress the pharmacological efficacy of drugs [114]. To overcome this biological barrier, Samarasinghe et al. designed alginate-enclosed chitosan-calcium phosphate nanocarriers (AEC-CP-NCs) encapsulating iron-saturated bovine lactoferrin (Fe-bLf) as a drug oral delivery system for attenuating the progression of OA (Fig. 10E) [115]. Fe-bLf is a protein with anti-inflammatory and anti-oxidative properties [116]. The AEC-CP-Fe-bLf-NCs significantly inhibited joint inflammation and decreased the level of catabolic genes, suggesting that the nanocarriers promoted the therapeutic efficacy of drugs for cartilage protection and effective OA treatment via oral administration.

Polymer conjugation with therapeutically relevant proteins is broadly used to enhance pharmacological effects. For instance, attaching PEG to proteins is termed PEGylation. McMasters et al. synthesized hollow PEGylated poly (N-isopropylacrylamide) (pNIPAM) nanoparticles modified with the 23-mer cell-penetrating anti-inflammatory peptide KAFAK, which modulated pro-inflammatory cytokines by inhibiting mitogen-activated protein kinase-activated protein kinase 2 (MK2) [117]. The PEGylated pNIPAM nanoparticles exhibited a continuous inhibitory effect on inflammation and suppressed the expression of IL-6 in bovine cartilage explants over 8 days, indicating a promising platform for the delivery of therapeutics.

Triblock copolymers are gaining attention in drug delivery systems due to their modulated release kinetics, high loading efficiency and biocompatible properties [118]. Poly (lactic-*co*-glycolic acid)-polyethyleneglycol-poly (lactic-*co*-glycolic acid) (PLGA--PEG-PLGA) triblock copolymeric NPs were used as drug carriers to deliver etoricoxib, a cyclooxygenase-2 (COX-2) selective inhibitor, into joints for pharmacological therapy of OA [100]. The etoricoxib-loaded PLGA-PEG-PLGA NPs attenuated cartilage destruction by down-regulating the expression of MMP-13 and Adamts-5. The triblock copolymeric NPs exhibited sustained drug release for up to 28 days *in vitro*. To slow down hydrolysis and thus increase release times, the PLGA block could be replaced by poly (ε-caprolactone-*co*-lactide) (PCLA) blocks [119]. Petit et al. developed an acetyl-capped PCLA-PEG-PCLA triblock copolymer loaded with celecoxib to yield temperature-responsive gelling systems for drug delivery with sustained intra-articular release (Fig. 11A) [120]. Celecoxib is a selective NSAID COX-2 inhibitor. The gel systems were typical free flowing sols at room temperature and gels at 37 °C. The thermogels showed a sustained release of celecoxib for 4–8 weeks in the knee joints of healthy rats,

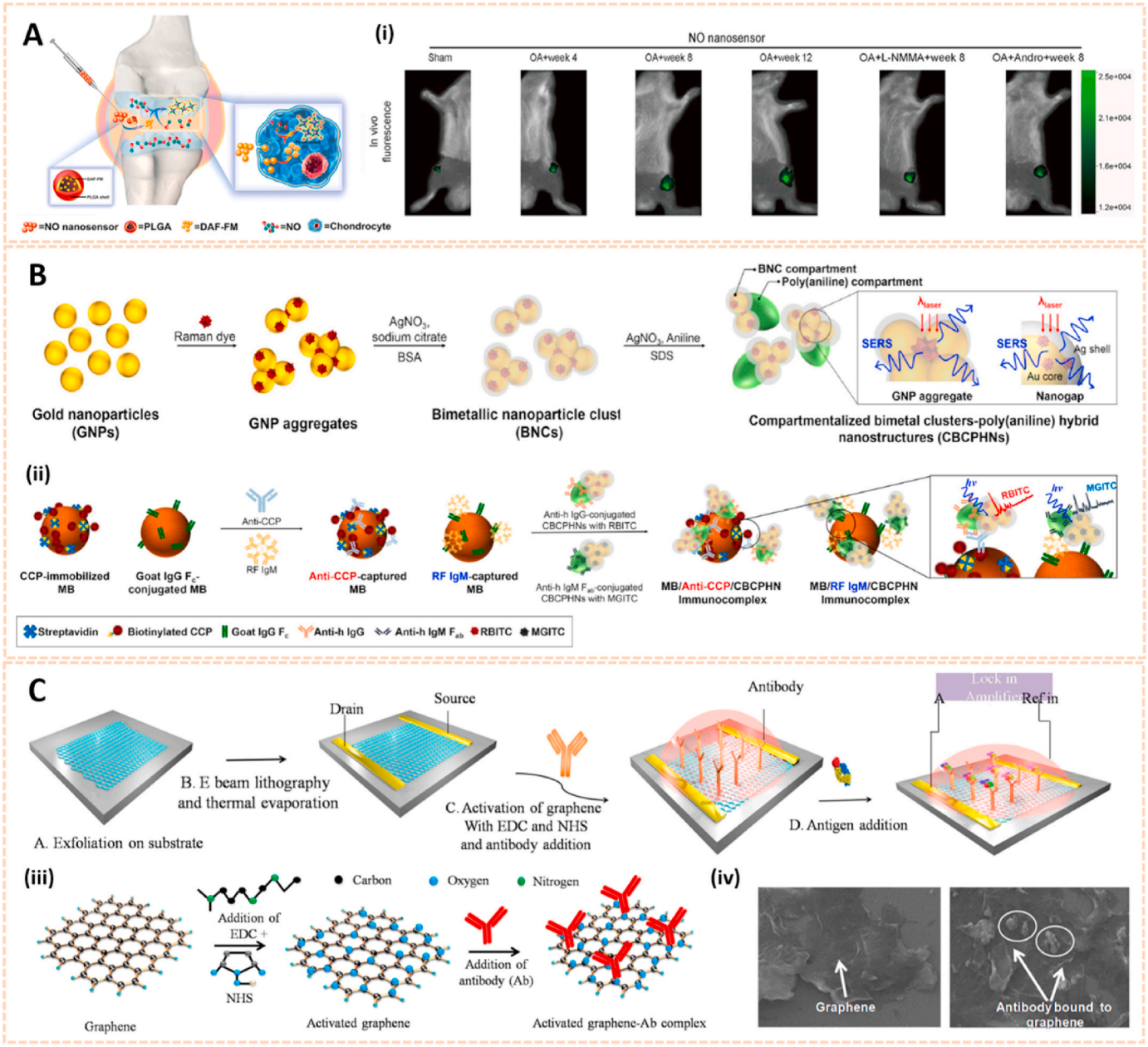

Fig. 9. Organic and graphene-based nanomaterials for biomarkers detection in human biofluids. A) Schematic illustration of NO nanosensors application for predicting OA development. (i) Tracking the NO secretion in the joints of OA animals with NO nanosensors [87]. The images reproduced with the permission from American Chemical Society. B) A scheme for preparation of CBCPHNs. (ii) Schematic illustrations of SERS-based multiplexing using CBCPHNs and MBs for two autoantibodies, anti-CCP, and RF IgM detection [85]. The images reproduced with the permission from Elsevier B.V. C) Fabrication of the graphene immunosensor. (iii) Activation procedure for antibody (Ab) conjugation to the graphene nanomaterial using the carbodiimide method. (iv) Scanning electron microscopy (SEM) analysis of the surface morphology of graphene and graphene-antibody bioconjugate [36]. The images reproduced with the permission from Elsevier B·V.

indicating a promising drug delivery system for the management of OA following subcutaneous administration.

Polyamidoamine (PAMAM) dendrimers are promising cargos for penetrating anionic cartilage tissue to target cells due to their small size, tunable surface charge, scalable synthesis, robust characterization, and flexibility properties. Geiger et al. fabricated PEGylated PAMAM dendrimers conjugated with insulin-like growth factor 1 (IGF-1) for cartilage protection [121]. The modified dendrimer increased IGF-1 retention in rat knee joints by 10-fold for up to 30 days and penetrated human-thickness cartilage at least 1 mm. Moreover, dendrimer-IGF-1 reduced the width of medial tibial cartilage degeneration by 60% and the volume of osteophytes in the joint by 80% relative to untreated rats at 1 month postoperatively (Fig. 11B). This novel nanocarrier paves the way for enhancing the therapeutic efficacy of drugs and subsequently accelerating the development of disease-modifying OA drugs.

3.1.2. Nanomaterials for gene therapy toward synoviocytes and chondrocytes

Nanomaterial-based gene delivery systems open novel perspectives for therapeutic approaches to OA by transferring exogenous nucleic acids into cells to alter protein expression profiles [122]. However, the clinical application of siRNA is severely limited by its low delivery efficiency. The siRNA cannot readily enter the cell owing to its high molecular weight, hydrophilicity and negative charge. Moreover, siRNA is highly unstable in the systemic circulation with a short half-life due to serum nucleases. Therefore, safer and more efficient delivery systems

Table 3
Summary of example nanomaterials for osteoarthritis.

Category	Nanomaterials	Active principle	Main results	Ref.
Drug carriers	Nanocrystal-polymer particles	PH-797804	• drug loading of ~31.5% (w/w) • good retention in the joint and adjacent tissues for up to 2 months • improve inflammation and joint degradation	[99]
	PLGA-PEG-PLGA triblock copolymeric nanoparticles	Etoricoxib	• sustained drug release over 28 days *in vitro* • decrease expression of COX-2, PGE2 and NO • inhibit expression of MMP13 and Adamts-5	[100]
	Solid lipid nanoparticles	Diacerein, polysaccharide chondroitin sulfate	• extended release up to 16 h • increase bioavailability of diacerein by 2.8 times	[101]
	Solid lipid nanoparticles	Aceclofenac, chondroitin sulfate	• sustained drug release over 24 h *in vitro* • enhanced accumulation at the knee joint due to specific interactions between CS and CD44/annexin/leptin receptors	[102]
Gene therapy	Copolymer self-assembling nanoparticles	IL-1 receptor antagonist	• bound specifically to target synoviocyte cells via surface IL-1 receptors • increase the retention time of IL-1Ra in vivo over 14 days with enhanced IL-1Ra half-life	[103]
	Polyethylenimine nanoparticles	Chondrocyte-affinity peptide, Hif-2α siRNA	• promote the local concentration and prolong the retention time of siRNA in the cartilage • decrease levels of Hif-2α, MMP13 and IL-1β	[104]
	Self-assembling peptidic nanoparticles	NF-κB p65 siRNA	• persisted therapeutic effect up to 3 weeks • attenuate chondrocyte apoptosis via inhibited IL-1β-induced p65 activity	[105]
Scaffolds for cartilage regeneration	PLGA, nano-sized calcium-deficient hydroxyapatite (nCDHA)	PLGA, nCDHA, arginine-glycine-aspartate, alginate	• provide the dimensional stability of the whole construct and a 3D environment for the chondrogenesis of hPMSCs	[106]
	PLGA layer	Ti, PLGA	• promote cartilage regeneration by promoting subchondral bone regeneration • provide mechanical support platform for cartilage	[107]
	Electrospun PDLA/PCL nanofibers	PDLA/PCL, chitosan	• increase expression of collagen type II and proteoglycans	[108]
	PLLA/silk fibroin nanofibers	PLLA/silk fibroin	• better hydrophilicity • support chondrocytes adhesion, proliferation and secretion of cartilage-specific ECM	[109]
	Hybrid peptide nanofibers	K-PA, hyaluronic acid	• present a tear-resistant scaffold • maintain cartilage-specific matrix proteins and preserve cartilage morphology	[110]

are vital for the clinical application of siRNA (Table 3). Chitosan (CS) is a well-known biodegradable polysaccharide used as a vector for gene therapy. Based on a hybrid hyaluronic acid (HA)/CS plasmid DNA strategy, Deng et al. designed HA/CS NPs conjugated with plasmid-DNA encoding IL-1Ra to form HA/CS/pIL-1Ra NPs to alleviate inflammation in synoviocytes [123]. The HA/CS/pIL-1Ra NPs exhibited protective effects on synovitis by decreasing the expression of MMP3, MMP13, COX-2 and iNOS with sustained release over 15 days. Similarly, Zhou et al. developed CS/HA NPs containing plasmid DNA encoding cytokine response modifier A (CrmA), a serpin-like protease inhibitor, to form HA/CS-CrmA NPs for cartilage protection in a rat OA model [124]. The HA/CS-CrmA NPs successfully transfected synoviocytes with a sustained release of plasmid DNA for more than 21 days. Moreover, these NPs possessed chondroprotective effects on cartilages and synovial tissues by dramatically inhibiting IL-1β generation.

Apart from plasmid DNA, RNA interference therapy has recently become popular for the treatment of OA by gene silencing. Chen et al. fabricated a photothermal-triggered nitric oxide nanogenerator loaded with Notch1-siRNA to form NO-Hb@siRNA@PLGA-PEG (NHsPP) for the precise therapy of OA by synergistic NO, siRNA and PTT treatment [125]. This combination therapy inhibited the expression of pro-inflammatory cytokines and the macrophage response, thus protecting cartilage from destruction (Fig. 12A). Additionally, hypoxia-inducible factor-2α (Hif-2α) siRNA transfection was conducted by chondrocyte-affinity peptide-polyethylenimine (CAP-PEI) nanoparticles to attenuate cartilage degeneration in an OA model [104]. This NP-mediated Hif-2α siRNA reduced the expression of catabolic factors with prolonged retention duration of siRNA in the cartilage and subsequently sustained cartilage integrity and attenuated synovial inflammation. Lipid nanoparticle (LNP) is a novel cartilage therapeutic tool for siRNA delivery owing to a small diameter and high encapsulation efficiency. Lipid-based NP combined with Indian Hedgehog (Ihh) siRNA was designed as a therapeutic strategy for ameliorating cartilage degeneration [126]. As we known, Ihh is correlated with OA progression in humans. This LNP-Ihh siRNA enabled cartilage penetration and exerted chondroprotective effects in a rat OA model by knocking down specific genes.

Carbon-based nanomaterials are one of the most widely used vectors for gene delivery due to their unique properties, including biosafety, flexibility, ease of formulation and high delivery efficiency. Carbon dots conjugated with sulfosuccinimidyl-4-(N-maleimidomethyl) cyclohexane-1-carboxylate (CD-SMCC) were developed as nanocarriers for transferring TNF-α siRNA to promote chondrogenesis of mesenchymal stem cells (Fig. 12B) [38]. CD-SMCC-siTnfα enhanced cartilage regeneration by suppressing inflammation, indicating a potential stem cell-based gene therapy for cartilage defects. In addition, Sacchetti et al. fabricated single-walled carbon nanotubes (SWCNTs) conjugated with polyethylene glycol (PEG) chains (PEG-SWCNTs) as an intra-articular gene delivery system for chondrocytes (Fig. 12C) [127]. The PEG-SWCNTs were capable of penetrating cartilage and transferring gene inhibitors into the chondrocytes of OA mice with a prolonged duration in the knee joint, suggesting as a novel nanovector for intra-articular gene delivery and therapy of OA.

3.1.3. Nanomaterial-based scaffolds for cartilage regeneration

Nanostructured scaffold is a novel therapeutic approach for cartilage tissue regeneration with favorable biocompatibility, controllable degradation rate, suitable pore size and porosity and appropriate mechanical properties [128]. Scaffolds are primarily manufactured using different polymers, such as poly (lactic-*co*-glycolic acid) (PLGA), poly (L-lactide) (PLLA) and poly (ε-caprolactone) (PCL), combined with functional groups by electrospinning, phase separation and self-assembly to facilitate cartilage repair (Table 3).

Electrospun nanofiber-based scaffolds have been broadly used in

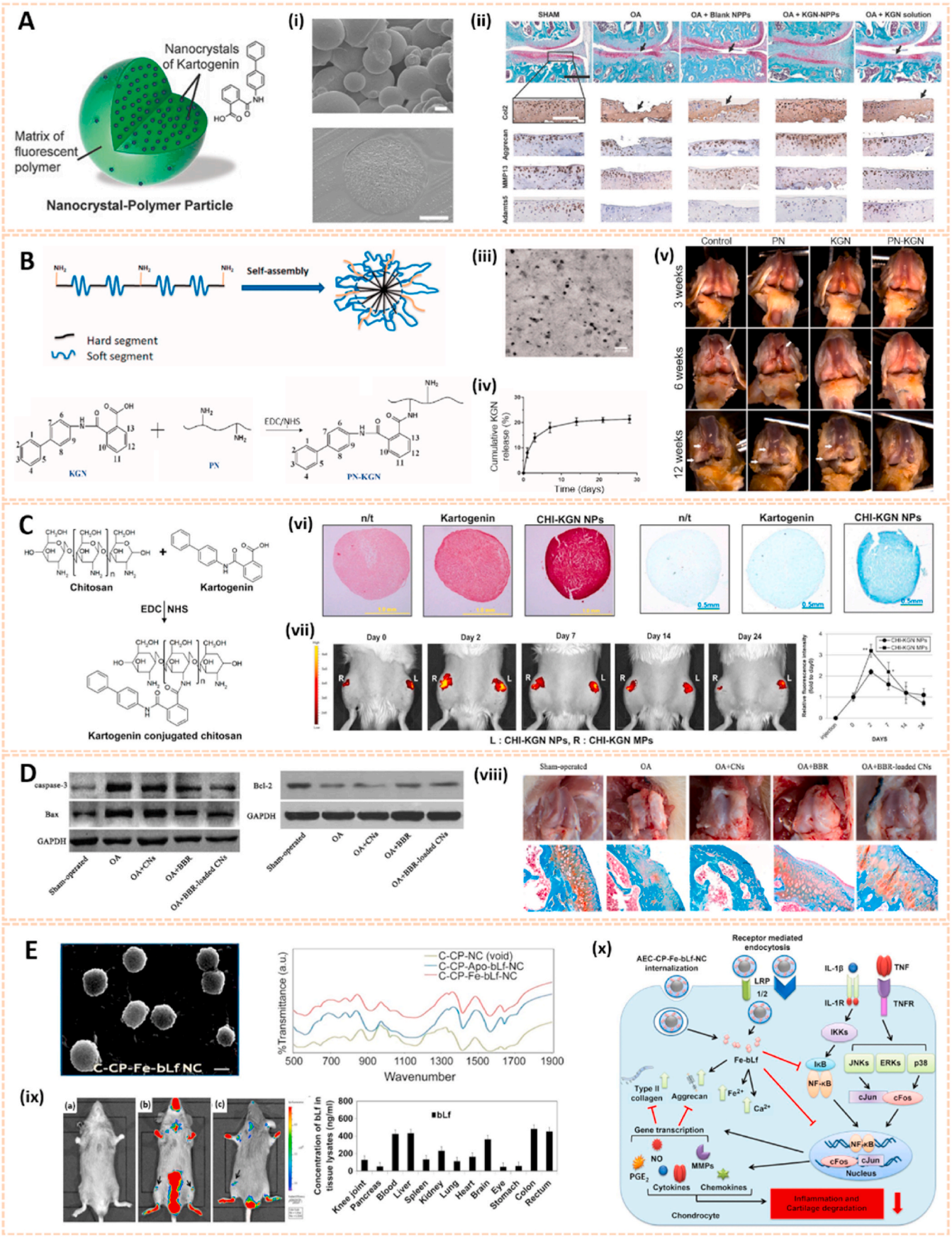

(caption on next page)

Fig. 10. Nanocrystal-polymer and chitosan-based nanocarriers for osteoarthritis therapy. A) Schematic representation of a KGN-NPP. (i) SEM of surface and core of KGN-NPPs. (ii) Representative safranin-O/fast green and IHC showing the medial side of the knee of mice at day 56. Femur (above), tibia (below). Arrows indicate cartilage erosion. Scale bar = 200 μm [97]. The images reproduced with the permission from WILEY-VCH. B) Illustration of the procedures to synthesize PN-KGN. (iii) TEM of PN-KGN. (iv) In vitro release of KGN from PN-KGN at 37 °C. (v) Macroscopic views of OA development at 3, 6, and 12 weeks after OA induction. Arrows indicate the locations of cartilage degeneration (n = 6 per group) [98]. The images reproduced with the permission from Taylor & Francis. C). Proposed reaction scheme of CHI-KGN conjugate. (vi) Safranin-O and Alcian-blue staining on day 21. (vii) In vivo fluorescence imaging and relative intensity using fluorescence dye-labeled CHI-KGN NPs (left knee) and CHI-KGN MPs (right knee) at various time points from rats in which OA was induced surgically 6 weeks before [111]. The images reproduced with the permission from Elsevier Ltd. D) Effects of BBR-loaded CNs on protein expressions of caspase-3, Bcl-2 and Bax in rat articular cartilage from each experimental group. (viii) Effect of BBR-loaded CNs on histological changes in articular cartilage of the rat ACLT + MMx model [113]. The images reproduced with the permission from Elsevier B.V. E) SEM of C-CP-Fe-bLf-NCs and chemical bonding analysed using FTIR analysis. (ix) Fluorescence and biodistribution of arthritic mice treated with (a) control diet and (b&c) Cy5.5 dye labeled AEC-CP-Fe-bLf-NC diet were fed orally 36 h prior to being euthanized and imaged. Arrows show the localization of NC in joint cartilage. (x) Schematic diagram illustrating the signaling mechanism modulated by AEC-CP-Fe-bLf-NCs in arthritis [115]. The images reproduced with the permission from Elsevier Ltd.

cartilage regeneration. Poly (D,L-lactide-*co*-glycolide) beads were electrospun into nonwoven fibers as PLGA nanofiber scaffolds to induce human mesenchymal stem cells differentiated into chondrogenic cells [129]. Chen et al. synthesized a modified 3D scaffold based on gelatin/PLA nanofibers and hyaluronic acid (HA) for cartilage tissue engineering (Fig. 13A) [130]. The preparation process of this 3D nanofibrous scaffold could be generally divided into three steps: (1) electrospinning, (2) freeze-drying and (3) cross-linking. Cross-linking of the scaffold was necessary for the formation of a stable and interconnected networks. This 3D scaffold exhibited hierarchical cellular structure and superabsorbent properties. In addition, the scaffold could bear a compressive strain as high as 60% and recovered its original shape after the stress released in the wet state. Moreover, the modified 3D scaffold enhanced the growth and proliferation of chondrocytes for cartilage tissue engineering. Additionally, Li et al. designed 3D biomimetic scaffolds containing electrospun gelatin-polycaprolactone nanofibers and DCECM (NF/DCECM) with good biocompatibility for chondrocyte proliferation (Fig. 13B) [131]. The NF/DCECM scaffolds exhibited strong mechanical properties and wet stability. Moreover, the electrospun nanofiber-based scaffold significantly facilitated early maturation of the cartilage lacuna and the secretion of collagen and glycosaminoglycan, indicating a promising tissue engineering scaffold for cartilage regeneration and cartilage defect repair.

Apart from electrospun nanofiber-based scaffolds, hydrogel scaffolds have also been applied for the treatment of OA owing to their injectability, adhesivity and chondrogenic properties. An alginate/poly (vinyl alcohol) (PVA) semi-interpenetrating network hydrogel scaffold construct with chondroitin sulfate nanoparticles (Chs-NPs) and nanohydroxyapatite (nHA) was fabricated with gradient interface to mimic the superficial cartilage and deep calcified layers [132]. The injectability and in situ sol–gel transformation ability of scaffold ensured integration of administered construct with irregular cartilage defects and enhanced mineralized subchondral bone regeneration and superficial hyaline cartilage in the corresponding zone of osteochondral tissue. In addition, Shi et al. developed an ultraviolet-response cross-linked HA hydrogel scaffold with kartogenin-encapsulated PLGA NPs using an innovative one-step technology for cartilage regeneration (Fig. 13C) [133]. The biodegradable scaffolds enabled the recruitment of marrow-derived and synovium-derived mesenchymal stem cells for chondrogenesis, suggesting a great potential for clinical translation.

Carbon-based nanomaterials such as carbon nanotube and graphene oxide scaffolds have also been developed in cartilage tissue engineering. Single-wall carbon nanotube (SWNT) nanocomposite scaffolds have been synthesized to enhance chondrogenic ability [134]. The –COOH surface of SWNTs regulated chondrocyte metabolic activity by increasing the expression of Col2a1 and fibronectin. Following a similar strategy, pristine carbon nanotube scaffolds have been used for chondrocyte growth [135]. In addition, graphene oxide (GO) nanosheets incorporated with photopolymerizable poly-D, l-lactic acid/polyethylene glycol (PDLLA) and transforming growth factor-β (TGF-β) were used as localized delivery scaffolds for cartilage tissue regeneration [136]. The TGF-β3-GO/PDLLA scaffolds promoted chondrogenic differentiation of hMSCs with a sustained release of TGF-β3 for more than 1 month, indicating a potential strategy for treating OA.

3.2. Nanomaterials in rheumatoid arthritis

3.2.1. Nanomaterials as passive targeting drug carriers

The main pathological characteristics of RA are enhanced vascular permeability and macrophage infiltration, which are similar to the mechanisms of tumors. Based on this, a passive targeting strategy for RA aims to increase the permeability and retention effect of nanocarriers to selectively accumulate and release drugs in the synovium [137]. A variety of nanomaterials, such as polymers, liposomes, metal NPs and quantum dots, could serve as nanocarriers for anti-rheumatoid arthritis drugs (Table 4).

Polymer nanomaterials have been broadly used as targeting drug carriers against RA with good biocompatibility, biodegradability, synthetic flexibility and appropriate mechanical properties [164–166]. Amphipathic poly (ethylene glycol)-block-poly (ε-caprolactone) (PCL-PEG) polymer micelles loaded with low-dose dexamethasone (Dex) were designed for targeted delivery to inflamed joints of rats with RA (Fig. 14A) [167]. The Dex-PCL-PEG micelles significantly attenuated joint swelling and bone destruction, and inhibited the expression of inflammatory cytokines. Qindeel et al. fabricated a polycaprolactone-polyethylene glycol-polycaprolactone (PCL-PEG-PCL) triblock copolymer as a nanocarrier for the targeted delivery of methotrexate (MTX)-loaded nanomicelles (NMs) against RA (Fig. 14B) [138]. The MTX-NMs possessed an encapsulation efficiency of 91% and were loaded into a carbopol 934-based hydrogel with eucalyptus oil for transdermal delivery. MTX-NMs obviously accumulated in the inflamed joints and thus improved the pharmacokinetics, oxidation protection and behavioral responses. In addition, Aloga et al. developed bioinspired reconstituted high-density lipoprotein (rHDL) NPs loaded with xylopic acid (XA), a diterpene kaurene with anti-inflammatory and analgesic properties, for the treatment of RA (Fig. 14C) [168]. The rHDL/XA passively aggregated in inflamed joints and subsequently inhibited mononuclear cell infiltration and joint progression via the amino acid and lipid metabolism pathways. The rHDL/XA nanoformulation provides a potential for RA therapy.

Liposomes serve as an effective delivery system composed of double lipid layers surrounding an aqueous core, which possess good biological, physical and chemical properties for the treatment of RA [169,170]. The polymerized stealth liposomes were developed by bis(10,12-tricosadiynoyl)-*sn*-glycero-3-phosphocholine ($DC_{8,9}PC$) and 1,2-distearoylsn-*glycero*-3-phospho-ethanolamine-poly (ethyleneglycol) ($DSPE\text{-}PEG_{2000}$) as a vehicle for Dex delivery against RA (Fig. 14D) [171]. The polymerized stealth liposomes selectively aggregated in the inflamed joints after intravenous administration and inhibited proinflammatory cytokine expression, thus attenuating swelling and bone erosion of inflamed joints. Additionally, iRGD peptide-functionalized echogenic liposomes (iELPs) loaded with MTX and indocyanine green (ICG) fluorescent probes were synthesized using a thin film-hydration method (Fig. 14E) [172]. The iELPs provide a nanoplatform for NIR

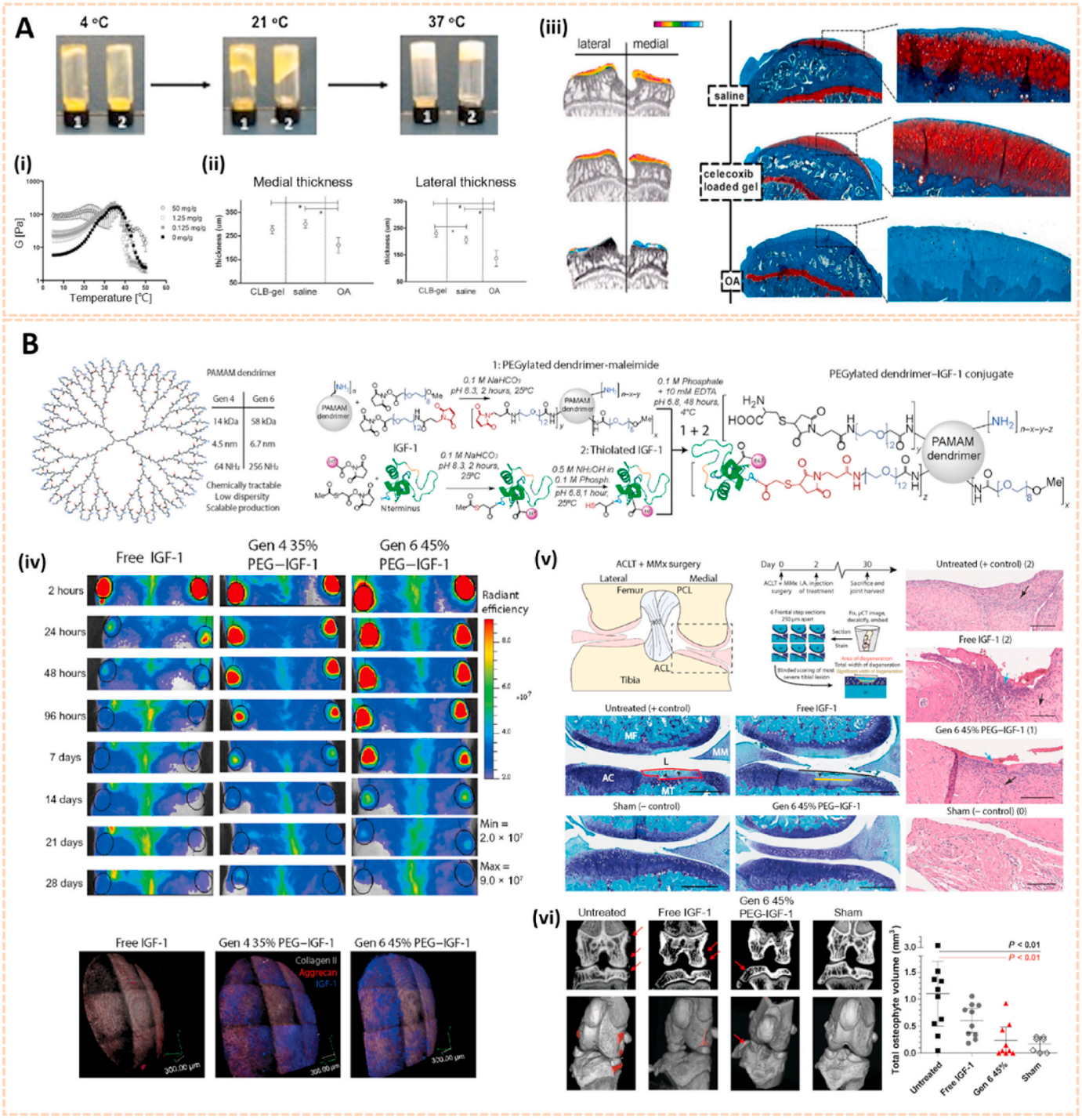

Fig. 11. Lipid, triblock copolymers and dendrimer-based nanocarriers for osteoarthritis therapy. A) Phase behavior of celecoxib-loaded PCLA-PEG-PCLA systems of 25% wt in PBS buffer pH 7.4. (i) Temperature-dependent storage modulus G′ of systems containing different celecoxib loadings (n = 3). (ii) Thickness of both the medial and lateral tibial plateau of the different groups. (iii) EPIC-μCT and Saf-O images of the three different groups [120]. The images reproduced with the permission from Elsevier Ltd. B) Design and synthesis of bioactive PEGylated dendrimer–IGF-1 conjugates as cartilage penetrating nanocarriers. (iv) PEGylated dendrimer nanocarriers extend joint residence and cartilage penetration of IGF-1 in rats. (v) Dendrimer-IGF-1 conjugate reduces cartilage degeneration 4 weeks after surgical traumatic joint injury. (vi) Dendrimer-IGF-1 conjugate reduces osteophyte burden in surgically injured rats 4 weeks after surgery [121]. The images reproduced with the permission from American Association for the Advancement of Science.

imaging and ultrasound-mediated therapy against RA by upregulating the expression of αvβ3 integrin. In addition, Ren et al. fabricated liposomes conjugated with varying amounts of PEG of different chain lengths using lipid film dispersion and extrusion for the treatment of RA (Fig. 14F) [37]. Of these, liposomes with 100 nm diameter and 10 wt% incorporation of 5 kDa PEG exhibited longer circulation time and high affinity to inflamed joints. The liposome-based nanocarrier ameliorated the progression of RA by enhancing the phagocytic abilities of synovial fibroblasts and macrophages, suggesting a potential passive targeting therapy against RA.

Metal nanomaterials are increasingly used as delivery platforms for the treatment of RA owing to their unique mechanical, chemical and

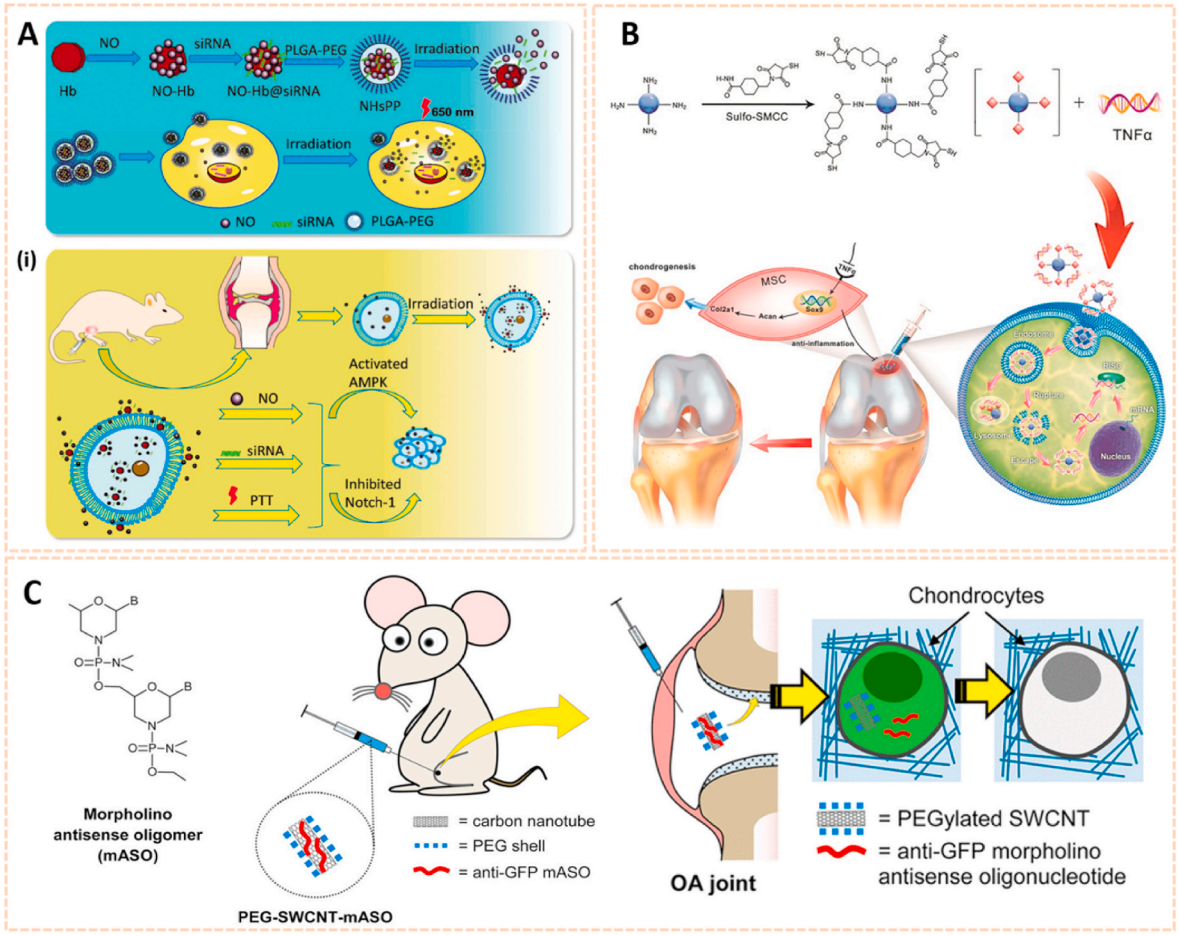

Fig. 12. Nanomaterials for gene therapy of OA. A) Assembly process for NHsPP nanoparticles with a photothermal response. (i) The process of NHsPP nanoparticles inhibiting the macrophage inflammatory response after being triggered by the photothermal effect [125]. The images reproduced with the permission from The Royal Society of Chemistry. B) Schematic illustration of the formation of carbon dot (CD)-succinimidyl-4-(N-maleimidomethyl) cyclohexane-1-carboxylate-silenced TNFα complexes and the CD-based nanocarrier for gene delivery and real-time monitoring of cellular trafficking *in vitro* and in vivo for enhancing cartilage repair [38]. The image reproduced with the permission from Oxford University Press. C) Scheme of PEG-SWCNTs as Chondrocyte-Specific Drug Delivery Systems [127]. The images reproduced with the permission from American Chemical Society.

physical features [173,174]. Kim et al. fabricated manganese ferrite/-ceria nanoparticle-anchored mesoporous silica nanoparticles (MFC-MSNs) loaded with MTX for RA therapy by scavenging ROS and generating O_2 (Fig. 15A) [175]. The MFC-MSNs attenuated the pathological features of the inflamed joints by inducing polarization of M1 to M2 macrophages. Similarly, triamcinolone-gold nanoparticles (Tri-am-AuNPs) were designed for targeted RA therapy through M1 macrophage apoptosis and M2 macrophage polarization (Fig. 15B) [141]. Additionally, hyaluronate-gold NPs loaded with tocilizumab (HA-AuNPs/TCZ) were synthesized for the treatment of RA by targeted binding to VEGF and IL-6R (Fig. 15C) [176]. In addition, Lima et al. developed gold nanoparticles (AuNPs) conjugated with liposomes and anti-IL-23 Abs for IL-23 capture and neutralization, thus inhibiting the production of IL-17A cytokine and articular destruction in RA (Fig. 15D) [177]. Therefore, these metal nanomaterial-based innovative strategies present a great potential to revolutionize RA treatment.

For passive targeting, the prepared drug carrier complex circulates through the bloodstream. In this approach, the timing of release is crucial as the drug will not reach the target site and it dissociates from the carrier very quickly, compromising the bioactivity and efficacy. By contrast, for active targeting, moieties, such as antibodies and peptides are coupled with drug delivery system to anchor to the receptor structures expressed at the target site. The drugs intended for direct release at the target sites can achieve more efficient delivery. Therefore, active targeting drug delivery is a more promising direction in the future.

3.2.2. *Nanomaterials as active targeting drug carriers*

An active targeting strategy could further improve the precision of drug delivery and therapeutic efficacy of RA. Surface modification with specific ligands allows nanomedicine to target several receptors of RA-related cells, such as macrophages, endothelial cells and neutrophils (Table 4).

Macrophages are activated in the inflamed joints of RA, which overexpressed a variety of specific receptors such as scavenger receptors (SR), folate receptor (FR), CD44 receptors, galactose receptors, mannose receptors, vasoactive intestinal peptide (VIP) receptors, folic acid receptors and CRIg [178–180]. For instance, Gong et al. fabricated palmitic acid-modified bovine serum albumin nanoparticles (PAB NPs) loaded with the anti-inflammatory drug celastrol (CLT) targeted to scavenger receptor-A (SR-A) on activated macrophages for RA treatment (Fig. 16A) [181]. The CLT-PAB NPs possessed enhanced electronegativity and introduced PA for SR-A targeting effects, and showed superior therapeutic efficacy with a lower dose of CLT in adjuvant-induced arthritis rats. In addition, methotrexate-conjugated polymer hybrid micelles (M-PHMs) were synthesized using MTX-PEI-LA and mPEG-LA and subsequently loaded with microRNA-124 for RA therapy (Fig. 16B) [182]. M-PHMs/miR-124 selectively aggregated in inflamed joints of RA rats and suppressed inflammation by folate receptor-mediated endocytosis, thus protecting bone from destruction. Additionally, HA-modified metal-organic frameworks (MOFs) were developed to targeted delivery MTX for RA therapy (Fig. 16C) [183].

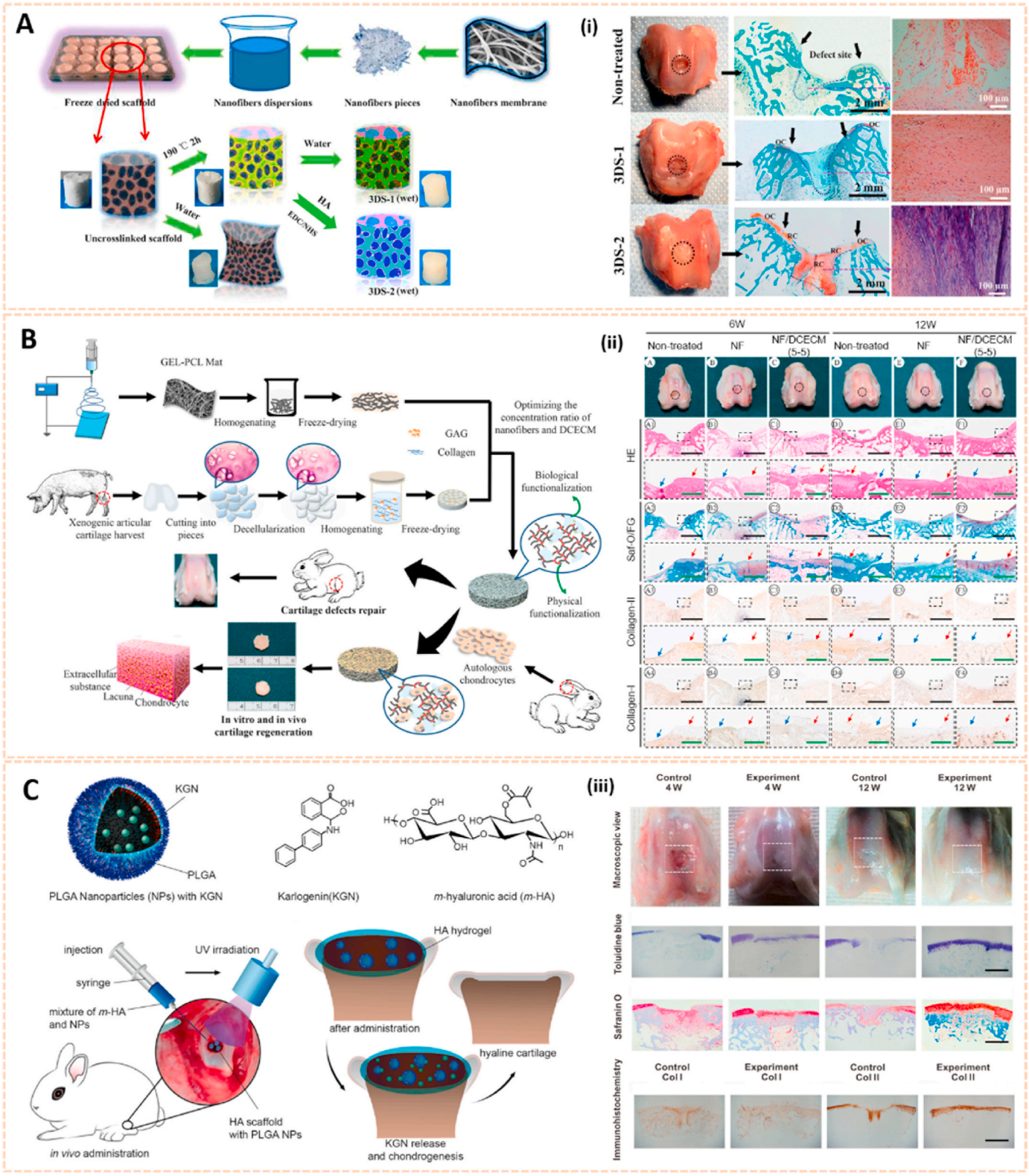

Fig. 13. Nanomaterials-based scaffolds for cartilage regeneration. A) Schematic illustration for 3D scaffold preparation. (i) Macroscopic images and histological analysis of cartilage defect area from three groups at 12 weeks after surgery [130]. The images reproduced with the permission from American Chemical Society. B) Schematic diagrams of the 3D scaffold synthesis and their application for cartilage tissue engineering. (ii) Gross view and histological evaluation of repaired region at 6 and 12 weeks postsurgery [131]. The images reproduced with the permission from American Chemical Society. C) Schematic of KGN-loaded PLGA nanoparticles, the surgical procedure for the cartilage defects repair and the hyaline cartilage chondrogenesis with photo-crosslinked HA scaffold encapsulated with KGN-loaded nanoparticles. (iii) Results of in vivo cartilage defects repair using KGN-loaded photo-cross-linkable scaffold [133]. The images reproduced with the permission from American Chemical Society.

Table 4
Summary of example nanomaterials for rheumatoid arthritis.

Category	Nanomaterials	Active principle	Main results	Ref.
Passive targeting drug carriers	PCL-PEG-PCL triblock copolymer	MTX-loaded nanomicelles	• encapsulation efficiency of 91% • improve the pharmacokinetic (4.34-fold greater half-life, 3.68-fold higher AUC0-t and 3.15-fold higher mean residence time)	[138]
	HSA-based nanoparticles	Prednisolone, curcumin	• drug loading efficiency of 85% • increase levels of anti-inflammatory cytokine • accumulate to a greater extent at inflamed joints	[139]
	Liposomes	amide prodrug of sulfapyridine	• longer retention in synovial joint with less polydispersity index	[140]
	Gold nanoparticles	Triamcinolone	• reduce ROS and inflammation levels • repolarize macrophages from M1 to M2	[141]
	Quantum dots	MPA-capped CdTe QDs, celecoxib	• enable bio-imaging for drug distribution	[142]
Active targeting drug carriers	Silver nanoparticles	folic acid, Ag^+	• M1 macrophages targeting delivery via folate receptor • release Ag^+ in response to intracellular GSH • facilitate M1 to M2 macrophages polarization	[143]
	Solid lipid nanoparticles	Prednisolone, hyaluronic acid	• bind to hyaluronic receptor CD44 • accumulate in affected joint tissue • reduce levels of inflammatory cytokines	[144]
	Hydroxyapatite nanoparticles	Methotrexate, teriflunomide, hyaluronic acid	• target for CD44 receptors overexpressed on inflamed macrophages • enhance the safety and efficacy of the treatment	[145]
	Nanoliposomes	Chondroitin sulfate, teriflunomide	• active targeting towards CD44 receptors • accumulate in synovial region with no signs of liver toxicity	[146]
	PLGA nanoparticles	Celastrol, RGD peptide	• high cellular uptake in OCs and macrophages via RGD-αvβ3 integrin interaction • induce the apoptosis of OCs and macrophages	[147]
Active targeting drug carriers	Micelles	MTX, sialic acid-dextran-octadecanoic acid	• target for E-selectin receptors in inflamed cells • sustained drug release behavior over 48 h • inhibit inflammatory response and diminish the adverse effects of MTX	[148]
	Human serum albumin nanoparticles	MTX, mannose	• target neutrophils via binding to mannose receptors • suppress angiogenesis and inflammatory cytokines	[149]
Gene therapy	Solid lipid nanoparticles	TNF-α siRNA	• high siRNA encapsulation efficiency (>90%) • a minimum burst release of siRNA (<5%) • increase siRNA delivery in chronic inflammation sites	[150]
	Calcium phosphate nanoparticles/liposome	NF-κB siRNA, MTX	• target for folate receptor • reduce expression of pro-inflammatory cytokines via NF-κB signaling pathway	[151]
	PEG nanoparticles	IL-1 receptor antagonist	• the half-life is boosted to the level of 30 h • bioavailability is boosted by 7 times	[152]
	Polymeric nanoparticles	Mcl-1 siRNA, PK3, folate	• pH-dependent siRNA release from nanocarriers with accelerated release at pH 5.0 • target for folate receptor	[153]
Gene therapy	PEG-b-PLGA nanoparticles	BTK siRNA	• inhibit BTK expression in macrophages and B cells • reduce joint inflammation with no toxicity	[154]
	Alginate nanoparticles	IL-10 plasmid DNA, tuftsin peptide	• active macrophage targeting • repolarize macrophages from M1 to M2 state	[155]
	Polymeric nanoparticles	miR-21, IL-4	• prolong blood circulation • passively accumulate in the inflamed joint • attenuate inflammation via NF-κB inhibition • promote macrophage polarization to M2a/M2c	[156]
Nanomaterials with Special Function	Metal oxide nanoparticles	Fe_3O_4	• display superior photothermal conversion ability upon the irradiation of NIR laser	[157]
	Nanogold-core dendrimer	Au, MTX	• offer photothermal benefit upon NIR laser irradiation • poly dispersibility index: 0.39 ± 0.02 • selective localize in arthritic tissue via folate receptors	[158]
	Palladium nanosheets	Palladium, MTX, RGD peptides	• show controlled MTX release under irradiation of 808 nm (0.3 W cm^{-2}) • inhibit the inflammatory response induced by VEGF and IL-1β	[159]
	Black phosphorus nanosheets, chitosan	Black phosphorus, platelet-rich plasma	• generate local heat upon near-infrared irradiation • deliver ROS to the inflamed joints • improve the adhesion and increase capacity of mesenchymal stem cells	[160]
	PLGA-quadrilateral ruthenium nanoparticles	Dextran sulfate, quadrilateral ruthenium, resveratrol	• exhibit photothermal effect • accumulate in lesion area with an exogenous stimulus • reverse the M1 type macrophages to the M2 type macrophages through an accurate release	[161]
	Polymeric nanoparticles	Neutrophil membrane	• neutralize proinflammatory cytokines • suppress synovial inflammation • target deep into the cartilage matrix	[162]
	Au@polydopamine nanoparticles	Tocilizumab, Au	• effectively scavenge oxygen free radicals • inhibit the formation of related inflammatory factors	[163]

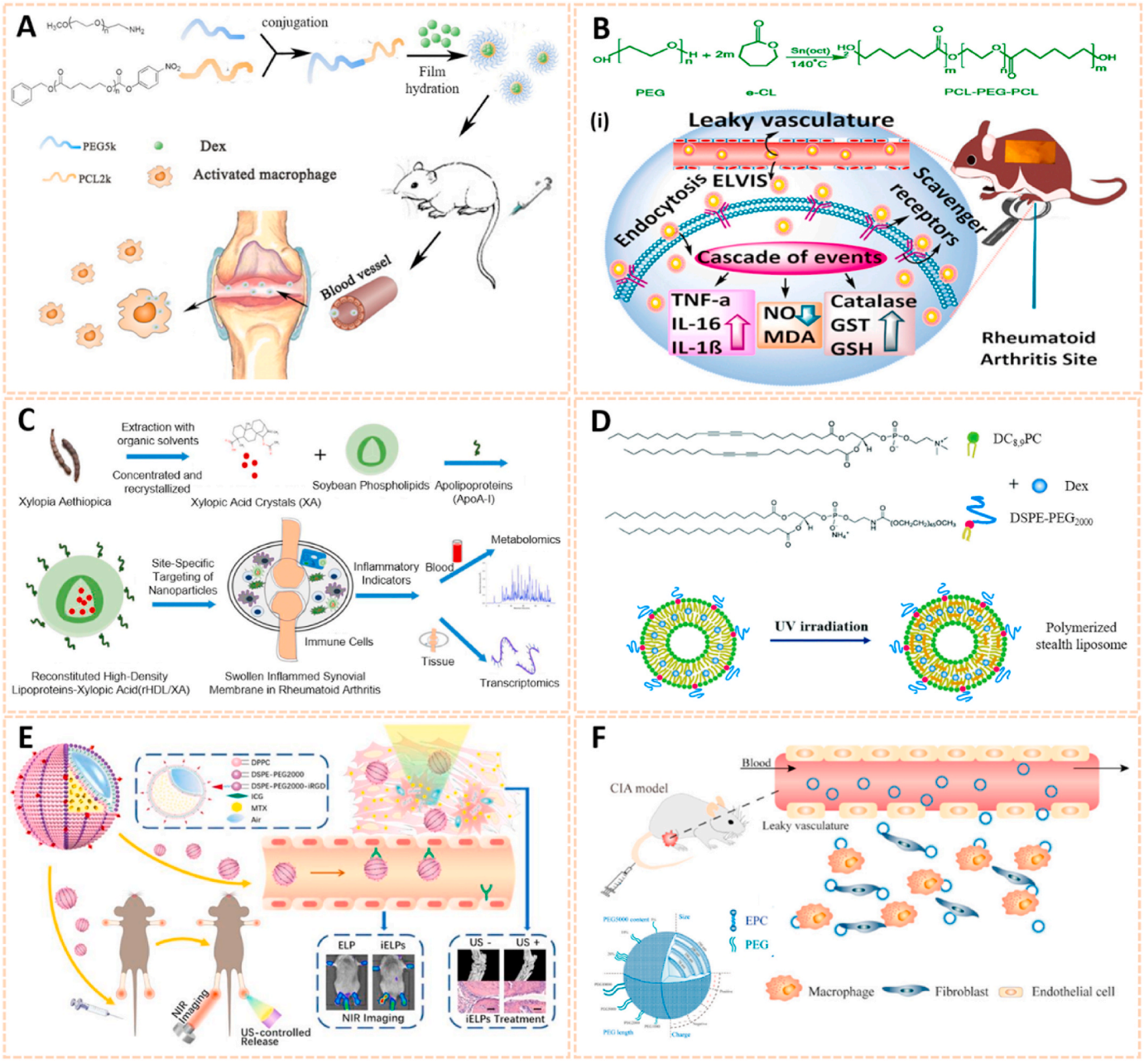

Fig. 14. Polymer and liposomes-based nanomaterials as passive targeting drug carriers. A) Schematic preparation and therapy of Micelles-Dex [167]. The image reproduced with the permission from Elsevier B.V. B) Reaction scheme for the synthesis of PCL-PEG-PCL. (i) Schematic mechanisms of MTX nanomicelles-based hydrogel against RA [138]. The image reproduced with the permission from American Chemical Society. C) Schematic summary of the entire study [168]. The image reproduced with the permission from Elsevier Ltd. D) Chemical structure of $DC_{8,9}PC$, $DSPE\text{-}PEG_{2000}$ and schematic of polymerized stealth liposomes with loaded Dex [171]. The image reproduced with the permission from The Royal Society of Chemistry. E) The schematic illustration of iELPs and the mechanism of NIR fluorescence imaging and treatment [172]. The image reproduced with the permission from Ivyspring. F) Schematic of the characteristics and RA targeting effect of liposomes in the inflammatory microenvironment of RA. Liposomes were mainly taken up by macrophages and fibroblasts after entering the joint cavity through the leaky vasculature. Fewer liposomes were taken up by endothelial cells [37]. The image reproduced with the permission from American Chemical Society.

The novel MOFs improved RA symptoms by targeting CD44 receptors with a drug loading of 45% and sustained drug release. These nanocarriers provide a great potential for RA treatment through active targeting toward macrophages.

Vascular endothelial cells (VECs) are critical cells in angiogenesis that increase the recruitment and adhesion of inflammatory cells in the progression of RA [184]. Actively targeting the receptors of activated VECs, such as integrin $\alpha_v\beta_3$ and E-selectins, has been adopted to treat RA [159,185]. The RGD peptide exhibits high affinity for integrin $\alpha_v\beta_3$. RGD-modified polymeric micelles loaded with MTX and nimesulide (R-M/N-PMs) were synthesized for RA therapy [186]. The R-M/N-PMs increased retention time in the inflamed joints and attenuated swelling of joints and bone destruction. Additionally, integrin $\alpha_v\beta_3$-targeted lipase-labile fumagillin prodrug nanoparticles were fabricated for RA treatment by suppression of inflammation. In addition, sialic acid-dextran-octadecanoic acid (SA-Dex-OA)-modified micelles loaded with MTX were designed as a multifunctional platform for drug delivery and bone regeneration of RA (Fig. 16D) [148]. The Dex-OA/MTX micelles targeted E-selectin and subsequently decreased the inflammatory response and promoted bone repair.

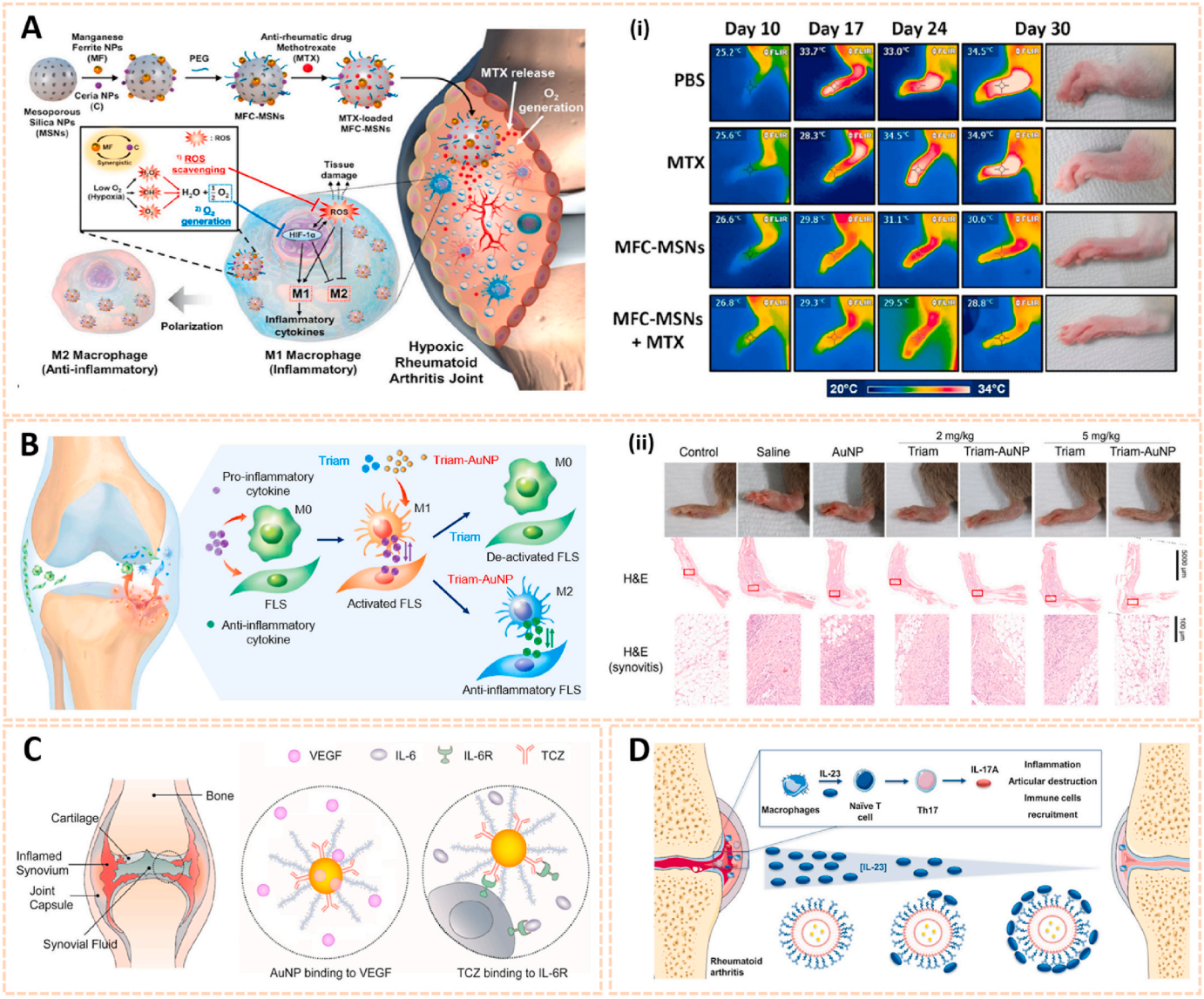

Fig. 15. Metal nanomaterials as passive targeting drug carriers. A) Schematic therapeutic mechanisms of MFC-MSNs in RA treatment. (i) Thermographic images of left hind paw and corresponding gross images of the paw [175]. The images reproduced with the permission from American Chemical Society. B) Schematic illustration showing the inflammatory crosstalk between FLSs and macrophages. (ii) Therapeutic effects of the nanodrug on CIA model mice [141]. The images reproduced with the permission from American Chemical Society. C) Schematic illustration of HA-AuNP/TCZ complex for the treatment of RA by the dual targeting to VEGF and IL-6R [176]. The image reproduced with the permission from American Chemical Society. D) Schematic illustration of the biofunctionalized liposomes role in rheumatoid arthritis treatment. The neutralization of IL-23 cytokine will inhibit the Th17 differentiation, and consequently, reduce inflammation and immune cells recruitment [177]. The image reproduced with the permission from Wiley-VCH GmbH.

Activated neutrophils are also a crucial type of RA-related cells that express abundant mannose receptors and PSGL-1. Lyu et al. developed human serum albumin nanoparticles conjugated with mannose and loaded with MTX (MTX-M-NPs) to target neutrophils for RA therapy (Fig. 16E) [149]. MTX-M-NPs significantly suppressed angiogenesis and inflammatory cytokines, thus improving joint swelling and bone destruction in the RA rat model. Additionally, a “shield and sword nanosoldiers” strategy for RA was established with low molecular weight heparin (LMWH)-d-α-tocopheryl succinate (TOS) nanoparticles (LT NPs) for multistage manipulation of neutrophils by targeting PSGL-1 (Fig. 16F) [187]. The activated neutrophil-targeted delivery of MTX to inflamed joints enhanced the therapeutic efficacy of RA.

On the other hand, although these active targeting nanocarriers improve the specificity of the nanostructures to target regions of the organism to a certain extent, there are still many challenges when the physiological variables of blood flow, disease status, and tissue architecture are taken into account. Meanwhile, few studies have been performed to evaluate the interaction of the moieties-appended in nanocarriers with cell membranes, and their uptake mechanism is still unclear. Moreover, some particular physicochemical characteristics of each delivery system make it difficult to standardize the mechanism of action/interaction of these systems in cells.

3.2.3. *Nanomaterials for gene therapy toward macrophages*

Although traditional anti-rheumatic drugs are clinically available, they often lead to unwanted adverse effects after frequent and long-term administration. Therefore, nanomaterials loaded with biological agents such as plasmid DNA, siRNA, miRNA and receptor antagonists have been adopted for RA therapy, (Table 4). IL-10 plasmid DNA was encapsulated into tuftsin-modified alginate nanoparticles to achieve targeted macrophage repolarization for RA treatment [155]. The NPs decreased the expression of pro-inflammatory cytokines by efficiently

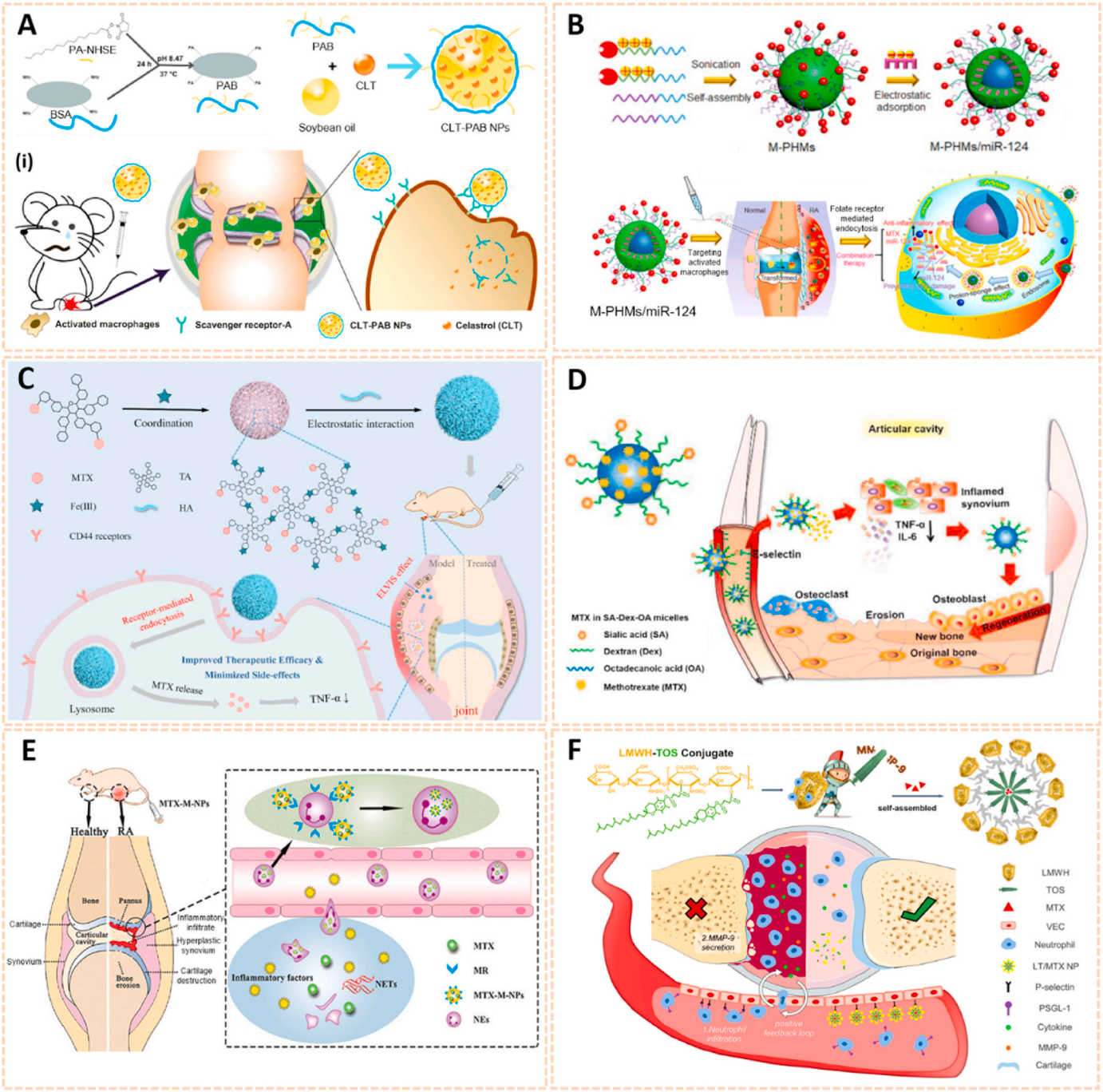

Fig. 16. Nanomaterials as active targeting drug carriers. A) Preparation and characterization of PAB and CLT-PAB NPs. (i) Schematic displaying the proposed mechanism by which CLT-PAB NPs target SR-A during treatment of rheumatoid arthritis [181]. The image reproduced with the permission from Elsevier Ltd. B) Schematic representation of MTX-conjugated polymer hybrid micelles co-loaded with miR-124 (M-PHMs/miR-124) preparation and combination therapy of M-PHMs/miR-124 in RA [182]. The image reproduced with the permission from Ivyspring. C) Schematic illustration the construction of MTX-TA/$Fe3^{+}$@HA for targeted RA treatment [183]. The image reproduced with the permission from Elsevier B.V. D) A multifunctional carrier for methotrexate delivery and bone repair of rheumatoid arthritis [148]. The image reproduced with the permission from The Royal Society of Chemistry. E) Treatment of rheumatoid arthritis by serum albumin nanoparticles coated with mannose to target neutrophils [149]. The image reproduced with the permission from American Chemical Society. F) Schematic illustration of the shield and sword nano-soldiers for RA by multi-stage manipulation of neutrophils [187]. The image reproduced with the permission from Elsevier B·V.

repolarizing macrophages from the M1 to the M2 state, thus preventing joint damage.

Apart from plasmid DNA, siRNA has been applied more frequently in gene therapy. Li et al. fabricated generation 5 (G5) poly (amidoamine) dendrimer-entrapped gold nanoparticles (Au DENPs) loaded with alpha-tocopheryl succinate (α-TOS) and TNF-α siRNA as a multifunctional nanoplatform for RA therapy (Fig. 17A) [188]. The α-TOS-modified Au DENPs/TNF-α siRNA NPs achieved synergistic antioxidation and anti-inflammation therapeutic efficacy for RA. IL-1β has also been identified as a therapeutic target for RA. Lipidoid-polymer hybrid nanoparticles (FS14-NPs) loaded with siRNA against IL-1β (siIL-1β) were synthesized to target macrophages and inhibit the progression of RA (Fig. 17B) [189]. The FS14-NP/siIL-1β significantly ameliorated joint swelling, cartilage erosion and bone damage in CIA mice. Abnormal

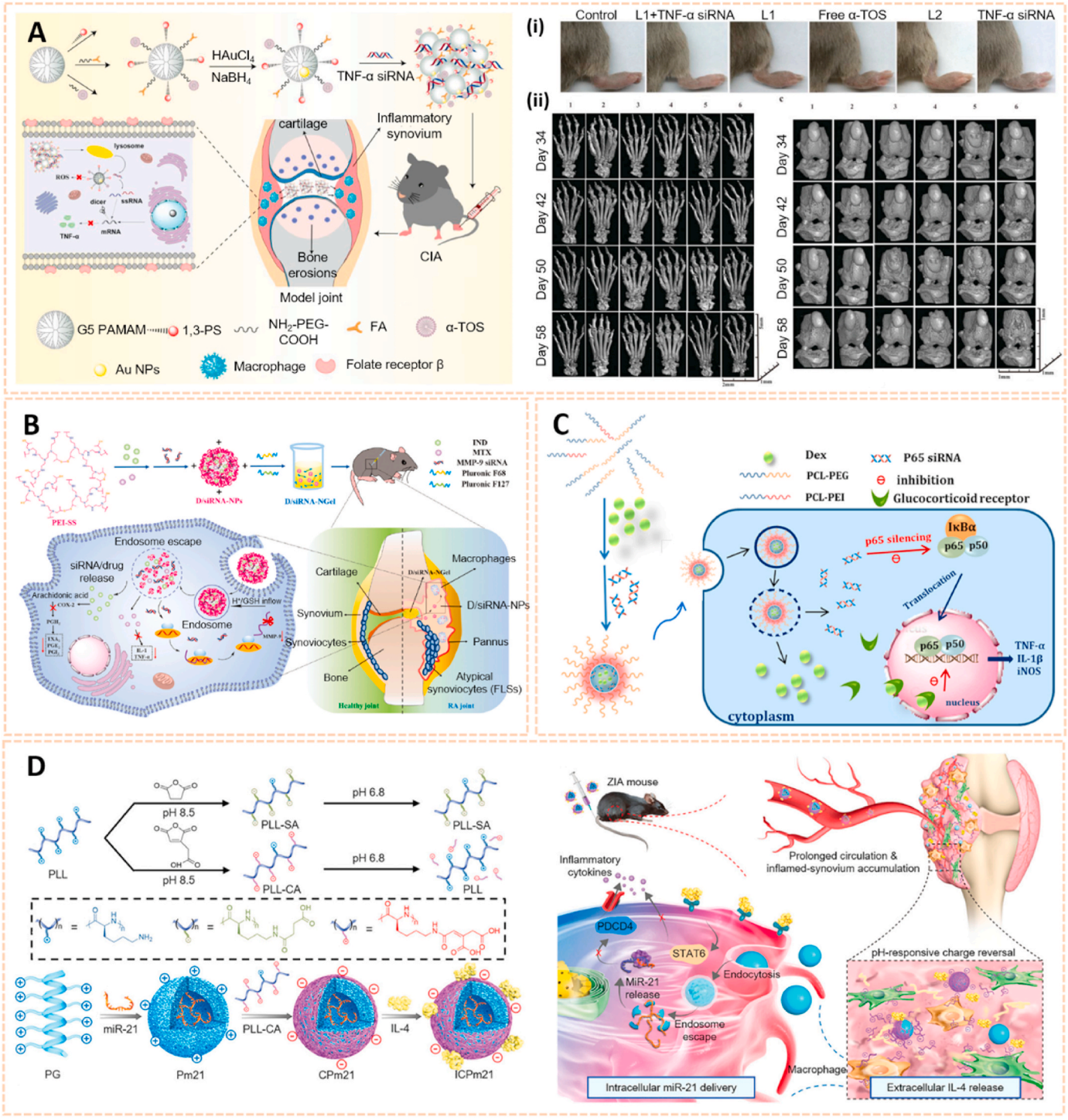

Fig. 17. Nanomaterials for gene therapy. A) Synthesis of $(Au^0)_{25}$-G5. NH_2-1,3-PS-(PEG-FA)-(PEG-TOS) DENPs/TNF-α siRNA polyplexes for combined antioxidative and anti-inflammatory RA therapy. (i) Representative hind paw images in different treatment groups at day 58. (ii) Micro-CT imaging of the ankle and knee joints of mice in different treatment groups at different time points [188]. The images reproduced with the permission from Wiley-VCH GmbH. B) Schematic illustration of the whole experimental process, including preparation, intra-articular injection and intracellular fate of D/siRNA-NGel [190]. The image reproduced with the permission from The Royal Society of Chemistry. C) Schematic of Dex and siRNA co-encapsulation in micelles and the intracellular fate of micelles [191]. The image reproduced with the permission from Elsevier Ltd. D) Schematic illustration showing the inflammation-instructed, hierarchical co-delivery of miR-21 and IL-4 mediated by acid-responsive, charge reversal NCs [156]. The images reproduced with the permission from Wiley-VCH GmbH.

secretion of matrix metalloproteinase 9 (MMP9) is involved in joint damage in RA. MMP9 siRNA, indomethacin (IND) and methotrexate (MTX) were loaded in hydrogel (D/siRNA-NGel) for the synergistic treatment of RA (Fig. 17C) [190]. D/siRNA-NGel possessed excellent anti-inflammatory ability and reversed articular cartilage degeneration and bone erosion. In addition, NF-κB signaling plays a key role in the pathogenesis of RA. Wang et al. designed polycaprolactone -polyethylenimine (PCL-PEI) and polycaprolactone-polyethyleneglycol

(PCL-PEG) hybrid micelles loaded with Dex and NF-κB p65 siRNA for RA treatment (Fig. 17D) [191]. The micelles decreased pro-inflammatory cytokines expression and repolarized macrophages to the M2 state by blocking the NF-κB signaling pathway. These siRNA delivery strategies indicated a promising potential for treating RA by silencing inflammatory cytokine genes and specific signaling pathways.

Additionally, miRNA-based gene therapy is also a novel approach for RA treatment to overcome clinical multidrug resistance [192]. Based on this strategy, Deng et al. fabricated PLL-cis-aconitic anhydride (CA) nanocomplexes (NCs) loaded with miR-21 and IL-4 for macrophages intracellular delivery against RA (Fig. 17E) [156]. The inflammation-instructed NCs enabled prolonged retention duration after intravenous administration and aggregated in the inflamed joints. The NCs regulated the osteoimmune microenvironment by enhancing macrophage polarization to the M2a/M2c phenotypes via NF-κB signaling, suggesting a novel strategy for RA treatment.

3.2.4. Nanomaterials with special function

Photothermal therapy (PTT) is an emerging approach to treat several diseases using electromagnetic radiation [193]. A variety of photothermal-based nanomaterials have been synthesized for RA treatment, such as metal NPs, metal oxide NPs, palladium nanosheets, black phosphorus nanosheets and polymeric nanocomposites [157, 159–161,194] (Table 4).

Metal nanomaterials can serve as photothermal agents with optical, physical and chemical properties. L-cysteine (Cys)-modified CuS NPs ($Cu_{7.2}S_4$ NPs) were developed using a facile one-step wet chemical method for combined PTT and photodynamic therapy (PDT) against RA [195]. The $Cu_{7.2}S_4$ NPs decreased the expression of proinflammatory cytokines and exhibited antibacterial ability against *Staphylococcus aureus* (*S. aureus*) and *Escherichia coli* (*E. coli*), subsequently suppressing synovial erosion and bone destruction. Additionally, Lee et al. designed RGD-modified gold half-shell nanoparticles loaded with MTX for targeted chemo-photothermal treatments of RA (Fig. 18A) [40]. The multifunctional NPs generated heat after NIR irradiation, and the release rate of the drug was increased, thus delivering heat and drug to the inflamed joints together. These NPs combined with PPT maximized the therapeutic efficacy of RA. In addition, a multifunctional nanoplatform based on an octahedral copper sulfide shell and gold nanorod core (Au NR@CuS) coated with hyaluronic acid (HA) and vasoactive intestinal peptide (VIP) was fabricated for PTT/PDT and targeted drug delivery tri-combined therapy for RA (Fig. 18B) [196]. The VIP-HA-Au NR@CuS exhibited a high photothermal conversion efficiency of 67.2% and generated •OH for synergistic treatment of RA.

Apart from metal nanomaterials, black phosphorus nanosheets have received attention owing to their excellent photothermal effects and potential osteogenic properties [197]. A platelet-rich plasma (PRP)-chitosan thermoresponsive hydrogel loaded with black phosphorus nanosheets (BPNs) was developed as an injectable therapeutic nanoplatform for the treatment of RA (Fig. 18C) [160]. The multifunctional hydrogel exhibited outstanding photothermal properties and enhanced phosphorus-driven bone formation, indicating a promising therapeutic approach for RA.

Inspired by natural biological systems, biomimetic nanomaterials coated with cell membranes of immune cells provides promising advantages in RA therapy [198]. The bionic technique reduces the immunogenicity of nanomaterials and prolongs the circulation duration [199]. For instance, neutrophil membrane-modified PLGA NPs were developed for the treatment of RA [162]. The direct use of effector cell membranes leads to the inhibition of synovial inflammation without the need to identify them and thus attenuates joint damage in RA. Similarly, Headland et al. designed neutrophil-derived annexin A1 microvesicles that could penetrate cartilage and protect the joints through inhibiting the expression of the stress-adaptive homeostatic mediators interleukin-8 and prostaglandin E2 [200]. Additionally, Topping et al. prepared extracellular vesicles (EVs) from human neutrophils combined with anti-ROS-CII for targeted anti-inflammatory treatment of arthritic joints [201]. In addition, macrophage-derived microvesicle (MMV)-modified PLGA NPs enhanced the targeting effect and inhibited the progression of RA [202]. Additionally, umbilical vein endothelial cell (UVEC) membrane-coated drug-loaded NPs conjugated with tumor necrosis factor-related apoptosis-inducing ligand (TRAIL) were synthesized as therapeutic nanoplatforms for RA therapy [203]. The biomimetic strategy could neutralize cytokines, inhibit synovial inflammation and subsequently protect joints from damage by penetrating into targeted inflamed tissues, which is of great potential for RA therapy and further clinical translation.

Overproduction of endogenous nitric oxide (NO) is closely related to the pathogenesis of RA development, which acts as a proinflammatory mediator to induce cartilage and bone tissue destruction. Therefore, nanomaterials with antioxidant property have gained increasing attention for the treatment of RA. NO-scavenging nanosized hydrogel (NO-Scv gel) was fabricated by solution polymerization between acrylamide and NO-cleavable cross-linker (NOCCL) for treating RA (Fig. 19A) [204]. The NO-Scv gel ameliorated bone resorption and joint destruction by removing NO and reducing the inflammation level of activated macrophages. Furthermore, polymeric aggregate-embodied hybrid NO scavenging and sequential drug-releasing hydrogel was designed for the combinatorial treatment of RA (Fig. 19B) [205]. In addition, a polypeptide nanogel methoxy poly (ethylene glycol)-poly (L-phenylalanine-*co*-L-cystine) (mPEG-P (LP-*co*-LC)) loaded with MTX was synthesized (Fig. 19C) [206]. These novel nanogels selectively distributed in the inflamed joints after intravenous administration and thus reduced synovitis and relieved RA progression by inhibiting the redox reaction. Metal nanomaterials also have potential antioxidant ability for RA treatment. Albumin-cerium oxide NPs (nanoceria) loaded with indocyanine green (ICG) were developed as an antioxidant theranostic platform for RA (Fig. 19D) [207]. The nanoceria-ICG normalized the disrupted reactive oxygen species (ROS) levels, repolarized pro-inflammatory M1 to anti-inflammatory M2 macrophages and provided real-time monitoring via optical/optoacoustic imaging. The inflammation-targeting, inherent contrast and therapeutic activity of this nanoplatform may make it a relevant agent for assessing severity in RA and other inflammatory diseases, and subsequently controlling inflammation with image-guidance. The design of these nanoplatforms will enable potential clinical translation as systemic therapies for RA.

3.3. Nanomaterials in osteoporosis

3.3.1. Nanomaterials as anti-osteoporosis drug carriers

The current therapeutic strategy for osteoporosis (OP) aims to decrease bone resorption and promote bone formation independently or in synergy. Various nanomaterials such as polymeric nanomaterials, mineral-based nanomaterials, metal-based nanomaterials and carbon-based nanomaterials have been developed as carriers for delivery of anti-osteoporosis drugs for preventing and treating OP (Table 5).

Polymers such as poly (lactic-*co*-glycolic acid) (PLGA), poly (ethylene glycol) (PEG) and chitosan have been used as drug nanocarriers for OP treatment and bone tissue regeneration with excellent biocompatibility and sustained release properties. Lipp et al. synthesized a monomethoxy PEG (mPEG) and PLGA thermosensitive triblock copolymer (mPEG-PLGA-mPEG)-based carrier for the controlled release of salmon calcitonin (sCT) for the treatment of OP [216]. The copolymer-based delivery system possessed excellent biocompatibility and released sCT over a period of 2 months after systemic administration, thus enhancing the therapeutic effect for OP. Similarly, triblock copolymer PLGA-PEG-PLGA thermosensitive hydrogel loaded with sCT and oxidized calcium alginate (sCT-OCA) complex was developed for long-term antiosteopenia therapy by subcutaneous injection [217] (Fig. 20A). The copolymer exhibited a sol-gel transition in situ at body temperature. Both hydrogel degradation and sCT-OCA complex decomposition determined the sustained release of sCT. Chitosan

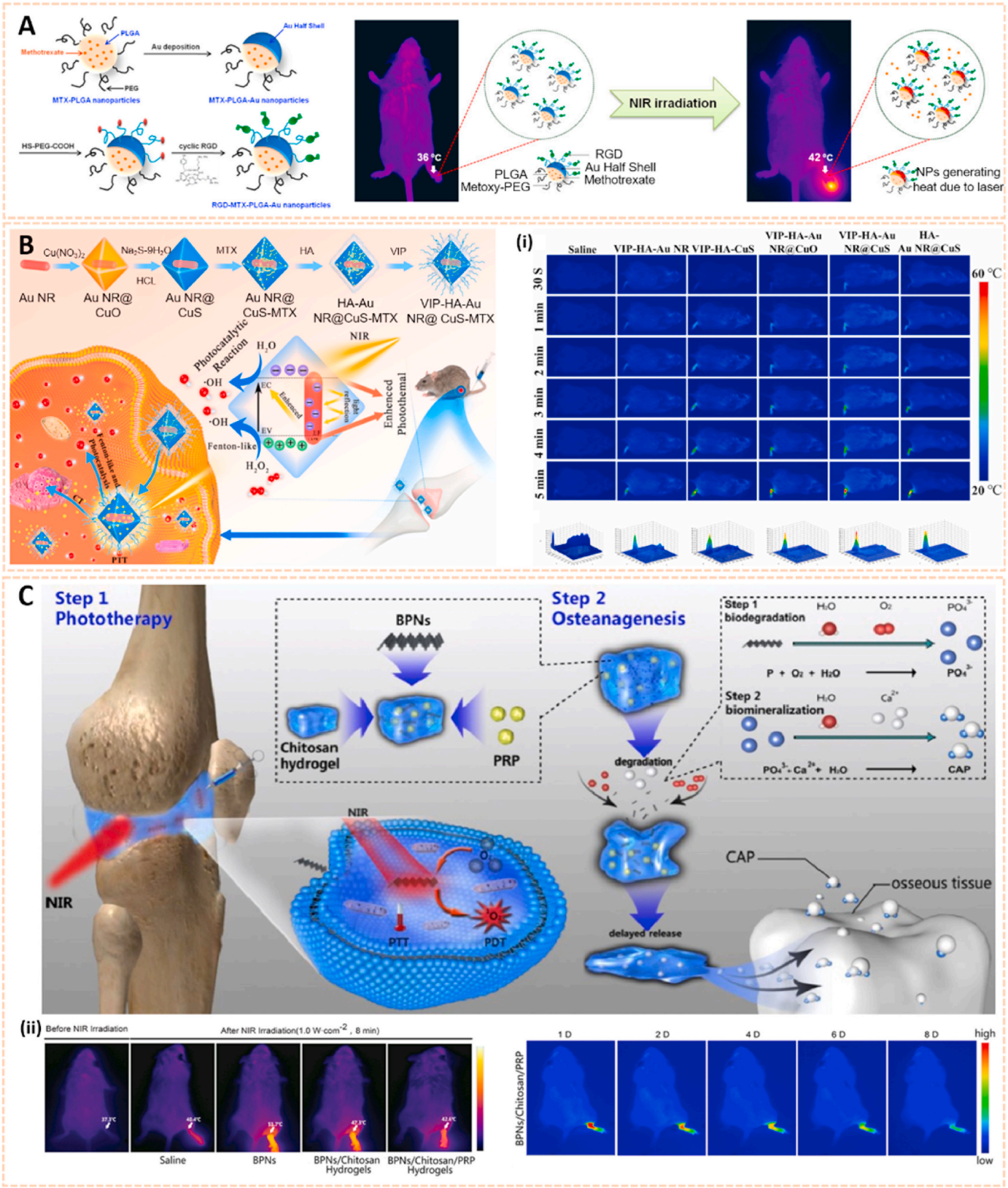

Fig. 18. Photothermal-based nanomaterials for RA treatment. A) Schematic fabrication process of RGD-MTX-PLGA-Au nanoparticles and targeted chemo-photothermal effect [40]. The image reproduced with the permission from American Chemical Society. B) Schematic illustration of the synthesis VIP-HA-Au NR@CuS NPs and synergistic treatment of rheumatoid arthritis. (i) Photothermal images of arthritis after treat with Saline, VIP-HA-Au NR, VIP-HA-CuS NPs, VIP-HA-Au NR@CuO NPs and VIP-HA-Au NR@CuS NPs [196]. The images reproduced with the permission from Elsevier Ltd. C) Schematic illustration of the PRP-Chitosan thermoresponsive hydrogel combined with black phosphorus nanosheets as injectable biomaterial for biotherapy and phototherapy treatment of RA. (ii) In vivo representative photothermal images of arthritis sites after of saline, BPNs, BPNs/Chitosan thermoresponsive hydrogel and BPNs/Chitosan/PRP thermoresponsive hydrogel as a function of the irradiation time under NIR irradiation [160]. The images reproduced with the permission from Elsevier Ltd.

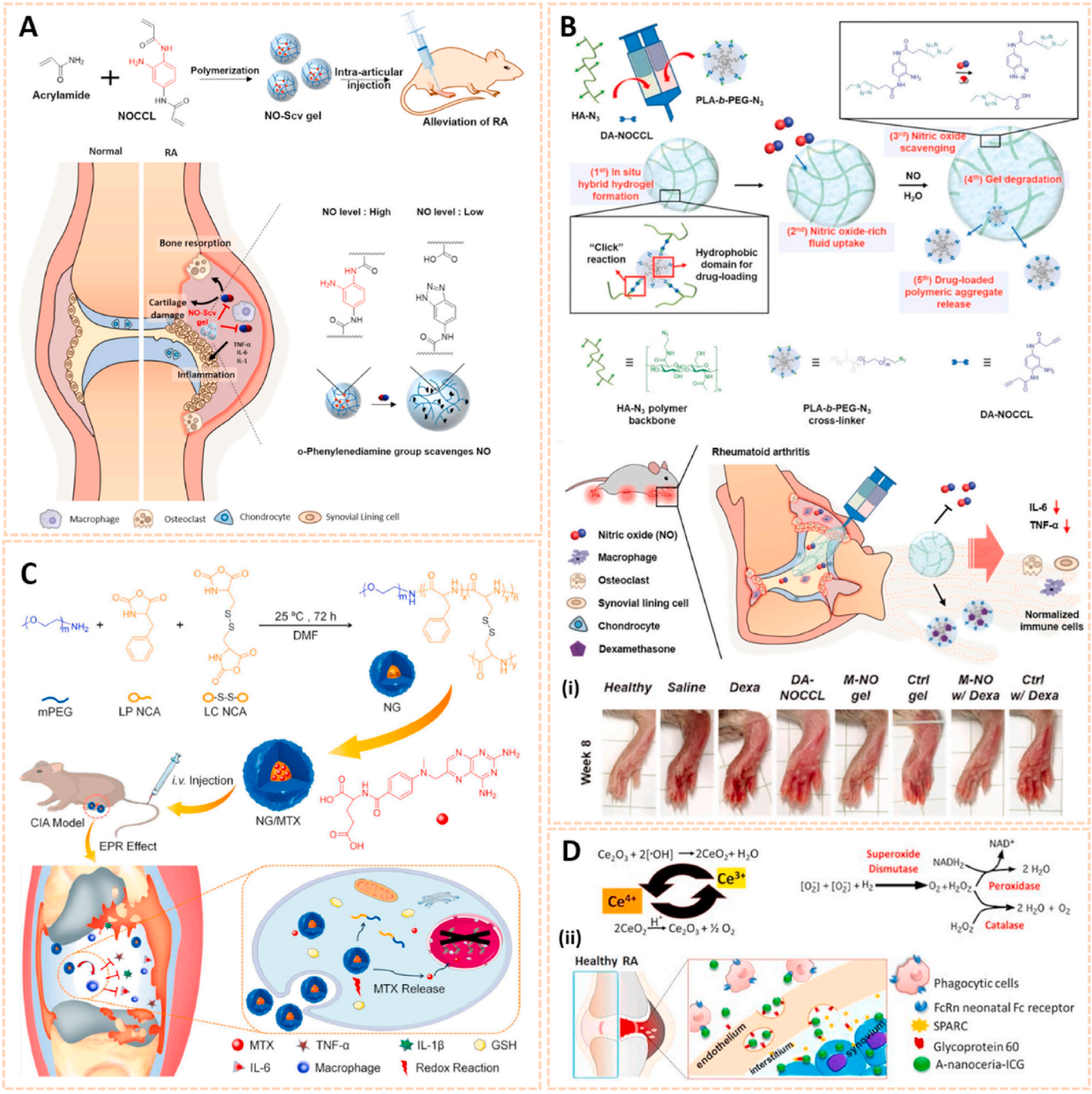

Fig. 19. Nanomaterials with antioxidant property for RA treatment. A) Schematic illustration of NO-Scv Gel-mediated anti-inflammation therapy for treating RA [204]. The image reproduced with the permission from American Chemical Society. B) Polymeric aggregate-embodied hybrid nitric oxide-scavenging "click" hydrogel for combinatorial treatment of rheumatoid arthritis. (i) Representative hind paw images of the sample-treated RA mice [205]. The images reproduced with the permission from Wiley-VCH GmbH. C) Schematic diagram of synthesis, treatment, and brief function mechanism of NG/MTX in treatment of CIA [206]. The image reproduced with the permission from American Chemical Society. D) Schematic representation of valence states recycling in nanoceria and enzymatic modes of nanoceria. (ii) Albumin-binding receptors interaction with A-nanoceria within inflamed RA joint [207]. The images reproduced with the permission from IVYSPRING.

nanoparticles are able to protect peptides from enzymatic degradation due to strong electrostatic interactions. Narayanan et al. formulated parathyroid hormone 1–34 (PTH 1–34)-loaded PEGylated chitosan NPs (PEG–CS–PTH NPs) with 40% encapsulation for OP treatment [209]. The PEG–CS–PTH NPs facilitated the transport of bioactive molecules across the intestinal epithelium with a remarkable oral bioavailability of 100–160 pg/ml PTH 1–34 over 2 days. These findings showed the protective effect of polymeric delivery systems to enhance the therapeutic efficiency of drugs from enzymatic degradation with sustained release.

Mineral-based nanomaterials such as nanocrystalline hydroxyapatite (nHA) have been used for bone tissue regeneration owing to their hardening ability, high surface area and in vivo osteoinductive properties. Fricain et al. designed an nHA-pullulan/dextran polysaccharide composite macroporous scaffold for promoting bone formation under OP conditions [210]. The platform could induce the deposition of a biological apatite layer and favor the formation of a dense mineralized

Table 5
Summary of example nanomaterials for osteoporosis.

Category	Nanomaterials	Active principle	Main results	Ref.
Drug carriers	Lipid nanoparticles	Hydroxyapatite, zoledronic acid	• typical biphasic release pattern [38.17 ± 2.12% (pH 7.4) and 64.2 ± 3.75% (pH 5) at 48 h] • exhibit a strong affinity towards HA	[208]
	PEGylated chitosan nanoparticles	PTH 1-34	• encapsulation efficiency of 40% • show an oral bioavailability of 100–160 pg/ml PTH 1–34 throughout 48 h	[209]
	Nanocrystalline hydroxyapatite particles	Pullulan/dextran polysaccharide	• retain subcutaneously local growth factors • induce the deposition of a biological apatite layer • favor the formation of a dense mineralized tissue subcutaneously in vivo	[210]
	Cerium nanoparticles	Cerium oxide, alendronate	• bone-targeted ability • pH-responsive activity • selectively eliminate mature osteoclasts without affecting preosteoclasts	[211]
	Nanodiamonds	Alendronate, nanodiamonds	• enhance ALP activity • effectively accumulate in bone tissues after intravenous administration	[212]
Gene therapy	Polyurethane nanomicelles	SDSSD peptide, anti-miR-214	• selectively bind to osteoblasts via periostin • enhance bone formation without overt toxicity or elicit an immune response	[213]
	Tetrahedral framework nucleic acids	miR-2861	• enable efficient miR-2861 unloading and deployment after intracellular delivery • inhibit the expression of HDAC5 and promote osteogenic differentiation	[214]
	PLGA nanoparticles	Polyethyleneimine-RANK siRNA	• significantly reduce (47%) RANK mRNA levels • suppress the differentiation of preosteoclasts to mature osteoclasts	[215]

tissue. Moreover, Lee et al. synthesized strontium-releasing nanoscale cement with dual therapeutic actions of osteoclastic inhibition and osteogenic stimulation to facilitate OP therapy (Fig. 20B) [218]. The nanoscale cement released triple ions Sr, silicate and Ca, of which Sr and Ca are considered to be osteo-promotive and silicate are proangiogenic, thus promoting bone formation and slowing down the bone resorption in osteoporotic pathological conditions.

Metal oxide NPs have been broadly used in biological applications owing to their good biocompatibility and intrinsic magnetic properties. The chemical coordination of alendronate and Fe_3O_4 with HA served as a multifunctional HA (Func-HA) enhanced bone remodeling under osteoporotic conditions (Fig. 20C) [219]. The Func-HA exhibited magnetic properties with dual regulation of osteoclasts (OCs) and osteoblasts (OBs) for osteoporotic bone reconstruction. In addition, superparamagnetic iron oxide nanoparticles conjugated with HA (SPIO@HA) were fabricated with a core-shell structure for the combined regulation of osteoclastogenesis and osteogenesis for OP therapy through systemic administration (Fig. 20D) [220]. SPIO@HA inhibited OC differentiation via TRAF6-p62-CYLD signaling and activated OB differentiation through the TGF-β, PI3K-AKT and calcium signaling pathways. In addition, cerium NPs have been developed as pH-sensitive enzymes with changeable oxidative activity. A biocompatible pH-responsive cerium nanosystem (CNS) was synthesized for anabolic therapy in OP (Fig. 20E) [211]. The CNS exhibits oxidative activity in response to the low-pH microenvironment created by mature osteoclasts (mOCs). Moreover, the CNS at neutral pH levels has no effect on preosteoclasts (pOCs). The cerium nanosystem provides a bone-targeted pH-responsive drug delivery platform for OP treatment.

In addition, carbon-based nanomaterials such as nanodiamond (NDs) have extended applications in biological fields owing to their surface functionality, spherical morphology and strong hardness [221]. Bone-targeted delivery of nanodiamond-based drug carriers loaded with alendronate (Alen-NDs) was designed for potential OP treatment through systemic administration [212]. The Alen-NDs effectively accumulated in bone tissues after intravenous administration due to high Hap affinity and subsequently enhanced ALP activity. In addition, hard nanodiamonds accumulated in bone tissue can increase the mechanical strength of bone by being incorporated into bone tissues. Therefore, the Alen-NDs can potentially be employed for osteoporosis treatment by delivering both NDs and Alen to bone tissues.

3.3.2. Nanomaterials for gene therapy toward bone cells

Gene therapy is considered a novel strategy for OP treatment through modulating gene expression by exogenous small nucleic acids such as miRNA and siRNA [222,223] (Table 5). Sun et al. fabricated osteoblast-targeting Ser-Asp-SerSer-Asp (SDSSD) peptide-modified polyurethane (PU) nanomicelles loaded with anti-miR-214 to improve bone microarchitecture in an OP mouse model (Fig. 21A) [213]. The SDSSD-PU NPs could selectively target OBs and subsequently enhance bone formation without overt toxicity or elicit an immune response. Relatively, a delivery system composed of the eight repeating sequences of aspartate (D-Asp 8) peptide and liposome-encapsulated antagomir-148a was developed specifically approaching bone resorption surfaces to downregulate miR-148a in OCs for OP treatment [224]. In addition, an RNase H-responsive sticky-end tetrahedral framework nucleic acid loaded with miR-2861 (stFNA-miR) was designed [214]. The bioswitchable nanocomposite separated miR-2861 after intracellular delivery and subsequently inhibited HDAC5 expression and promoted osteogenesis. These findings demonstrated the capability and editability of nanocomposites to improve the delivery efficacy of miRs for bone regeneration.

Targeted delivery of specific siRNA through nanocarriers could facilitate the therapeutic efficacy of OP treatment [225]. Zhang et al. designed dioleoyl trimethylammonium propane (DOTAP)-based cationic liposomes conjugated with six repetitive sequences of aspartate, serine, and serine ($(AspSerSer)_6$) for OP treatment (Fig. 21B) [226]. The nanocarriers delivered osteogenic pleckstrin homology domain-containing family O member 1 (Plekho1) siRNA specifically to bone formation surfaces, indicating a potential approach for the clinical translation of RNA interference-based bone anabolic therapy. Furthermore, CH6 aptamer-functionalized lipid nanoparticles encapsulating Plekho1 siRNA (CH6-LNPs-siRNA) were synthesized as a novel RNAi-based therapy for OP (Fig. 21C) [227]. The CH6-LNP-siRNA system selectively achieved OB delivery at the cellular level and promoted bone formation in osteopenic rodents. These siRNA delivery systems have the potential to be used as a novel alternative approach for the systemic treatment of osteoporosis.

3.4. Nanomaterials in bone cancer

3.4.1. Nanomaterials for chemotherapy

Standard chemotherapy is the first-line treatment for primary bone cancers such as osteosarcoma (OS) and bone metastasis from other malignant tumors. However, a high dose of chemotherapeutic agents that would cause considerable toxicity is usually required due to the reduced permeability and low blood flow of bone tissues. Advancements in nanomaterials have made it possible to minimize the toxicity and improve the efficacy of chemotherapy with adverse effects [228]. A

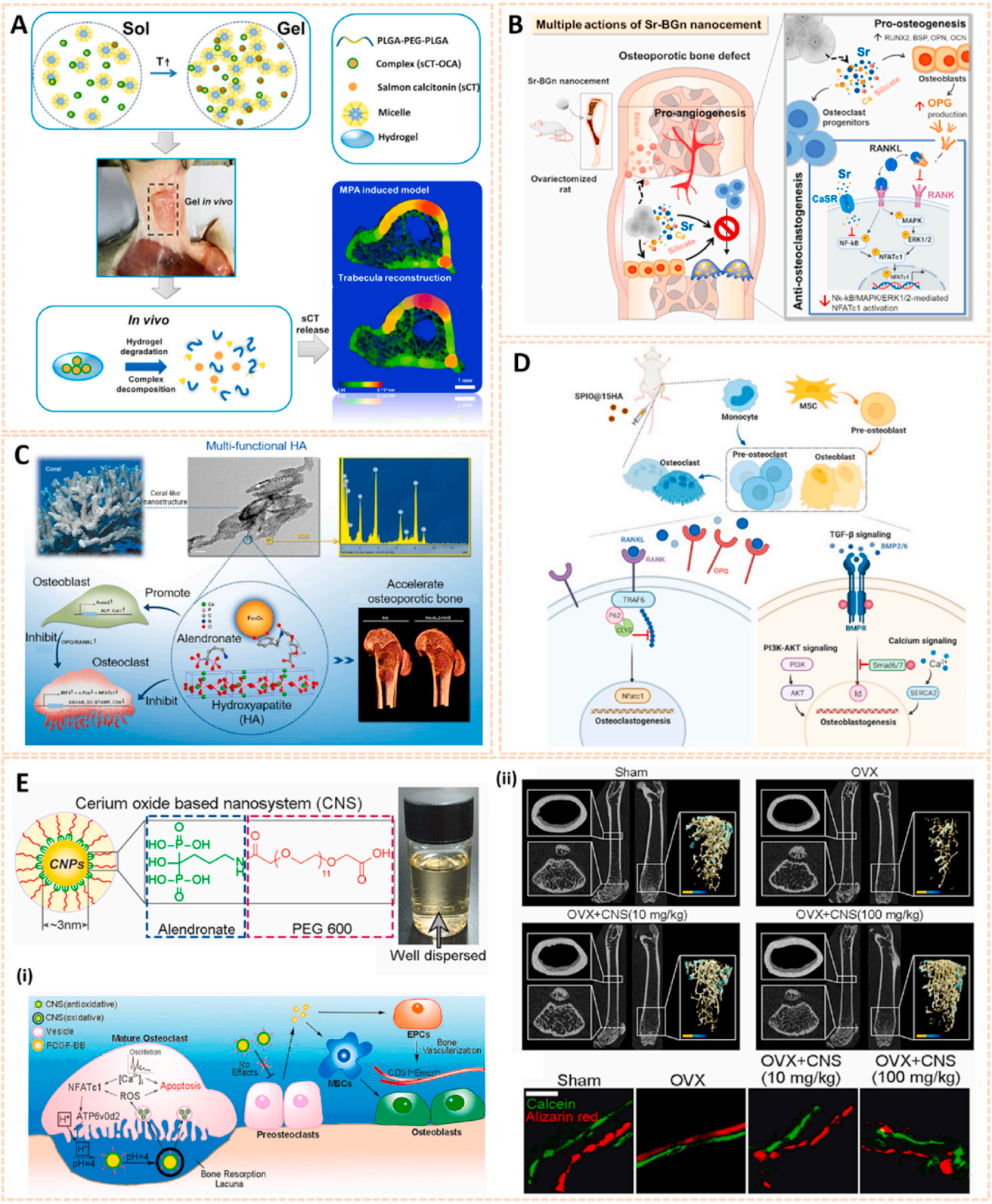

Fig. 20. Nanomaterials as drug carriers for OP treatment. A) Application of the sCT-OCA complex loaded thermosensitive PLGA-PEG-PLGA hydrogel for controlled sCT release [217]. The image reproduced with the permission from American Chemical Society. B) Schematic summarizing the multiple-actions of Sr-BGnC in the regeneration of osteoporotic bone defect [218]. The image reproduced with the permission from Elsevier Ltd. C) Chemical self-assembly of multifunctional hydroxyapatite with a coral-like nanostructure for osteoporotic bone reconstruction [219]. The image reproduced with the permission from American Chemical Society. D) Illustration of SPIO@15HA nanocomposites' impacts on BMMs oriented osteoclastogenesis and MSCs oriented osteogenesis [220]. The image reproduced with the permission from Oxford University Press. E) Schematic illustration of CNS. Synthesized CNS was well dispersed in water with bright yellow color. (i) Schematic diagram of the mechanism of CNS functioning as a pro-anabolic therapy in treating OVX mice. (ii) CNS attenuates bone loss in OVX mice [211]. The images reproduced with the permission from Elsevier B·V.

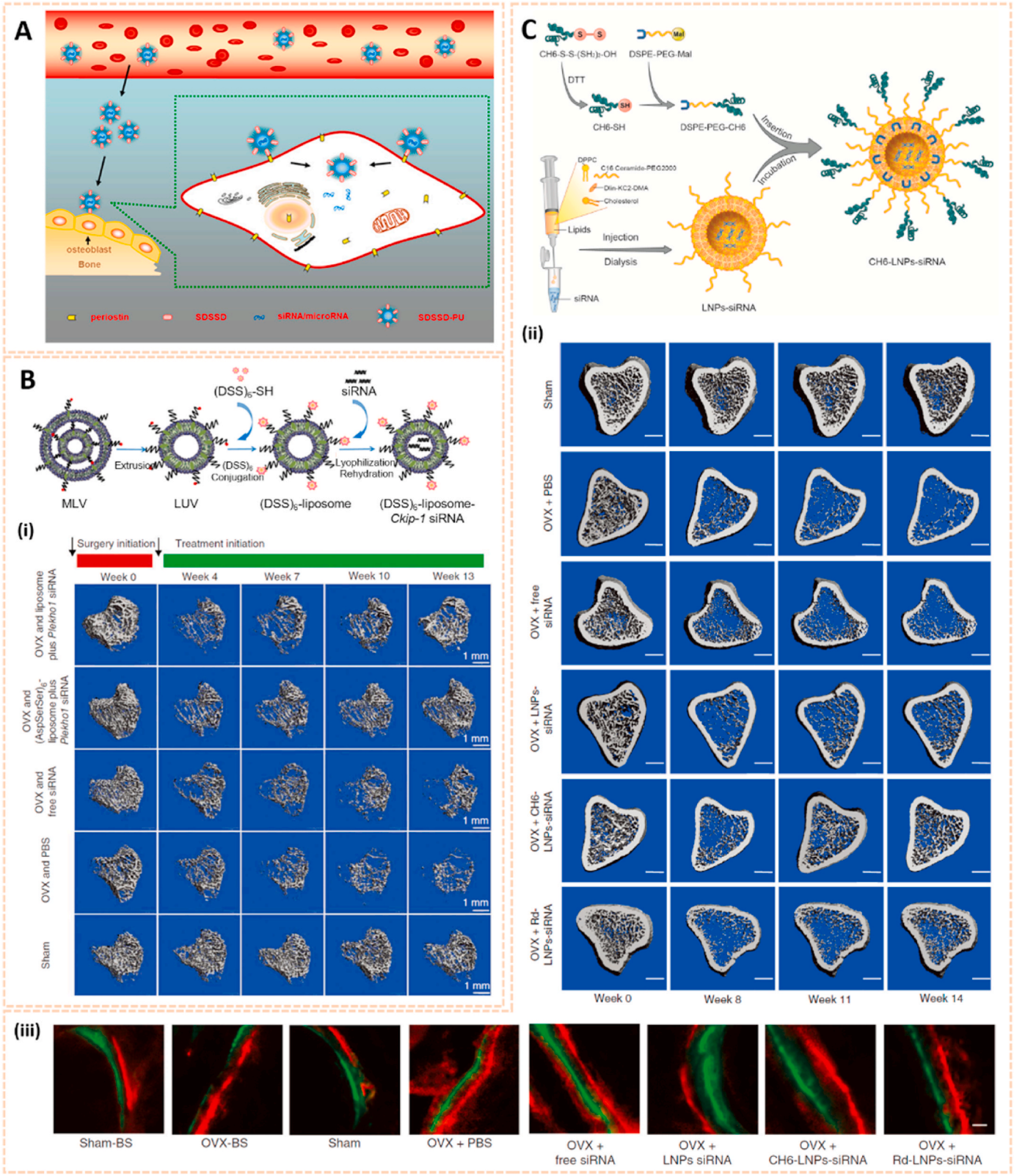

Fig. 21. Nanomaterials for gene-based therapy of OP. A) Osteoblast-targeting-peptide modified nanoparticle for siRNA/microRNA delivery [213]. The image reproduced with the permission from American Chemical Society. B) Schematic diagrams illustrating the preparation of $(DSS)_6$-liposome-siRNA. (i) In vivo microCT examination of the three-dimensional trabecular architecture in OVX-treated rats [226]. The images reproduced with the permission from Nature America, lnc. C) Preparation of CH6-LNPs-siRNA. (ii) Representative 3D microarchitecture of the proximal tibia in each group (n = 9), obtained by in vivo microCT examination. (iii) Bone formation examined by sequential labeling with fluorescent dye in non-decalcified bone sections [227]. The images reproduced with the permission from Nature America, lnc.

variety of nanomaterials, including mesoporous silica NPs, polymeric NPs, metal NPs, calcium phosphate NPs, metal oxide NPs, polydopamine NPs, liposomes, chitosan and dendrimers, have been used to enhance chemotherapeutic efficacy for osteosarcoma (Table 6).

For instance, mesoporous silica-coated bismuth sulfide NPs conjugated with RGD peptide (RGD-Bi_2S_3@MSN NPs) were developed to deliver the anticancer drug doxorubicin (DOX) to enhance osteosarcoma killing (Fig. 22A) [75]. The mesoporous pores and large surface areas were promising for drug protection and encapsulation (DOX, 99.85%). In addition, the RGD-Bi_2S_3@MSN NPs exhibited a high specificity for OS and finally accumulated in the tumor cells (10-fold more than peritumoral tissues). The drug release was triggered by NIR laser and subsequently ablated OS through the mitochondrial apoptosis pathway. This smart ultrahigh drug loading and NIR-responsive theranostic platform is a promising candidate for OS treatment.

Polymeric NPs have been widely developed in OS treatment due to their good biocompatibility and biodegradability [252]. Yin et al. synthesized polylactide NPs loaded with DOX and subsequently conjugated them with bone-seeking pamidronate (Pam-DOX-NPs) for targeted therapy of OS (Fig. 22B) [253]. The Pam-DOX-NPs selectively accumulated in bone tumors and prolonged the retention duration, thus dramatically inhibiting OS progression and skeletal malignant osteolysis. Additionally, RGD peptide-installed biodegradable polymeric micelles loaded with DOX (RGD-DOX-PM) were fabricated for high-efficiency targeted chemotherapy of OS [254]. The RGD-DOX-PM had nano-scaled particle size with a drug loading efficiency of 57%–73%. Moreover, the RGD-DOX-PM exhibited specific OS cell targeting and killing ability over healthy osteoblast cells *in vitro*.

Metal NPs have also shown great advancement in OS therapy owing to their size, conformation and thermally stable properties [255]. Wang et al. fabricated nanozyme-triggered nanomotors by decorating platinum NPs with gold nanocups and loading them with indocyanine green and human transferrin (GNCs-Pt-ICG/Tf) [256]. The nanomotors with peroxidase-like activity functioned as continuous O_2 generators by catalyzing endogenous H_2O_2 decomposition to promote active cellular targeting photodynamic therapy. In addition, albumin-bioinspired iridium oxide NPs were designed through a one-step biomineralization approach as a DOX-loaded nanoplatform with high photothermal conversion efficiency for combined chemo-photothermal therapy of OS (Fig. 22C) [257]. Additionally, Wang et al. synthesized alendronate-conjugated polydopamine NPs loaded with the chemodrug SN38 for bone-targeted chemo-photothermal therapy of malignant bone tumors and reduced the osteolytic damage of bones (Fig. 22D) [258]. These findings provide insightful perspectives for the fabrication of active targeting nanocarriers with photodynamic/photothermal therapy in a variety of biomedical applications.

To treat cancer bone metastasis, multiple targeted drug delivery systems based on nanomaterials, such as mesoporous silica NPs, calcium phosphate NPs, liposomes, metal-organic frameworks, polymeric NPs, micelles, quantum dots, metal NPs, bisphosphonate NPs and dendrimers have been developed (Table 6). For instance, mesoporous silica NPs encapsulated in gold nanorods and subsequently conjugated with zoledronic acid (Au@MSNs-ZOL) were fabricated as a bone-targeted nanoplatform for the treatment of bone metastasis (Fig. 23A) [259]. The combination of ZOL and photothermal therapy inhibited tumor growth and bone resorption through the apoptosis pathway. Similarly, mesoporous silica-covered gadolinium (III) upconversion NPs loaded with ZOL and plumbagin were developed to target osteocytes to ameliorate early bone metastasis (Fig. 23B) [260]. This multifunctional nanoplatform targeted osteocytes and released plumbagin controlled by pH, subsequently decreasing osteocytic RANKL expression. Cancer bone metastasis and osteoclastogenesis could both be attenuated significantly in vivo. These works highlight the significance of theranostic nanomedicine and bone cell-targeting therapy for bone metastasis treatment.

Micelle-based nanocarriers are also used in bone metastasis therapy. Bortezomib-loaded micelles conjugated with ALN were fabricated for bone-targeted and aryl boronate-based pH-responsive drug release for antimetastatic therapy (Fig. 23C) [261]. Additionally, integrin avβ3-targeted micelle NPs loaded with docetaxel enable targeted chemotherapy to breast cancer cells within the bone at the metastatic site [262]. This nanosystem enabled targeted delivery of the chemotherapeutic docetaxel, thus bone tumor burden could be reduced significantly with less bone destruction and less hepatotoxicity. Dendrimer-based nanoplatforms are also broadly adopted in the treatment of bone metastasis owing to their monodisperse nature, well-defined molecular weight and surface functionality properties. Arg-Gly-Asp (RGD)-targeted polyamidoamine (PAMAM) dendrimers modified with catechol and PEG ligands were synthesized for bortezomib delivery to metastatic bone tumors [263]. Bortezomib was loaded on the dendrimer via a boronate-catechol linkage with pH-responsive property. The cRGD ligand enabled internalization of the bortezomib complex by breast cancer cells. This targeted nanosystem could significantly inhibit the progression of metastatic bone cancer and tumor-associated osteolysis.

Nanoscale metal-organic framework (nMOF) drug delivery systems can also be used to promote the biodistribution of ZOL to tumors and improve its anticancer activity. Au et al. designed folate-targeted pH-responsive calcium ZOL nMOFs for the treatment of cancer bone metastasis (Fig. 23D) [239]. The modified nMOF enhanced the direct antitumor effect of ZOL by over 80% through suppression of tumor neovasculature, cell proliferation and apoptosis induction. For polymeric NPs, Vanderburgh et al. synthesized a diblock copolymer of poly-[(propylene sulfide)-*block*-(alendronate acrylamide-*co*-N,N-dimethylacrylamide)] [PPS-*b*-P(Aln-*co*-DMA)] loaded with the Gli 2 inhibitor GANT58 as a targeted delivery system to bone-associated tumors [264]. Ten mol % alendronates in the hydrophilic block exhibited a favorable balance of systemic pharmacokinetics and bone binding with the highest bone/liver biodistribution ratio. The formulation decreased the tumor-associated bone lesion area by 3-fold and increased the bone volume fraction by 2.5-fold in tibia bone metastasis. These targeted nanoplatforms provide the potential to inhibit tumor-driven OC activation and subsequent bone destruction in patients with cancer bone metastasis.

3.4.2. Nanomaterials for gene therapy toward OS cells

In addition to chemotherapy, gene therapy of bone cancer overcomes drug resistance by modulating intracellular gene expression using miRNA, siRNA and plasmid DNA (Table 6). Based on a miRNA strategy, Tiram et al. first identified three novel regulators of OS, miR-43a, miR-93 and miR-200c [245]. Then, aminated polyglycerol dendritic nanocarriers loaded with miRNA (dPG–NH_2–microRNA) were fabricated for OS therapy by reducing the expression of target genes and inhibiting cancer angiogenesis and cancer cell migration.

For the siRNA strategy of bone cancer, functionalized large pore mesoporous silica NPs with magnetic core-shell structures were designed as biocompatible siRNA nanocarriers against OS [265]. The nanocarriers exhibited a high loading capacity of siRNA (2 wt%) and strong magnetic response under an external magnetic field. The superparamagnetic magnetite nanocrystal cluster coating also increased the dispersion stability of the siRNA-loaded carrier and served as a pH-responsive release switch. Functional siRNA could be delivered into the cytoplasm of human osteosarcoma cancer cells using these nanocarriers. In addition, cationic liposomes conjugated with distearoyl-phosphatidylethanolamine-methyl-poly (ethylene glycol) (DSPE–mPEG) and subsequently loaded with DOX and JNK-interacting protein 1 (JIP1) siRNA were developed for metastatic OS treatment [266]. The DOX-loaded liposomes exhibited dual-targeted extracellular effects against EphA2 and intracellular effects against JIP1, thus overcoming OS multidrug resistance and enhancing toxicity toward OS cells.

Plasmid DNA also plays a key role in inhibiting cancer cell growth. Dextran-graft-polyethylenimine (DEX-*g*-PEI) copolymer loaded with adriamycin and plasmid pEGFP-N1 was developed against OS with low

Table 6
Summary of example nanomaterials for bone cancer.

Category	Nanomaterials	Active principle	Main results	Ref.
Chemotherapy (osteosarcoma)	Silica nanoparticles	Cancer cell membrane, ICG	• specifically target the homogenous 143B cells both *in vitro* and in vivo • enhance anticancer efficacy	[229]
	Poly (ester amide) nanoparticles	Apatinib	• distribute increasingly inside the tumor • suppress osteosarcoma stemness and enhance osteosarcoma stem-like cell apoptosis with minimal side effects	[230]
	Silver nanoparticles	Rhizophora apiculate, Ag	• reduce the precursor silver nitrate into silver nanoparticles of favorable size for tumor infiltration • possess significant cytotoxic effects against MG-63 cells	[231]
	Polydopamine nanoparticles	Paclitaxel, alendronate	• keep stable in PBS (pH 7.4), 5% glucose, plasma • display sustained drug release behavior • have stronger cytotoxicity against K_7M_2 wt osteosarcoma cells	[232]
	Liposomes	hyaluronic acid, H_2S-releasing doxorubicin	• deliver the drug within the endoplasmic reticulum (ER), inducing protein sulfhydration and ubiquitination • activate an ER stress pro-apoptotic response mediated by CHOP	[233]
	Dendrimers	Platinum, carboxyl-	• predominantly accumulate at the osteolytic lesions around bone tumors • suppress bone tumors and osteolysis mediated by photothermal ablation	[234]
	Mesoporous silica nanoparticles	Doxorubicin, lectin	• exhibit a noticeable higher internalization degree into human OS cells compared to healthy preosteoblast cells • have a cytotoxicity on tumor cells 8-fold higher than that caused by the free drug	[235]
	Platinum Nanoparticles	Doxorubicin,	• inhibit OS epithelial cells viability and proliferation in a dose-dependent manner • increase 8-oxo-G levels and induce apoptosis	[236]
	Chitosan	Methotrexate, poloxamer	• show high accumulation in cell cytoplasm region through energy-dependent endocytosis process • exhibit increased cytotoxicity in MG63 cells via apoptosis effect	[237]
Chemotherapy (cancer bone metastasis)	Liposomes	Doxorubicin, Asp_8, folate	• exclusively deliver drugs to bone • bind selectively to folate receptor-positive tumors	[238]
	Nanoscale metal-organic frameworks	Calcium zoledronate	• inhibit cell proliferation and induce apoptosis in FR-overexpressing tumor cells • increase the direct antitumor activity of Zol by 80–85%	[239]
	Micelles	Alendronate, docetaxel	• exhibit the recruitment, differentiation and resorption activity of osteoclasts • attenuate the tumorigenesis and improve animal lifespan	[240]
	Quantum dots	Doxorubicin, alendronate, Ag_2S	• ensure the long circulation time of the nanodrugs • exhibit high affinity to the bone tissue • facilitate the on-site killing of cancer cells and minimize toxicity to normal tissue • provide a facile real-time feedback on the tumor growth and therapeutic efficacy via bioluminescence	[241]
	Na_xWO_3 nanoparticles	oxygen vacancy-rich tungsten bronze	• provide PTT effects under laser irradiation (980 nm) • exhibit significant cytotoxicity against breast cancer 4T1 cell *in vitro* dose-dependently	[242]
	PAMAM dendrimers	Docetaxel, hyaluronic acid, alendronate	• show osteoclasts and tumor cells dual-targeting ability • endocytosis by the tumor cells via CD44 receptor • inhibit the activity of osteoclasts	[243]
	Polymeric nanoparticles	Paclitaxel, folic acid, alendronate	• exhibit high affinity for bone tissue • promote uptake by folate receptor-overexpressing cancer cells to augment PTX cytotoxicity • improve the survival rate of treated mice	[244]
Gene Therapy	Dendrimers	miR-34a, miR-93, miR-200c	• attenuate angiogenic capabilities of fast-growing OS • prolong the dormancy period of fast-growing OS	[245]
	Nanodiamonds	EWS-Fli-1 siRNA	• deliver siRNA into Ewing sarcoma cells and inhibit EWS/Fli-1 gene expression	[246]
	Lipopolymer	CRISPR/Cas9 plasmids	• facilitate selective distribution of CRISPR/Cas9 in both orthotopic OS and lung metastasis • enhance effective VEGFA genome editing in tumor • reduce angiogenesis and bone lesion with no detectable toxicity	[247]
Scaffolds for bone regeneration	Graphene oxide nanosheets	Tricalcium silicate	• exhibit excellent photothermal performance with the irradiation of NIR • inhibit the growth of subcutaneous tumor tissue • promote cell proliferation and the ALP activity of MC3T3-E1	[248]
	Metal-organic framework nanosheets	β-tricalcium phosphate, Cu ions	• kill osteosarcoma cells through released heat energy after exposure to NIR light (1.0 W cm^{-2}, 10 min) • support the attachments of HBMSCs and HUVECs • stimulate osteogenesis and angiogenesis	[249]
	Chitosan scaffolds	$SrFe_{12}O_{19}$, $CaSiO_3$, doxorubicin	• possess anti-tumor efficacy via the synergetic effect of DOX drug release and hyperthermia ablation • promote proliferation and osteogenic differentiation via BMP-2/Smad/Runx 2 pathway	[250]
	$CuFeSe_2$ nanocrystals	Bioactive glass	• endow scaffolds excellent photothermal performance • ablate the bone tumor cells (Saos-2 cells) and inhibit bone tumor growth • stimulate osteogenic gene expressions	[251]

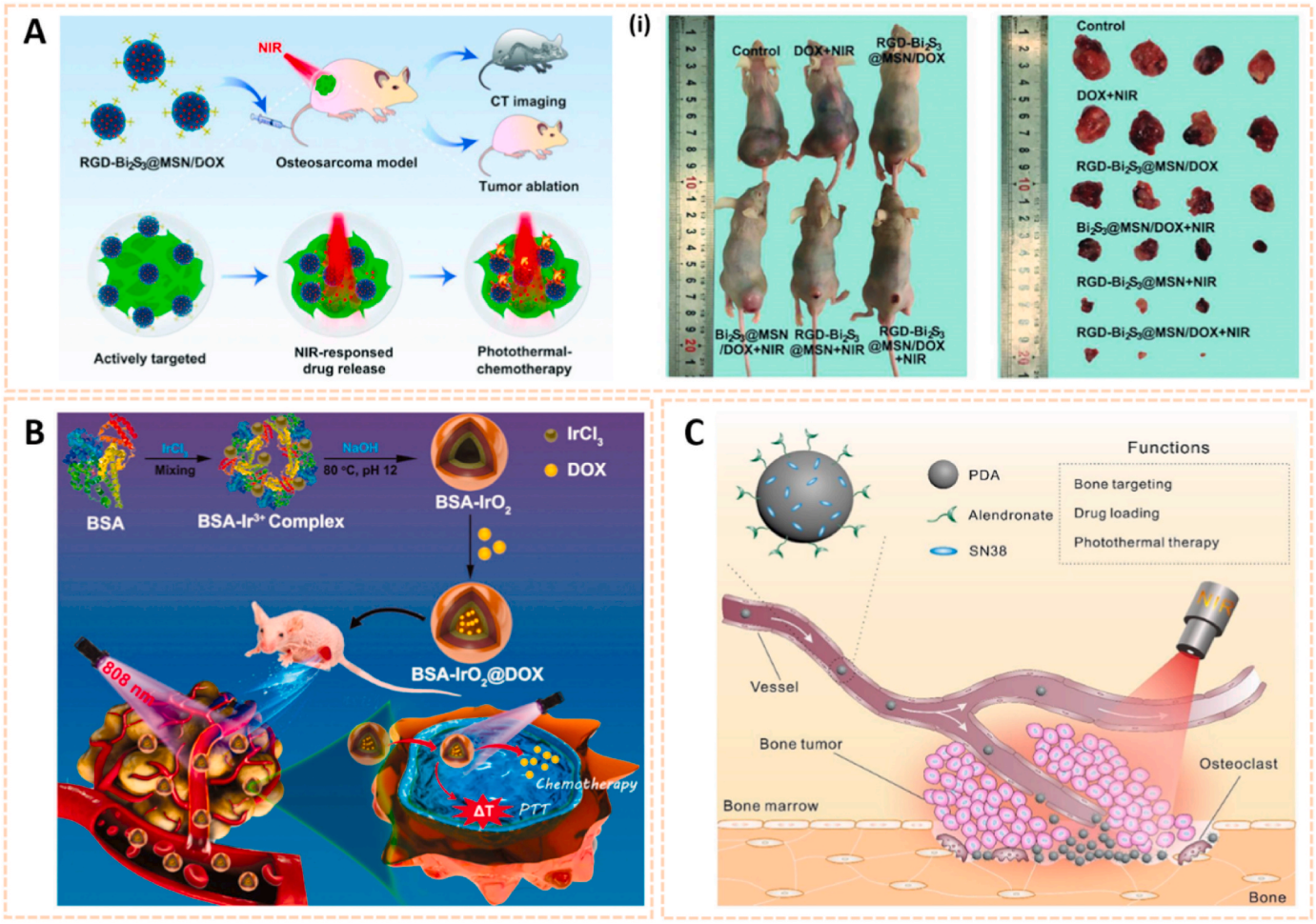

Fig. 22. Nanomaterials for chemotherapy of OS. A) The smart RGD–Bi_2S_3@MSN/DOX nanoplatform for OS real-time X-ray CT imaging and NIR-responsive photothermal therapy-chemotherapy. (i) Representative images of tumor bearing mice from different treatment groups [75]. The images reproduced with the permission from WILEY-VCH. B) Schematic illustration of the preparation of BSA-IrO_2@DOX and served as a versatile nanoplatform for mild hyperthermia-induced DOX release and synergistic chemo-photothermal therapy [257]. The image reproduced with the permission from Informa UK. C) Illustration depicts PDA-ALN/SN38-associated bone-targeted chemo-photothermal treatment of malignant bone tumor [258]. The image reproduced with the permission from Elsevier Ltd.

cytotoxicity [267]. Additionally, chitosan NPs loaded with Dz13, a DNA enzyme designed to cleave human c-Jun mRNA, were synthesized for enhanced therapeutic efficacy of OS [268]. Since vascular endothelial growth factor A (VEGFA) is highly expressed in OS, Liang et al. fabricated aptamer-functionalized PEG-PEI-Cholestero lipopolymer loaded with CRISPR/Cas9 plasmids targeted to tumor cells [247]. The functionalized nanosystem facilitated selective distribution of CRISPR/Cas9 in both orthotopic OS and lung metastasis and subsequently enhanced effective VEGFA genome editing in tumors. The nanosystem also inhibited angiogenesis and bone lesions with no detectable toxicity. These delivery systems restrained specific signaling pathways in tumor cells and could facilitate translation of plasmid DNA into clinical bone cancer treatment.

3.4.3. *Nanomaterial-based scaffolds for bone regeneration*

With a deeper understanding of nano bio-interactions and development in nanomaterial fabrication, various therapeutic strategies based on scaffolds have been formulated for the treatment of bone cancer and resultant bone defects simultaneously. These scaffolds, such as carbon-based scaffolds, nanosheet-based scaffolds, chitosan scaffolds and nanocrystal scaffolds are broadly used for photothermal therapy of OS and bone tissue engineering (Table 6).

Black phosphorus (BP) nanosheets are emerging as 2D layer-structured nanomaterials owing to their unique photothermal properties and degradability [269]. Yang et al. developed a 2D-BP nanosheet-reinforced 3D-printed BG scaffold for localized treatment of OS (Fig. 24A) [270]. The scaffolds were capable of photothermal ablation of OS and enhancing newborn cranial bone tissue. In addition, 2D borocarbonitride (BCN) nanosheet-engineered akermanite ($Ca_2MgSi_2O_7$, AKT) bioceramic scaffolds were designed as a bifunctional platform for integrating OS therapy and bone regeneration through activation of the BMP2 signaling pathway [271]. Additionally, a combination of MoS_2 nanosheets with BG scaffolds was used for the treatment of OS and bone repair (Fig. 24B) [272]. These scaffolds could rapidly and effectively elevate temperature and exhibit excellent photothermal stability under NIR irradiation. Moreover, the scaffolds inhibited the viability of bone tumor cells and increased the expression of osteogenic genes, therefore are highly promising for the treatment of bone cancer-related bone defects.

Considering the good thermal conductivity of graphene oxide (GO), GO-modified scaffolds are widely used in the treatment of cancer. Ma et al. synthesized GO-modified β-tricalcium phosphate (GO-TCP) composite scaffolds with a high photothermal effect for OS under irradiation with 808 nm NIR and a significant improvement in bone-forming ability [273]. Carbon dots (CDs) are also used to modify bone repair scaffolds. CD-doped chitosan/nanohydroxyapatite (CS/nHA/CD) scaffolds were formulated by a facile freeze-drying method [274]. The CS/nHA/CD scaffolds promoted bone regeneration, OS ablation and bacterial

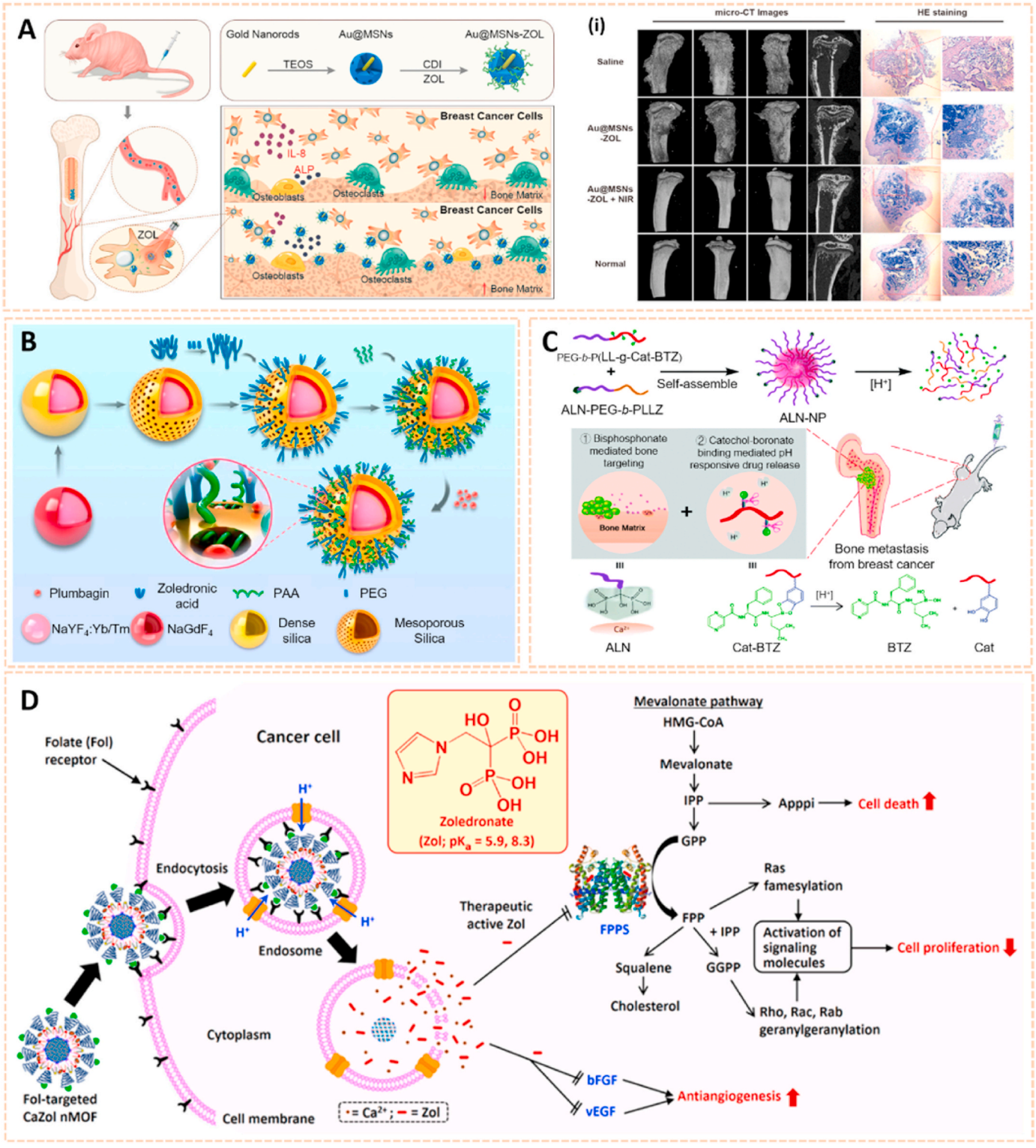

Fig. 23. Nanomaterials for chemotherapy of bone metastasis. A) Bone-targeted nanoplatform combining zoledronate and photothermal therapy to treat breast cancer bone metastasis. (i) CT images of tibias from different angles and micrographs of H&E-stained tibias [259]. The images reproduced with the permission from American Chemical Society. B) Schematic illustration of the synthesis of theranostic bone-targeting Gd(III)-doped upconversion nanoparticles PUCZP [260]. The image reproduced with the permission from American Chemical Society. C) The formation of ALN-NPs and the mechanism of combining bone targeting and pH-responsive release of bortezomib based on aryl boronate linkage for anti-metastasis therapy [261]. The image reproduced with the permission from The Royal Society of Chemistry. D) Direct anticancer activity of Fol-targeted CaZol nMOFs against a Fol-receptor-overexpressed cancer cell [239]. The image reproduced with the permission from Elsevier Ltd.

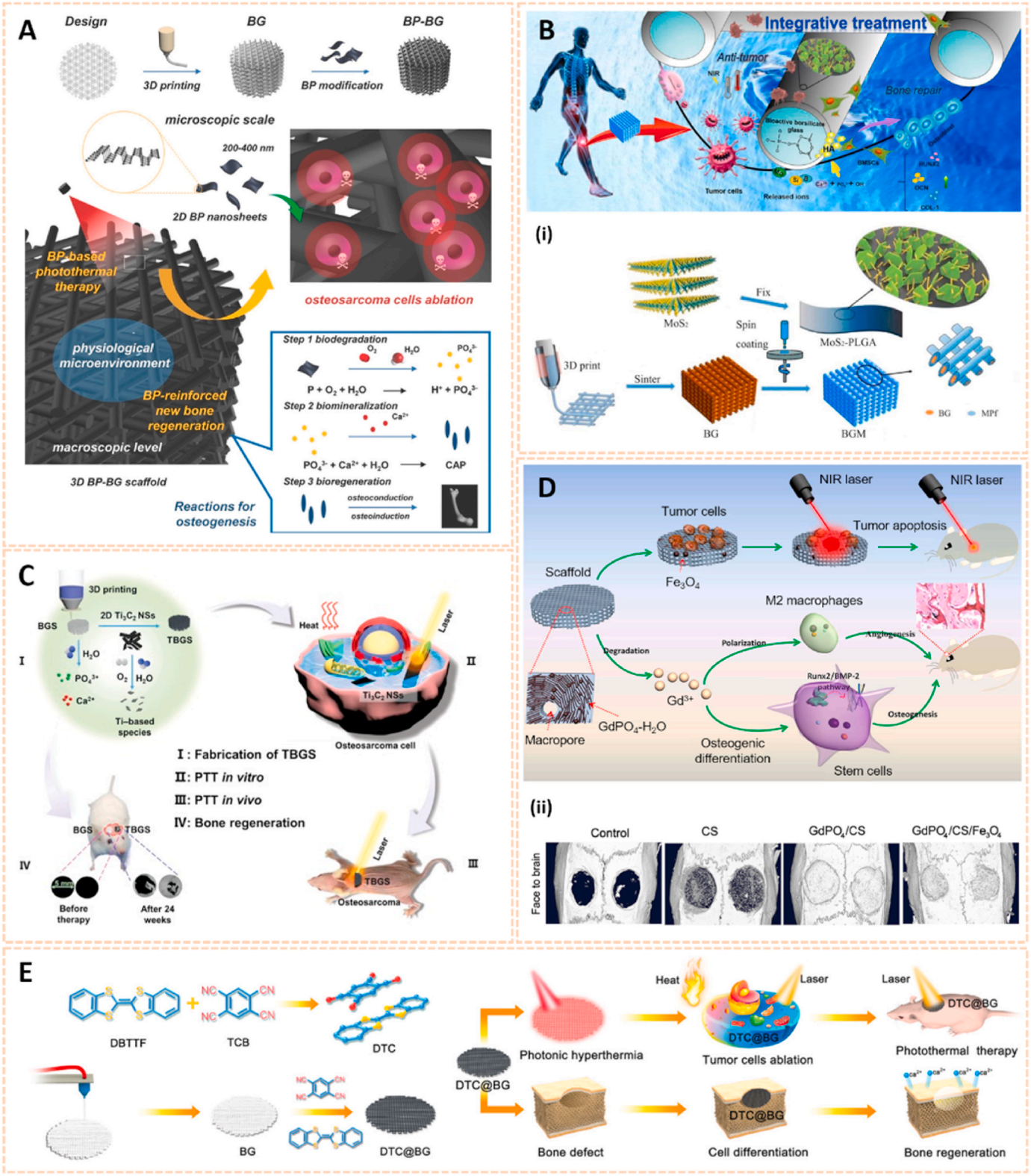

Fig. 24. Nanomaterials-based scaffolds for OS therapy and bone tissue engineering. A) Schematic illustration of the fabrication process for BP-BG scaffold and the stepwise therapeutic strategy for the elimination of osteosarcoma followed by osteogenesis using BP-BG [270]. The image reproduced with the permission from WILEY-VCH. B) Schematic diagram for investigation on the integrative treatment of anti-tumor/bone repairing with 3D printing BGM scaffolds. (i) Scheme of fabrication the integrative anti-tumor/bone repair BGM scaffolds [272]. The images reproduced with the permission from Elsevier B.V. C) Schematic illustration of the fabrication of TBGS, ablation of bone cancer, and regeneration of bone tissue [275]. The image reproduced with the permission from WILEY-VCH. D) Ordered arrangement of hydrated $GdPO_4$ nanorods in magnetic chitosan matrix promotes tumor photothermal therapy and bone regeneration against breast cancer bone metastases. (ii) Micro-CT images of calvarial defects repair model at 3 months after surgery [276]. The images reproduced with the permission from Elsevier B.V. E) Schematic illustration of the fabrication and biomedical applications of DTC@BG scaffolds [39]. The image reproduced with the permission from WILEY-VCH.

eradication. In addition, 2D Ti_3C_2 MXene-integrated 3D-printed BG scaffolds were developed to augment OS therapy (Fig. 24C) [275]. The designed scaffolds induced bone-tumor ablation by NIR-triggered photothermal hyperthermia. Meanwhile, the integration of 2D Ti_3C_2 MXene efficiently accelerated the growth of newborn bone tissue. The dual functionality of bone-tumor killing and bone tissue regeneration make these carbon-based scaffolds promising for the applications in bone tissue engineering.

In addition, magnetic Fe_3O_4 NPs and hydrated $GdPO_4$ nanorod-modified chitosan matrices scaffolds were designed for oncotherapy and bone defect healing through the BMP-2/Smad/RUNX2 signaling pathway (Fig. 24D) [276]. Similarly, magnetic $SrFe_{12}O_{19}$ NP-modified BG/CS porous scaffolds were fabricated for bone regeneration and photothermal therapy of bone cancer [277]. Additionally, NIR-absorbing organic cocrystal (DTC)-modified BG scaffolds enabled photonic OS hyperthermia and facilitated bone defect regeneration (Fig. 24E) [39]. These findings offer a new avenue to ablate malignant bone tumors and facilitate new bone formation for the treatment of bone cancer and resultant bone defects.

3.5. Nanomaterials in bone infection

3.5.1. Nanomaterials as implant coatings with antibacterial activity

Implants are the most commonly used materials in orthopaedic surgeries, aiming to reconstruct bone and joints. However, implant-related infection is a catastrophic complication after surgery due to its potential for reoperation, long-term use of antibiotics, prolonged length of stay, distress for patients and economic burden on societies [278]. Therefore, various nanomaterials have been developed as implant coatings for preventing and treating implant-related infection (Table 7).

Fabricating coating with specific metal nanomaterials can endow implants with antibacterial properties. TiO_2 nanotubes with embedded silver oxide NPs were prepared with long lasting antibacterial property [289]. The Ag^+ released from the coating strongly killed *Escherichia coli* and *Staphylococcus aureus* without showing cytotoxicity on the osteoblasts. In addition, a hybrid magnesium/zinc-metal organic framework coating (Mg/Zn-MOF74) was fabricated on alkali-heat treated titanium surface (Fig. 25A) [290]. The Mg/Zn-MOF74 coating was sensitive to the bacterial acid microenvironment and displayed strong antibacterial ability against *Escherichia coli* and *Staphylococcus aureus*. The coating also exhibited anti-inflammatory property as compared to the pristine Ti substrates. These metal nanomaterial-based coatings could inhibit bacterial infection and promote bone regeneration around implants after implantation.

Smart systems prepared from various nanomaterials have provided great opportunities to treat bone infection and serve as multifunctional systems for the delivery of antibiotics. These systems respond to multiple microenvironmental stimuli, such as NIR-light, pH and enzymes [283,291,292]. Su et al. designed a sulfur (S)-doping Ti implant with oxygen deficiency for the treatment of bacterial infected bone implants by photo-sonotherapy (Fig. 25B) [293]. This coating exhibited a superior bactericidal efficiency of over 99.9% against *Staphylococcus aureus* under 15 min NIR and ultrasound treatment. In addition, Yuan et al. fabricated a multifunctional hybrid coating consisting of mesoporous polydopamine NPs, photosensitizer indocyanine green and RGD peptide to eradicate biofilms on implant via NIR triggered photothermal and photodynamic therapy (Fig. 25C) [294]. The therapeutic coating effectively killed *Staphylococcus aureus* biofilms with an efficiency of 95.4% under NIR. Moreover, the coating exhibited osteogenesis and osseointegration properties after biofilm eradication. Additionally, Hong et al. synthesized a hybrid coating of Bi_2S_3 nanorod arrays loaded with Ag_3PO_4 NPs to eliminate biofilm on bone implants upon NIR (Fig. 25D) [295]. The coating exhibited a high antibacterial efficiency of 99.45% against *Staphylococcus aureus* and 99.74% against *Escherichia coli* after 15 min NIR irradiation. Moreover, Wu et al. proposed a win-win strategy for both delivering antibacterial therapy and fostering bone regeneration [296]. Black phosphorus nanosheets (BPs) and zinc sulfonate ligand (ZnL_2) were integrated into the surface of a hydroxylapatite (HA) framework. The BPs contribute to photothermal effects and BPs-ZnL_2 causes envelope stress to bacteria under NIR irradiation and subsequently releases Zn^{2+} and PO_4^{3-} to facilitate osteogenesis. These NIR light-mediated strategies not only can be used to eradicate biofilm in vivo in a remotely controllable fashion but also provide insights into the design of multifunctional biomaterials in other fields. However, there are still some notable points, including the laser power density, temperature and duration of NIR light irradiation. The NIR-induced photothermal effect should be well controlled below the threshold to achieve bacteria eradication and avoid damage to normal cells and

Table 7
Summary of example nanomaterials for bone infection.

Category	Nanomaterials	Active principle	Main results	Ref.
Implant coating	Silver nanoparticles/PLGA coating	Ag^+	• exhibit strong antibacterial activity • promote pre-osteoblasts proliferation and maturation	[279]
	Bioactive glass nanoparticles/PCL coating	Cu^{2+}	• induce more calcium phosphate formation on the coating surface • inhibit the growth of *S. carnosus* and *E. coli* by Cu^{2+}	[280]
	Ti nanocolumn coating	Ti nanocolumn	• exhibit strongly impaired *S. aureus* adhesion and subsequent biofilm formation	[281]
	TiO_2 nanorod coating	Polydopamine, TiO_2, MoS_2, RGD	• kill bacteria noninvasively upon co-irradiation of 660 nm visible light and 808 nm NIR light through generating hyperthermia and ROS • promote the osteogenic activity	[282]
	Chitosan coating	hyaluronic acid, gentamicin, deferoxamine	• drug release was associated with degradation of multilayers triggered by exogenous hyaluronidase • display effective antifouling and antibacterial properties against *E. coli* and *S. aureus* • enhance the adhesion, proliferation and osteo/angio-genic differentiation of MSCs	[283]
	Polymeric coating	Vancomycin, niosomes	• prolong drug release up to two weeks • exhibit no cytotoxic effects towards normal cells • control bacterial colonization and biofilms formation	[284]
Platforms for bone infection	Chitosan scaffolds	Vancomycin, ZIF8 nanocrystals	• vancomycin encapsulation efficiency for ZIF8 nanocrystals was 99.3% • vancomycin was released in a pH-controlled manner • inhibit the activity of *S. aureus*	[285]
	nano-hydroxyapatite scaffolds	Ag^+, nano-hydroxyapatite	• exhibit an initial burst release of Ag^+ and followed by a slow controlled release up to 39 days	[286]
	Black phosphorus nanosheets	Black phosphorus	• exhibit excellent NIR photothermal performance and good biocompatibility • enhance mineralization and bone regeneration	[287]
	MoOx-hydroxyapatite nanoparticles	Hydroxyapatite, MoOx	• promote the death of pathogen microorganisms • serve as a real-time imaging nanoplatform against bone infection	[288]

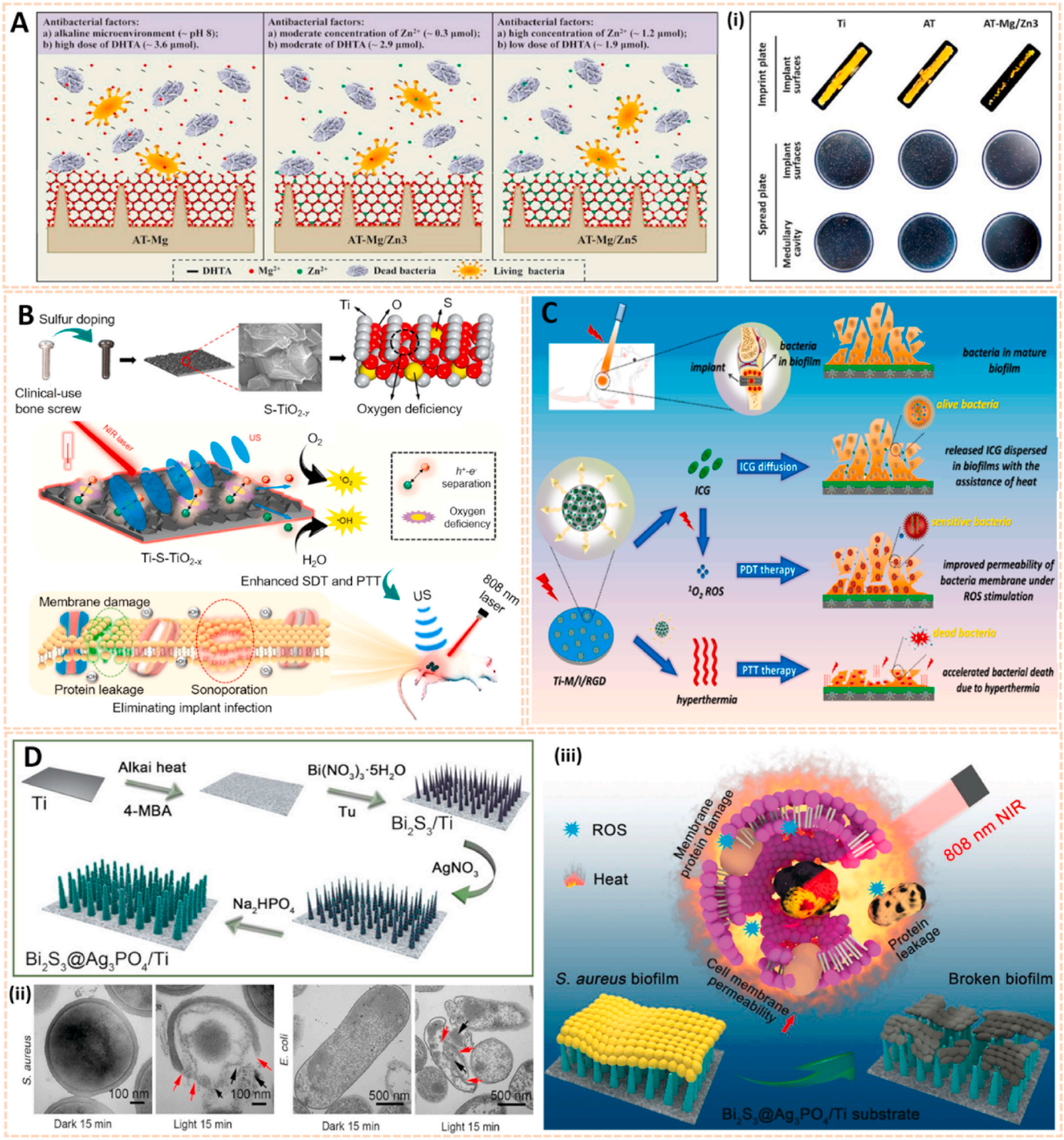

Fig. 25. Nanomaterials as implant coating with antibacterial activity. A) illustration scheme of potential antibacterial mechanisms of AT-Mg, AT-Mg/Zn3 and AT-Mg/Zn5 substrates. (i) imprint and spread plate images of *S. aureus* seeding on different implant surfaces or surrounding medullary cavities after implantation for 3 d with bacterial infection [290]. The images reproduced with the permission from Elsevier Ltd. B) Schematic illustration that shows the sulfur-doped clinically used bone screw has enhanced sonocatalytic-photothermal ability by creating oxygen deficiency and exhibits efficient bone infection therapy [293]. The image reproduced with the permission from American Chemical Society. C) Schematic illustration revealing the elimination process of already-established *S. aureus* biofilm on Ti-M/I/RGD implant in vivo, through NIR triggering remotely controlled PDT/PTT synergistic strategy [294]. The image reproduced with the permission from Elsevier Ltd. D) Illustration for the synthesis procedures for Bi_2S_3@Ag_3PO_4 nanorod arrays on Ti plates. (ii) Antibacterial efficiency against *S. aureus* and *E. coli*. (iii) The antibiofilm mechanism diagram of PDT and PTT induced by Bi_2S_3@Ag_3PO_4/Ti under 808 nm NIR light illumination toward bacteria [295]. The images reproduced with the permission from WILEY-VCH Verlag GmbH.

tissues. Commonly, mild local hyperthermia (40–42 °C) is recommended to promote the mineralization process and enhance bone healing without affecting cell viability [297]. Therefore, the development of more sensitive and accurate monitoring systems is needed to adjust NIR irradiation, avoid overheating and subsequent damage. In addition, the role of different stimuli on nanomaterial properties and performances should be fully understood in the future.

Several nanomaterials that respond to pH changes have been developed to treat bone infection. Tobramycin-loaded micelles in nanostructured multilayer coatings of chitosan/heparin were fabricated as a novel pH-responsive strategy to treat implant-related infection [298]. Tobramycin-embedded micelles showed fast release at pH 7.4 and slow release under acid conditions owing to the electrostatic interaction between tobramycin and heparin. In addition, Tao et al. designed a pH-responsive levofloxacin-loaded zeolitic imidazolate framework-8 (ZIF-8@Levo) layer-by-layer coating for inhibiting bacteria-associated infection and enhancing osseointegration (Fig. 26A) [299]. This coating eliminated *E. coli* and *S. aureus* by creating a marginally alkaline microenvironment and releasing Zn^{2+} and levofloxacin. Additionally, pH-sensitive naringin-zinc oxide NPs were designed as a novel coating on Ti substrate for eradicating bacteria, enhancing osteogenesis and inhibiting osteosarcoma (Fig. 26B) [300]. The accumulation of ROS induced by the coating could eliminate bacteria and induce osteosarcoma cell apoptosis via ROS/ERK signaling pathway. These pH-response strategies combat bacteria-mediated acidification of the local microenvironment and enhance bone formation for potential orthopaedic applications.

Enzymes are one of the common invasion factors utilized by bacteria to adhere to implants. Sutrisno et al. developed hyaluronidase-responsive biocompatible multilayers of chitosan (Chi)/sodium hyaluronate-lauric acid (SL) onto the surface of BMP2 loaded Ti nanotubes to prevent bacterial infection [301]. The degradation of SL multilayer was triggered by exogenous hyaluronidase at the initial stage of implantation and subsequently exhibited antibacterial properties against both *E. coli* and *S. aureus*. In addition, hydrolytically degradable nanolayered implant coatings loaded with antibiotics gentamicin and BMP2 were fabricated for eradication of biofilms and bone tissue repair (Fig. 26C) [302]. The gentamicin in the top layers was released rapidly to eradicate infection at the beginning. Following sustained release over several weeks, the underlying BMP2 induced significant mechanically competent bone formation. The multilayered implants with the host tissue improved bone-implant interfacial strength 15-fold compared with the uncoated one. These findings show the potential of enzyme-responsive layered release strategy for the treatment of implant-related infection.

3.5.2. *Nanomaterial-based platforms for bone infection*

Treatment of bone infection such as osteomyelitis remains a great challenge in the clinic. Uncontrolled bone infection leads to serious sepsis, bone erosion and even potential lifethreatening. Therefore, several nanomaterial-based strategies have been developed to treat osteomyelitis (Table 7).

Composited scaffolds can serve as therapeutic platforms for antibiotics and antibacterial ions. Feng et al. synthesized nanocomposites consisting of hollow metal-organic framework (HNTM), MoS_2 nanosheets and a red cell (RBC) membrane for the efficient treatment of

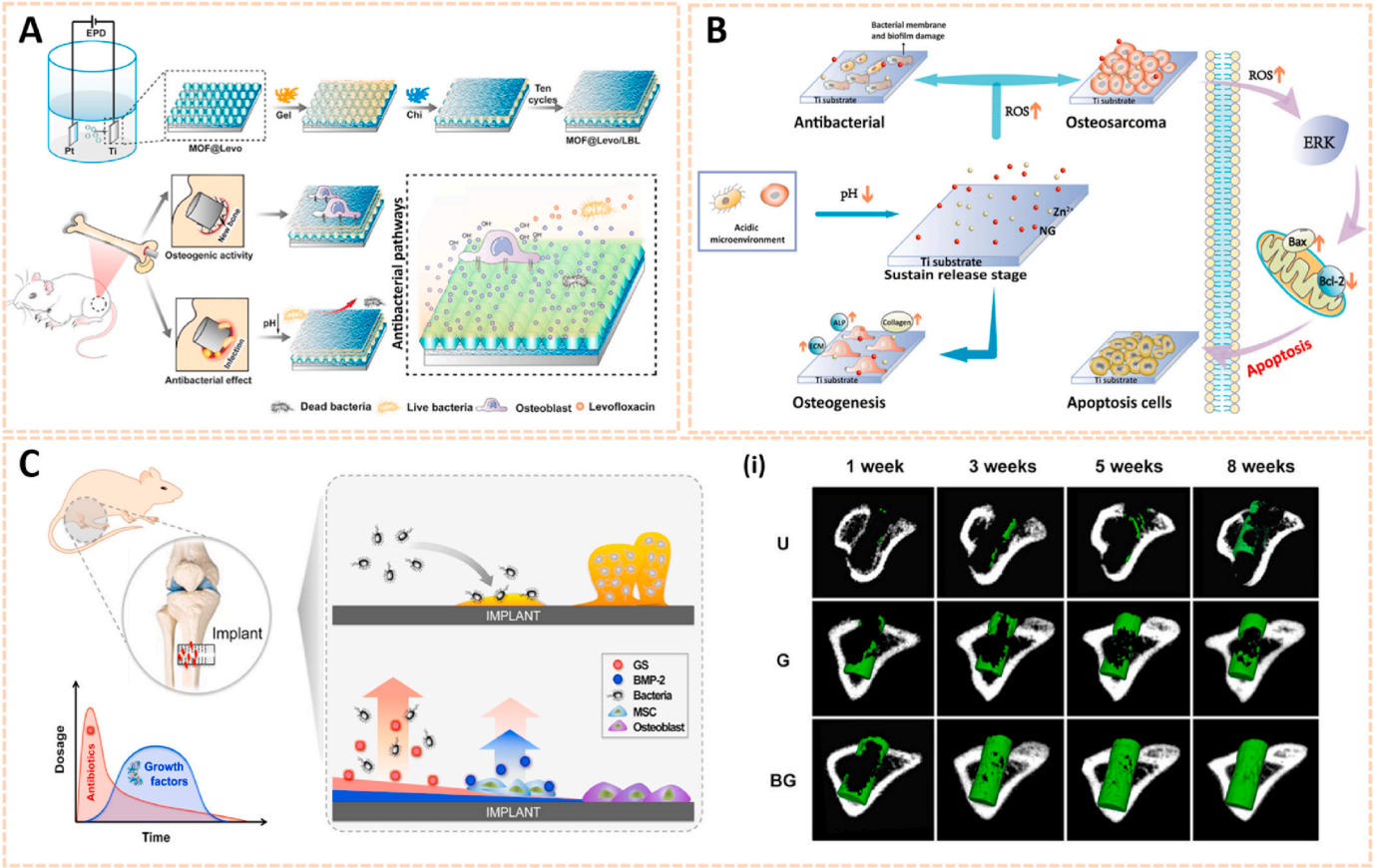

Fig. 26. pH-responsive and hydrolytically degradable nanomaterials for implant-related infection. A) Schematic illustration of ZIF-8@Levo coating onto Ti implant and potential antibacterial pathways of the ZIF-8@Levo/LBL implant for infected femur treatment [299]. The image reproduced with the permission from Elsevier B. V. B) Schematic diagram of the regulation mechanism of Ti–ZnO-PBA-NG on the cellular molecular level [300]. The image reproduced with the permission from Wiley Periodicals, lnc. C) Programmed sequential dual therapy delivery strategy to win the "Race to the Surface" against bacteria. (i) Radiographs and 3D reconstruction of new bone around implants at 1, 3, 5, and 8 weeks after revision [302]. The images reproduced with the permission from American Chemical Society.

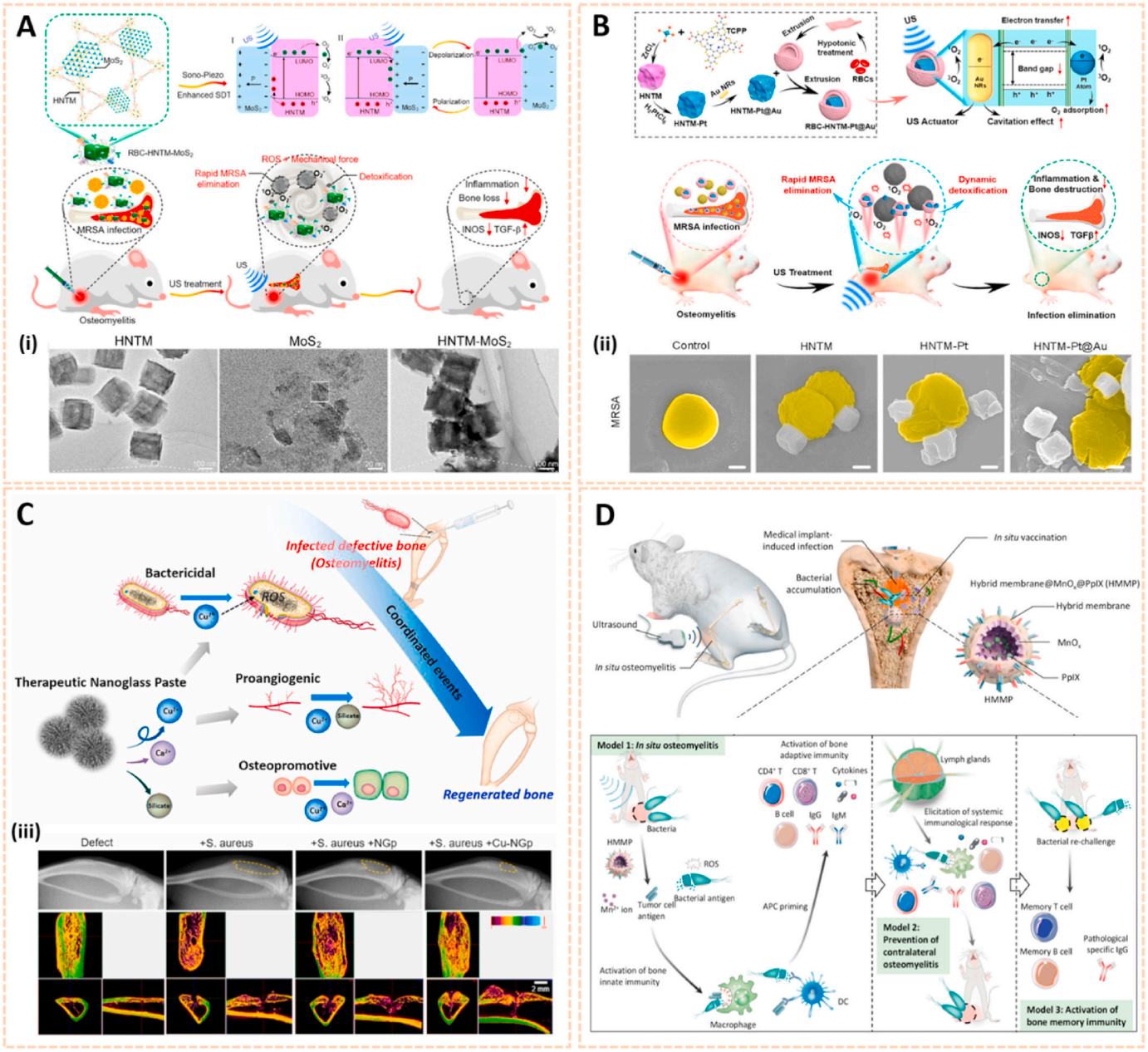

Fig. 27. Nanomaterials-based platforms for bone infection. A) Sonocatalytic mechanism of HNTM-MoS_2 and the efficient SDT treatment of osteomyelitis through rapid MRSA elimination and detoxification. (i) HRTEM images of HNTM, MoS_2 nanosheets, and HNTM-MoS_2 [303]. The images reproduced with the permission from American Chemical Society. B) Synthesis of the RBC-HNTM-Pt@Au, sonocatalytic mechanism, and the treatment of osteomyelitis through efficient SDT (ii) Corresponding SEM images of the MRSA [304]. The images reproduced with the permission from American Chemical Society. C). Schematic summarizing the multiple therapeutic actions of Cu-NGp coordinated in the osteomyelitis treatment (iii) X-ray images and the densitometry analyses [305]. The images reproduced with the permission from Elsevier Ltd. D). Schematics of HMMP In Situ Nanovaccination [307]. The image reproduced with the permission from American Chemical Society.

osteomyelitis (Fig. 27A) [303]. The RBC-HNTM-MoS_2 exhibited strongly antibacterial efficiency of 98.5% against *MRSA* under 15 min ultrasound treatment. Similarly, Au nanorod, HNTM and RBC were engineered as an ultrasound-activated single-atom catalyst for effectively treating *MRSA*-infected osteomyelitis under ultrasound irradiation (Fig. 27B) [304]. The RBC-HNTM-Pt@Au exhibited an efficient ultrasound propelled ability to dynamically neutralize the secreted toxins of *MRSA*. In addition, nanoglass paste loaded with silicate, calcium and copper was prepared as a multifunctional platform with antibacterial, proangiogenic and osteogenic properties (Fig. 27C) [305]. The copper in the nanoglass paste effectively killed gram-positive and -negative bacteria by inducing high intracellular ROS levels. Additionally, vancomycin loaded chitosan/gelatin-strontium incorporated hydroxyapatite scaffolds were synthesized against chronic osteomyelitis infection [306]. The scaffolds exhibited effective antibacterial activity combating *MRSA* and *methicillin-sensitive Staphylococcus aureus* (*MSSA*) with a sustained release of vancomycin.

Interestingly, an in situ vaccination strategy for innate and adaptive immunity activation has been proposed for the treatment of bacterial osteomyelitis (Fig. 27D) [307]. PpIX-encapsulated hollow MnOx coated with a hybrid membrane derived from both macrophage and tumor cell lines was engineered as a biomimetic nanomedicine. The in situ nanovaccination evoked local and systemic antibacterial immunological responses, together with memory adaptive immunity against bacterial relapse. Hydrogels have also been widely used as antibacterial nanomaterials. Peng et al. designed a biodegradable thermosensitive

mPEG-PLGA based hydrogel loaded with teicoplanin for effectively treating osteomyelitis in rabbits [308]. The injectable hydrogel provided a 100% encapsulated rate, sustained release of teicoplanin and in situ gelling at the targeted tissue. These multifunctional nanoplatforms hold great promise for the therapy of bone infection.

3.6. Nanomaterials in other bone-related diseases

Various nanotherapeutic systems have been employed in other bone-related diseases, such as bone fracture, bone defect and spinal cord injury. For the treatment of bone fracture, there are numerous therapeutic agents. However, the blood concentration of these agents is almost always limited to showing pharmacological action at the fracture site. Therefore, targeted delivery systems such as nanoparticles and hydrogels have been developed for fracture healing [309,310].

The migration and proliferation of endogenous MSCs at the fracture site is a key step for accelerating bone fracture healing [311]. Based on this, porous Se quantum dot-modified SiO_2 nanocomposites were fabricated for the treatment of bone fracture [312]. Se@SiO_2 enhanced the migration and osteogenic differentiation of MSCs through the SDF-1/CXCR4 signaling pathway and reversed H_2O_2-induced apoptosis, thus promoting bone fracture healing. In addition, peptide-functionalized poly (styrene-*alt*-maleic anhydride)-*b*-poly (styrene) NPs loaded with β-catenin agonists were synthesized as a fracture site-targeted delivery platform for expediting fracture healing (Fig. 28A) [313]. Specifically, increased bone bridging, ~4-fold greater torsional rigidity, and greater volumes of newly deposited bone were observed after 1-month treatment, indicating expedited fracture healing. For improved treatment of delayed fracture union, bone-targeted liposomes loaded with the bone anabolic agent salvianic acid A (SAA-BTL) were

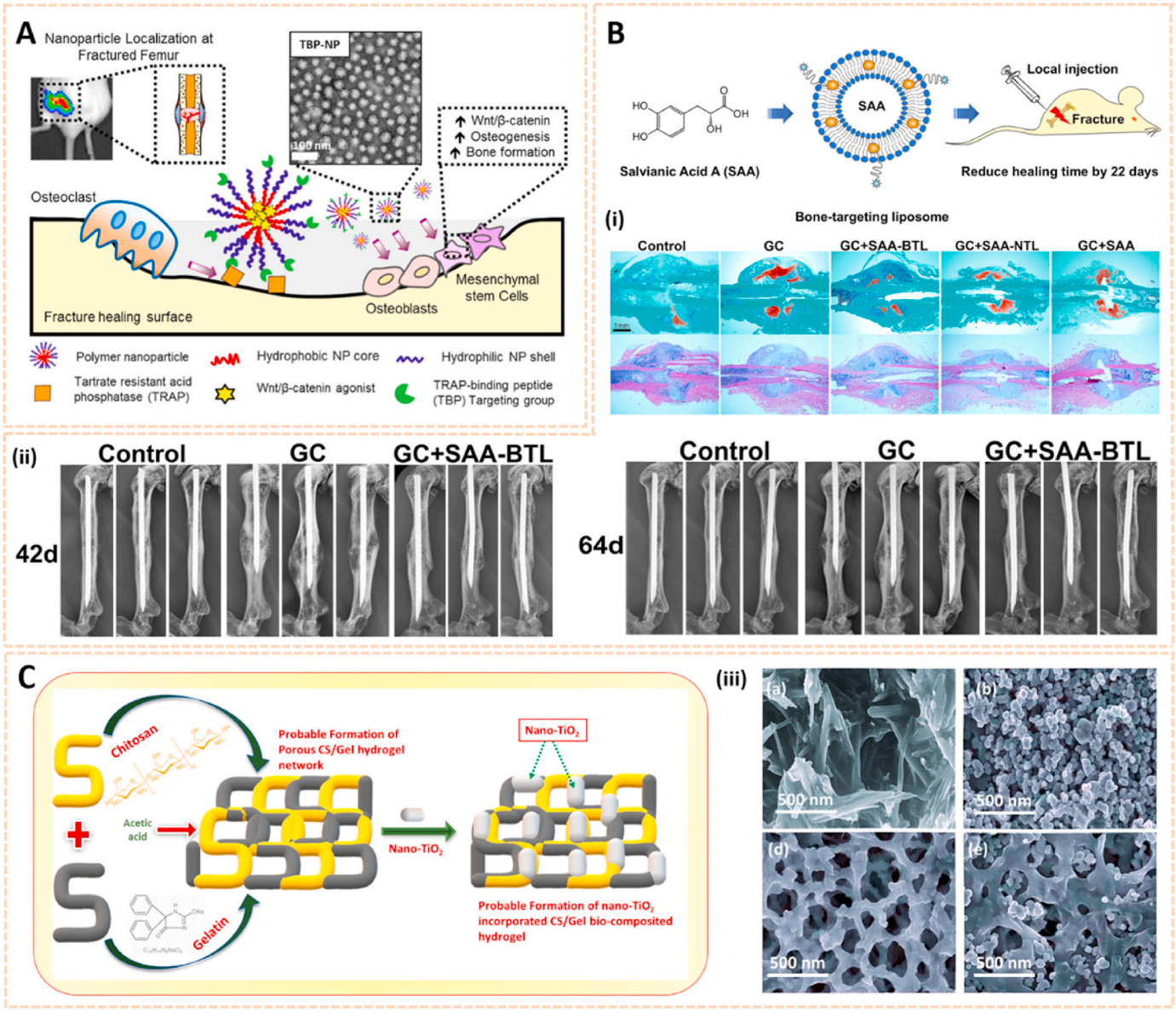

Fig. 28. Nanomaterials for bone fracture therapy. A) Schematic representation of TRAP-binding peptide-functionalized NPs for targeted delivery of β-catenin agonist for fracture healing [313]. The image reproduced with the permission from American Chemical Society. B) Bone-targeting SAA liposome for delayed fracture union. (i) Representative Safranin O and H&E staining of fracture callus at 18th day post closed femoral fracture. (ii) Series of representative lateral radiographs comparison of the fracture sites at 42 and 64 days post fracture of different treatment groups [314]. The images reproduced with the permission from Elsevier Inc. C) Experimental scheme exhibits the probable formation of TiO_2 incorporated Ge/CS biocomposite hydrogel structure. (iii) The FE-SEM morphological observations of prepared samples ((a) Chitosan, (b) TiO_2, (d) Gelatin/chitosan and (e) TiO2-Gel/CS bio-composites hydrogel) [316]. The images reproduced with the permission from Elsevier Ltd.

developed with pyrophosphorylated cholesterol (Fig. 2BCE) [314]. Locally administered nanomedicine significantly improved fracture callus formation and micro-architecture with an accelerated mineralization rate in the callus, indicating a promising therapeutic candidate for delayed bone fracture union.

Hydrogels are crosslinked hydrophilic polymeric networks that can be swelled but not dissolved in water [315]. A titanium oxide (TiO_2) NP-incorporated gelatin/chitosan matrix was designed as a bio-composited hydrogel system (Fig. 28C) [316]. The TiO_2 incorporated hydrogel enhanced osteoblasts survival with no toxicity, thus accelerating bone fracture healing. In addition, chitosan-based injectable hydrogels conjugated with cellulose nanocrystals were fabricated for vertebral compression fracture repair [317]. These nanosystems show a great potential for bone tissue engineering.

The angiogenesis in the defect area is a key factor for promoting bone formation and functional restoration. Based on this strategy, several nanomaterial-based scaffolds have been fabricated to drive angiogenesis or deliver angiogenic agents to the target tissues for vascularized bone regeneration. The common method is incorporating nanoparticles, nanosheets or nanofibers with different natural or synthetic materials, such as graphene oxide [318], bioceramics [319], silk fibroin [320], polycaprolactone [321], metal [322] and collagen [323]. For instance, graphene oxide-copper nanocomposites (GO-Cu) were used to coat porous calcium phosphate scaffolds [324]. The GO-Cu nanocomposites distributed uniformly on the surfaces of scaffold with prolonged release of copper icons. The GO-Cu coating could activate HIF-1α and increase the expression of VEGF and BMP-2, thus enhanced vascularized bone regeneration through ERK1/2 signaling pathway. In addition, nanofibrin stabilized calcium sulfate incorporated chitin (chitin-CaSO4-nFibrin) hydrogel system was synthesized [325]. The chitin-CaSO4-nFibrin gel was injectable with good moldability and temperature stable. The gel system could improve early cell attachment and promote osteo-differentiation via enhanced angiogenesis. Nano-bioactive glass could also be added to the scaffolds for bone tissue engineering. PLGA incorporated micro-nano bioactive glass porous scaffold was designed through a simple phase separation method [326]. The scaffold enhanced the attachment and proliferation of HUVECs and BMSCs, subsequently up-regulated the expression of angiogenic marker CD31 and osteogenic marker ALP. Nanoscaffolds could also perform as carriers of drugs or proteins with angiogenesis effect. Mesoporous silicate nanoparticles incorporated 3D nanofibrous gelatin scaffold was developed for dual-delivery of BMP2 and deferoxamine (DFO) [327]. The DFO and BMP2 were released from scaffold with different release rates (10 days and 28 days). The early release of DFO activated HIF-1α and trigger angiogenesis, subsequently improved BMP2-induced osteogenesis for bone tissue engineering.

Despite advances of therapeutic scaffolds synthesized to enhance angiogenesis and osteogenesis, most studies have simply focused on the histological manifestations of angiogenesis. However, the crosstalk between endothelial cells and osteoblasts have not been fully elucidated. Moreover, the spatial and temporal dynamics connections of bone tissues with an active vascular network is also a major concern for bone tissue repair and reconstruction. Therefore, a deeper understanding of the crosstalk and spatiotemporal regulation of angiogenesis and osteogenesis is still an urgent challenge for bone tissue engineering scaffolds.

Apart from bone tissue engineering, several nanomaterials are widely used for the treatment of spinal cord injury. Polycaprolactone-based nanoparticles loaded with methylprednisolone sodium succinate (MPSS) were synthesized as a localized delivery platform for spinal cord injury therapy [328]. The nanodelivery system inhibited the expression of inflammatory cytokines and rescued the damaged spinal cord. Additionally, Gaudin et al. developed lipid squalene conjugated with squalenoyl adenosine, and the subsequent formation of nanoassemblies provided neuroprotection against spinal cord injury [329]. Additionally, a multifunctional tetrahedral framework nucleic acid (tFNAs) system was established with miRNA-22 to modulate the crosstalk between Schwann cells (SCs) and macrophages for more effective rehabilitation of peripheral nerves [330]. The nanosystem could amplify the ability of SCs to recruit macrophages and promote their pro-healing M2 polarization. These nanomaterials represent a new possibility for enhancing spinal cord repair and may provide direction for future research in this area.

4. Conclusion and future perspectives

Timely diagnosis, prompt management and treatment of bone-related diseases have become considerable challenges for all clinical and research personnel. With advances in nanotechnology, various nanomaterials with special functions and unique structures have been fabricated for bone-related disease medical applications. In this review, we provide a comprehensive overview of updated nanomaterials for biological imaging, biomarker detection and therapy of orthopaedic disorders. Despite the impressive progress of these advanced theranostic nanomaterials, critical problems remain that make them difficult to translate into the clinic.

The nanotoxicity of nanomaterials has attracted much attention due to their chemical or physical damage to healthy cells [331]. Unlike regular chemical toxicants, the potential toxicity related to nanomaterials is synthetically affected by numerous factors, including size, shape, surface charge, chemical composition, dose and solubility. For instance, NPs with a smaller size could cause greater toxicity than large-size NPs owing to their ability to penetrate the skin, lungs and brain [332]. Moreover, the measured size might not be the same as the actual size after administration due to possible reactions caused by dispersion within the physicochemical microenvironment. Such reactions might make it difficult to determine the actual source of toxicity. In addition, NPs with spherical shapes usually undergo endocytosis much easier and faster than tube- and fiber-shaped NPs. Moreover, the cationic surface charge exhibits greater toxicity [333]. Therefore, endogenous biomimetic nanomaterials indicate a direction for nanomaterial fabrication to reduce immunogenicity and enhance biological security.

Regarding the drug-loading capacity and delivery efficiency of nanomaterials, there is still much room for improvement. Although the surface area of nanomaterials is large for high loading capacity, the drug concentration is usually limited to reach therapeutic effects in most cases [334]. Moreover, when the drugs only weakly interact with the surface of nanomaterials, the drugs are consumed before reaching the targeted position. Additionally, organs such as the liver, kidney and spleen might trap nanomaterials as foreign substances and subsequently eliminate them [335]. As a result, repeated administration with a large dose is needed, thus leading to more adverse effects. Therefore, there is an urgent need to develop nanomaterials with higher loading efficiency and physiochemical stability, and a systematic understanding of the interactions of nanomaterials with organs is required to reduce the filtration and elimination of nanomaterials before they reach therapeutic sites.

Controlled multiphase drug release kinetics are gaining popularity due to their ability to enhance drug synergism and therapeutic efficacy [336]. Multiphasic delivery systems have been developed to automatically respond to self-regulated stimuli, such as endogenous pH, NIR and specific molecules in the microenvironment [337]. However, there are still some notable points. For instance, the NIR-induced photothermal effect should be well controlled below the threshold to avoid damage to normal cells and tissues. For the treatment of bone-related diseases, mild local hyperthermia (40–42 °C) is recommended due to its ability to promote the mineralization process and enhance bone healing in bone-tissue engineering [297]. Therefore, the development of more sensitive and accurate monitoring systems is needed to adjust NIR irradiation, avoid overheating and subsequently damage. In addition, the microenvironment such as synovial fluid may also interact with intra-articular nanomaterials. The synovial fluid could increase the size

and reverse the charge of cationic NPs, thus inhibiting NPs loading into cartilage [338]. Therefore, the role of different stimuli on nanomaterial properties and performance is important to fully understand in the future.

Nanomaterials with multiple functions have been developed for the treatment of bone-related diseases with better therapeutic activity and fewer adverse effects. For instance, nanomaterials with additional functionalities allow the precise diagnosis of disease and facilitate the therapeutic index simultaneously. Moreover, this strategy also combines various therapeutic agents, such as drugs and plasmid DNA, to act together for synergistic therapeutic efficacy of drugs and gene loads [339]. However, fully understanding the biological and pharmacological actions of co-delivery therapeutic agents is necessary to avoid systemic toxicity. Furthermore, the mechanisms underlying the interaction, regulation and other multiple roles of nanomaterials in bone-related diseases are essential to gain a deeper insight.

The combination of various nanomaterials with different properties can allow synergetic nanomedical platforms for multimodal imaging and simultaneous therapy. Moreover, the conjugation of targeting moieties on the surface of these nanomaterials gives them specific targeted imaging and therapeutic properties. For example, iron oxide nanoparticles, gold nanoparticles or fluorescent organic dyes can allow the detection of bone-related diseases through non-invasive MRI and optical guidance. The encapsulation of magnetic nanoparticles and anticancer drugs in a nanostructured matrix enables the simultaneous diagnosis and targeted chemotherapy. Additionally, the combination of magnetic nanoparticles and therapeutic genes can track gene delivery using MRI and achieve gene therapy. In addition, several nanomaterials that strongly absorb NIR irradiation, such as gold nanoshells, gold nanorods and single-wall carbon nanotubes, can be used for simultaneous optical imaging and photothermal therapy. Therefore, future research directions in creating novel nanomaterials may focus on targeted multimodal imaging and simultaneous diagnosis and therapy.

Overall, nanomaterials have opened an avenue for the diagnosis and therapy of bone-related diseases. Advances in nanomaterials have enormous potential to revolutionize the detection, treatment and prevention of orthopaedic disorders. However, transferring these nanomaterials into routine clinical practice remains a challenge. Continued efforts toward the development of highly accurate and real-time sensitive diagnosis nanosystems and the fabrication of nanoplatforms with higher drug loading efficacy, sequential release kinetics, multiple functions and less biotoxicity should further proceed. We hope that the concepts, highlighted results, remaining challenges and future directions presented in this review will stimulate interest and further advances in the diagnosis and therapy of bone-related diseases.

Ethics approval and consent to participate

Ethical approval and consent to participate were waived by the local Ethics Committee of the First Affiliated Hospital of Soochow University in view of the nature of the review.

Declaration of competing interest

The authors declare no competing financial interest.

Acknowledgements

This review work was supported by the National Natural Science Foundation of China (82072425, 82072498, 81871788, 21875092, 31922040, 82272157), the Natural Science Foundation of Jiangsu Province (BK2021650 and BK20220059), the “Jiangsu Specially-Appointed Professor” Program, the Priority Academic Program Development of Jiangsu Higher Education Institutions (PAPD), Jiangsu Medical Research Project (ZD2022021), and Special Project of Diagnosis; Treatment Technology for Key Clinical Diseases in Suzhou (LCZX202003) and Postgraduate Research & Practice Innovation Program of Jiangsu Province (KYCX22_3217).

References

[1] M.C. Walsh, N. Takegahara, H. Kim, Y. Choi, Updating osteoimmunology: regulation of bone cells by innate and adaptive immunity, Nat. Rev. Rheumatol. 14 (3) (2018) 146–156, https://doi.org/10.1038/nrrheum.2017.213.
[2] K.E. Ensrud, C.J. Crandall, Osteoporosis, Ann. Intern. Med. 167 (3) (2017) 17–32, https://doi.org/10.7326/AITC201708010.
[3] J.N. Katz, K.R. Arant, R.F. Loeser, Diagnosis and treatment of hip and knee osteoarthritis: a review, JAMA 325 (6) (2021) 568–578, https://doi.org/10.1001/jama.2020.22171.
[4] J.S. Smolen, D. Aletaha, I.B. McInnes, Rheumatoid arthritis, Lancet 388 (10055) (2016) 2023–2038, https://doi.org/10.1016/S0140-6736(16)30173-8.
[5] T.A. Einhorn, L.C. Gerstenfeld, Fracture healing: mechanisms and interventions, Nat. Rev. Rheumatol. 11 (1) (2015) 45–54, https://doi.org/10.1038/nrrheum.2014.164.
[6] P. Clezardin, R. Coleman, M. Puppo, P. Ottewell, E. Bonnelye, F. Paycha, C. B. Confavreux, I. Holen, Bone metastasis: mechanisms, therapies, and biomarkers, Physiol. Rev. 101 (3) (2021) 797–855, https://doi.org/10.1152/physrev.00012.2019.
[7] Z.Y. Chen, S. Gao, Y.W. Zhang, R.B. Zhou, F. Zhou, Antibacterial biomaterials in bone tissue engineering, J. Mater. Chem. B 9 (11) (2021) 2594–2612, https://doi.org/10.1039/d0tb02983a.
[8] C.B. Johnston, M. Dagar, Osteoporosis in older adults, Med. Clin. North Am. 104 (5) (2020) 873–884, https://doi.org/10.1016/j.mcna.2020.06.004.
[9] X. Sun, X. Zhen, X. Hu, Y. Li, S. Gu, Y. Gu, H. Dong, Osteoarthritis in the middle-aged and elderly in China: prevalence and influencing factors, Int. J. Environ. Res. Publ. Health 16 (23) (2019) 1–18, https://doi.org/10.3390/ijerph16234701.
[10] O.O. Olumuyiwa-Akeredolu, M.J. Page, P. Soma, E. Pretorius, Platelets: emerging facilitators of cellular crosstalk in rheumatoid arthritis, Nat. Rev. Rheumatol. 15 (4) (2019) 237–248, https://doi.org/10.1038/s41584-019-0187-9.
[11] J.S. Biermann, W. Chow, D.R. Reed, D. Lucas, D.R. Adkins, M. Agulnik, R. S. Benjamin, B. Brigman, G.T. Budd, W.T. Curry, A. Didwania, N. Fabbri, F. J. Hornicek, J.B. Kuechle, D. Lindskog, J. Mayerson, S.V. McGarry, L. Million, C. D. Morris, S. Movva, R.J. O'Donnell, R.L. Randall, P. Rose, V.M. Santana, R. L. Satcher, H. Schwartz, H.J. Siegel, K. Thornton, V. Villalobos, M.A. Bergman, J. L. Scavone, NCCN guidelines insights: bone cancer, version 2.2017, J. Natl. Compr. Cancer Netw. 15 (2) (2017) 155–167, https://doi.org/10.6004/jnccn.2017.0017.
[12] E.J. Ryan, A.J. Ryan, A. Gonzalez-Vazquez, A. Philippart, F.E. Ciraldo, C. Hobbs, V. Nicolosi, A.R. Boccaccini, C.J. Kearney, F.J. O'Brien, Collagen scaffolds functionalised with copper-eluting bioactive glass reduce infection and enhance osteogenesis and angiogenesis both in vitro and in vivo, Biomaterials 197 (2019) 405–416, https://doi.org/10.1016/j.biomaterials.2019.01.031.
[13] C.Y. Wenham, A.J. Grainger, P.G. Conaghan, The role of imaging modalities in the diagnosis, differential diagnosis and clinical assessment of peripheral joint osteoarthritis, Osteoarthritis Cartilage 22 (10) (2014) 1692–1702, https://doi.org/10.1016/j.joca.2014.06.005.
[14] P.S. Meltzer, L.J. Helman, New horizons in the treatment of osteosarcoma, N. Engl. J. Med. 385 (22) (2021) 2066–2076, https://doi.org/10.1056/NEJMra2103423.
[15] P.M. Camacho, 2021 updates on osteoporosis diagnosis and therapy, Endocrinol Metab. Clin. N. Am. 50 (2) (2021), https://doi.org/10.1016/j.ecl.2021.03.011.
[16] M. Lotz, J. Martel-Pelletier, C. Christiansen, M.L. Brandi, O. Bruyere, R. Chapurlat, J. Collette, C. Cooper, G. Giacovelli, J.A. Kanis, M.A. Karsdal, V. Kraus, W.F. Lems, I. Meulenbelt, J.P. Pelletier, J.P. Raynauld, S. Reiter-Niesert, R. Rizzoli, L.J. Sandell, W.E. Van Spil, J.Y. Reginster, Republished: value of biomarkers in osteoarthritis: current status and perspectives, Postgrad. Med. 90 (1061) (2014) 171–178, https://doi.org/10.1136/postgradmedj-2013-203726rep.
[17] J.E. Compston, M.R. McClung, W.D. Leslie, Osteoporosis, Lancet 393 (10169) (2019) 364–376, https://doi.org/10.1016/S0140-6736(18)32112-3.
[18] W.F. Lems, K.E. Dreinhofer, H. Bischoff-Ferrari, M. Blauth, E. Czerwinski, J. da Silva, A. Herrera, P. Hoffmeyer, T. Kvien, G. Maalouf, D. Marsh, J. Puget, W. Puhl, G. Poor, L. Rasch, C. Roux, S. Schuler, B. Seriolo, U. Tarantino, T. van Geel, A. Woolf, C. Wyers, P. Geusens, EULAR/EFORT recommendations for management of patients older than 50 years with a fragility fracture and prevention of subsequent fractures, Ann. Rheum. Dis. 76 (5) (2017) 802–810, https://doi.org/10.1136/annrheumdis-2016-210289.
[19] G.R. Burmester, J.E. Pope, Novel treatment strategies in rheumatoid arthritis, Lancet 389 (10086) (2017) 2338–2348, https://doi.org/10.1016/S0140-6736(17)31491-5.
[20] B. Abramoff, F.E. Caldera, Osteoarthritis: pathology, diagnosis, and treatment options, Med. Clin. North Am. 104 (2) (2020) 293–311, https://doi.org/10.1016/j.mcna.2019.10.007.
[21] N. Kohli, V. Sharma, A. Orera, P. Sawadkar, N. Owji, O.G. Frost, R.J. Bailey, M. Snow, J.C. Knowles, G.W. Blunn, E. Garcia-Gareta, Pro-angiogenic and osteogenic composite scaffolds of fibrin, alginate and calcium phosphate for bone tissue engineering, J. Tissue Eng. 12 (2021), https://doi.org/10.1177/20417314211005610.
[22] J. Ritter, S.S. Bielack, Osteosarcoma, Ann. Oncol. 21 (Suppl 7) (2010) 320–325, https://doi.org/10.1093/annonc/mdq276.

[23] A. Italiano, O. Mir, S. Mathoulin-Pelissier, N. Penel, S. Piperno-Neumann, E. Bompas, C. Chevreau, F. Duffaud, N. Entz-Werle, E. Saada, I. Ray-Coquard, C. Lervat, N. Gaspar, P. Marec-Berard, H. Pacquement, J. Wright, M. Toulmonde, A. Bessede, A. Crombe, M. Kind, C. Bellera, J.Y. Blay, Cabozantinib in patients with advanced Ewing sarcoma or osteosarcoma (CABONE): a multicentre, single-arm, phase 2 trial, Lancet Oncol. 21 (3) (2020) 446–455, https://doi.org/10.1016/S1470-2045(19)30825-3.
[24] A. Grothey, J.Y. Blay, N. Pavlakis, T. Yoshino, J. Bruix, Evolving role of regorafenib for the treatment of advanced cancers, Cancer Treat Rev. 86 (2020) 1–17, https://doi.org/10.1016/j.ctrv.2020.101993.
[25] D. Romero, Sorafenib prevents AML relapse after allo-HSCT, Nat. Rev. Clin. Oncol. 17 (10) (2020) 591, https://doi.org/10.1038/s41571-020-00431-7.
[26] D.K. Mills, U. Jammalamadaka, K. Tappa, J. Weisman, Studies on the cytocompatibility, mechanical and antimicrobial properties of 3D printed poly (methyl methacrylate) beads, Bioact. Mater. 3 (2) (2018) 157–166, https://doi.org/10.1016/j.bioactmat.2018.01.006.
[27] A. Mero, M. Campisi, M. Favero, C. Barbera, C. Secchieri, J.M. Dayer, M. B. Goldring, S.R. Goldring, G. Pasut, A hyaluronic acid-salmon calcitonin conjugate for the local treatment of osteoarthritis: chondro-protective effect in a rabbit model of early OA, J. Contr. Release 187 (2014) 30–38, https://doi.org/10.1016/j.jconrel.2014.05.008.
[28] M.C. Chen, F.L. Mi, Z.X. Liao, C.W. Hsiao, K. Sonaje, M.F. Chung, L.W. Hsu, H. W. Sung, Recent advances in chitosan-based nanoparticles for oral delivery of macromolecules, Adv. Drug Deliv. Rev. 65 (6) (2013) 865–879, https://doi.org/10.1016/j.addr.2012.10.010.
[29] X. Yang, Z. Pan, M.R. Choudhury, Z. Yuan, A. Anifowose, B. Yu, W. Wang, B. Wang, Making smart drugs smarter: the importance of linker chemistry in targeted drug delivery, Med. Res. Rev. 40 (6) (2020) 2682–2713, https://doi.org/10.1002/med.21720.
[30] D.G.J. Larsson, C.F. Flach, Antibiotic resistance in the environment, Nat. Rev. Microbiol. 20 (5) (2022) 257–269, https://doi.org/10.1038/s41579-021-00649-x.
[31] J. Raphel, M. Holodniy, S.B. Goodman, S.C. Heilshorn, Multifunctional coatings to simultaneously promote osseointegration and prevent infection of orthopaedic implants, Biomaterials 84 (2016) 301–314, https://doi.org/10.1016/j.biomaterials.2016.01.016.
[32] X. Tong, L. Zhu, K. Wang, Z. Shi, S. Huang, Y. Li, J. Ma, C. Wen, J. Lin, Impact of gadolinium on mechanical properties, corrosion resistance, and biocompatibility of Zn-1Mg-xGd alloys for biodegradable bone-implant applications, Acta Biomater. 142 (2022) 361–373, https://doi.org/10.1016/j.actbio.2022.02.015.
[33] A. Gharieh, S. Khoee, A.R. Mahdavian, Emulsion and miniemulsion techniques in preparation of polymer nanoparticles with versatile characteristics, Adv. Colloid Interface Sci. 269 (2019) 152–186, https://doi.org/10.1016/j.cis.2019.04.010.
[34] K. Khalid, X. Tan, H.F. Mohd Zaid, Y. Tao, C. Lye Chew, D.T. Chu, M.K. Lam, Y. C. Ho, J.W. Lim, L. Chin Wei, Advanced in developmental organic and inorganic nanomaterial: a review, Bioengineered 11 (1) (2020) 328–355, https://doi.org/10.1080/21655979.2020.1736240.
[35] J. Chen, J. Qi, C. Chen, J. Chen, L. Liu, R. Gao, T. Zhang, L. Song, D. Ding, P. Zhang, C. Liu, Tocilizumab-conjugated polymer nanoparticles for NIR-II photoacoustic-imaging-guided therapy of rheumatoid arthritis, Adv. Mater. 32 (37) (2020), e2003399, https://doi.org/10.1002/adma.202003399.
[36] S. Islam, S. Shukla, V.K. Bajpai, Y.K. Han, Y.S. Huh, A. Kumar, A. Ghosh, S. Gandhi, A smart nanosensor for the detection of human immunodeficiency virus and associated cardiovascular and arthritis diseases using functionalized graphene-based transistors, Biosens. Bioelectron. 126 (2019) 792–799, https://doi.org/10.1016/j.bios.2018.11.041.
[37] H. Ren, Y. He, J. Liang, Z. Cheng, M. Zhang, Y. Zhu, C. Hong, J. Qin, X. Xu, J. Wang, Role of liposome size, surface charge, and PEGylation on rheumatoid arthritis targeting therapy, ACS Appl. Mater. Interfaces 11 (22) (2019) 20304–20315, https://doi.org/10.1021/acsami.8b22693.
[38] J. Liu, T. Jiang, C. Li, Y. Wu, M. He, J. Zhao, L. Zheng, X. Zhang, Bioconjugated carbon dots for delivery of siTnfalpha to enhance chondrogenesis of mesenchymal stem cells by suppression of inflammation, Stem Cells Transl. Med. 8 (7) (2019) 724–736, https://doi.org/10.1002/sctm.18-0289.
[39] H. Xiang, Q. Yang, Y. Gao, D. Zhu, S. Pan, T. Xu, Y. Chen, Cocrystal strategy toward multifunctional 3D-printing scaffolds enables NIR-activated photonic osteosarcoma hyperthermia and enhanced bone defect regeneration, Adv. Funct. Mater. 30 (25) (2020), https://doi.org/10.1002/adfm.201909938.
[40] S.M. Lee, H.J. Kim, Y.J. Ha, Y.N. Park, S.K. Lee, Y.B. Park, K.H. Yoo, Targeted chemo-photothermal treatments of rheumatoid arthritis using gold half-shell multifunctional nanoparticles, ACS Nano 7 (1) (2013) 50–57, https://doi.org/10.1021/nn301215q.
[41] A.S. Krishna, C. Radhakumary, K. Sreenivasan, In vitro detection of calcium in bone by modified carbon dots, Analyst 138 (23) (2013) 7107–7111, https://doi.org/10.1039/c3an01239e.
[42] F. Ostadhossein, L. Benig, I. Tripathi, S.K. Misra, D. Pan, Fluorescence detection of bone microcracks using monophosphonated carbon dots, ACS Appl. Mater. Interfaces 10 (23) (2018) 19408–19415, https://doi.org/10.1021/acsami.8b03727.
[43] A.M. Lutz, C. Seemayer, C. Corot, R.E. Gay, K. Goepfert, B.A. Michel, B. Marincek, S. Gay, D. Weishaupt, Detection of synovial macrophages in an experimental rabbit model of antigen-induced arthritis: ultrasmall superparamagnetic iron oxide-enhanced MR imaging, Radiology 233 (1) (2004) 149–157, https://doi.org/10.1148/radiol.2331031402.
[44] P. Periyathambi, T.P. Sastry, S.K. Anandasadagopan, K. Manickavasagam, Macrophages mediated diagnosis of rheumatoid arthritis using fibrin based magnetic nanoparticles as MRI contrast agents, Biochim. Biophys. Acta Gen. Subj. 1861 (1) (2017) 2992–3001, https://doi.org/10.1016/j.bbagen.2016.09.018.
[45] S. Mohanty, K. Yerneni, J.L. Theruvath, C.M. Graef, H. Nejadnik, O. Lenkov, L. Pisani, J. Rosenberg, S. Mitra, A.S. Cordero, S. Cheshier, H.E. Daldrup-Link, Nanoparticle enhanced MRI can monitor macrophage response to CD47 mAb immunotherapy in osteosarcoma, Cell Death Dis. 10 (2) (2019) 36, https://doi.org/10.1038/s41419-018-1285-3.
[46] Z. Ma, H. Qin, H. Chen, H. Yang, J. Xu, S. Yang, J. Hu, D. Xing, Phage display-derived oligopeptide-functionalized probes for in vivo specific photoacoustic imaging of osteosarcoma, Nanomedicine 13 (1) (2017) 111–121, https://doi.org/10.1016/j.nano.2016.09.002.
[47] J. Vonnemann, N. Beziere, C. Bottcher, S.B. Riese, C. Kuehne, J. Dernedde, K. Licha, C. von Schacky, Y. Kosanke, M. Kimm, R. Meier, V. Ntziachristos, R. Haag, Polyglycerolsulfate functionalized gold nanorods as optoacoustic signal nanoamplifiers for in vivo bioimaging of rheumatoid arthritis, Theranostics 4 (6) (2014) 629–641, https://doi.org/10.7150/thno.8518.
[48] Y. Jin, D. Ni, L. Gao, X. Meng, Y. Lv, F. Han, H. Zhang, Y. Liu, Z. Yao, X. Feng, W. Bu, J. Zhang, Harness the power of upconversion nanoparticles for spectral computed tomography diagnosis of osteosarcoma, Adv. Funct. Mater. 28 (33) (2018), https://doi.org/10.1002/adfm.201802656.
[49] H. Vu-Quang, M.S. Vinding, M. Jakobsen, P. Song, F. Dagnaes-Hansen, N. C. Nielsen, J. Kjems, Imaging rheumatoid arthritis in mice using combined near infrared and (19)F magnetic resonance modalities, Sci. Rep. 9 (1) (2019), 14314, https://doi.org/10.1038/s41598-019-50043-0.
[50] A. Saranti, A. Tiron-Stathopoulos, L. Papaioannou, C. Gioti, A. Ioannou, M. A. Karakassides, K. Avgoustakis, I. Koutselas, K. Dimos, 3D-printed bioactive scaffolds for bone regeneration bearing carbon dots for bioimaging purposes, Smart Mater. Med. 3 (2022) 12–19, https://doi.org/10.1016/j.smaim.2021.11.002.
[51] A.S. Krishna, C. Radhakumary, M. Antony, K. Sreenivasan, Functionalized carbon dots enable simultaneous bone crack detection and drug deposition, J. Mater. Chem. B 2 (48) (2014) 8626–8632, https://doi.org/10.1039/c4tb00918e.
[52] D. Shao, M. Lu, D. Xu, X. Zheng, Y. Pan, Y. Song, J. Xu, M. Li, M. Zhang, J. Li, G. Chi, L. Chen, B. Yang, Carbon dots for tracking and promoting the osteogenic differentiation of mesenchymal stem cells, Biomater. Sci. 5 (9) (2017) 1820–1827, https://doi.org/10.1039/c7bm00358g.
[53] S. Li, I. Skromne, Z. Peng, J. Dallman, A.O. Al-Youbi, A.S. Bashammakh, M.S. El-Shahawi, R.M. Leblanc, Dark" carbon dots specifically "light-up" calcified zebrafish bones, J. Mater. Chem. B 4 (46) (2016) 7398–7405, https://doi.org/10.1039/c6tb02241c.
[54] Z. Peng, E.H. Miyanji, Y. Zhou, J. Pardo, S.D. Hettiarachchi, S. Li, P. L. Blackwelder, I. Skromne, R.M. Leblanc, Carbon dots: promising biomaterials for bone-specific imaging and drug delivery, Nanoscale 9 (44) (2017) 17533–17543, https://doi.org/10.1039/c7nr05731h.
[55] A. Nagy, A. Steinbruck, J. Gao, N. Doggett, J.A. Hollingsworth, R. Iyer, Comprehensive analysis of the effects of CdSe quantum dot size, surface charge, and functionalization on primary human lung cells, ACS Nano 6 (6) (2012) 4748–4762, https://doi.org/10.1021/nn204886b.
[56] M. Muthiah, I.K. Park, C.S. Cho, Surface modification of iron oxide nanoparticles by biocompatible polymers for tissue imaging and targeting, Biotechnol. Adv. 31 (8) (2013) 1224–1236, https://doi.org/10.1016/j.biotechadv.2013.03.005.
[57] F. Dai, M. Du, Y. Liu, G. Liu, Q. Liu, X. Zhang, Folic acid-conjugated glucose and dextran coated iron oxide nanoparticles as MRI contrast agents for diagnosis and treatment response of rheumatoid arthritis, J. Mater. Chem. B 2 (16) (2014) 2240–2247, https://doi.org/10.1039/c3tb21732a.
[58] C.L. Chen, T.Y. Siow, C.H. Chou, C.H. Lin, M.H. Lin, Y.C. Chen, W.Y. Hsieh, S. J. Wang, C. Chang, Targeted superparamagnetic iron oxide nanoparticles for in vivo magnetic resonance imaging of T-cells in rheumatoid arthritis, Mol. Imag. Biol. 19 (2) (2017) 233–244, https://doi.org/10.1007/s11307-016-1001-6.
[59] A. Panahifar, M. Mahmoudi, M.R. Doschak, Synthesis and in vitro evaluation of bone-seeking superparamagnetic iron oxide nanoparticles as contrast agents for imaging bone metabolic activity, ACS Appl. Mater. Interfaces 5 (11) (2013), https://doi.org/10.1021/am4010495, 5219-5126.
[60] L. Pourtau, H. Oliveira, J. Thevenot, Y. Wan, A.R. Brisson, O. Sandre, S. Miraux, E. Thiaudiere, S. Lecommandoux, Antibody-functionalized magnetic polymersomes: in vivo targeting and imaging of bone metastases using high resolution MRI, Adv. Healthc. Mater. 2 (11) (2013) 1420–1424, https://doi.org/10.1002/adhm.201300061.
[61] S.D. Brown, P. Nativo, J.A. Smith, D. Stirling, P.R. Edwards, B. Venugopal, D. J. Flint, J.A. Plumb, D. Graham, N.J. Wheate, Gold nanoparticles for the improved anticancer drug delivery of the active component of oxaliplatin, J. Am. Chem. Soc. 132 (13) (2010) 4678–4684, https://doi.org/10.1021/ja908117a.
[62] J. Ma, X. Liu, R. Wang, J. Zhang, P. Jiang, Y. Wang, G. Tu, Bimetallic core–shell nanostars with tunable surface plasmon resonance for surface-enhanced Raman scattering, ACS Appl. Nano Mater. 3 (11) (2020) 10885–10894, https://doi.org/10.1021/acsanm.0c02144.
[63] M. Fournelle, W. Bost, I.H. Tarner, T. Lehmberg, E. Weiss, R. Lemor, R. Dinser, Antitumor necrosis factor-alpha antibody-coupled gold nanorods as nanoprobes for molecular optoacoustic imaging in arthritis, Nanomedicine 8 (3) (2012) 346–354, https://doi.org/10.1016/j.nano.2011.06.020.
[64] H. Lee, K. Lee, I.K. Kim, T.G. Park, Synthesis, characterization, and in vivo diagnostic applications of hyaluronic acid immobilized gold nanoprobes, Biomaterials 29 (35) (2008) 4709–4718, https://doi.org/10.1016/j.biomaterials.2008.08.038.
[65] D. Natarajan, Z. Ye, L. Wang, L. Ge, J.L. Pathak, Rare earth smart nanomaterials for bone tissue engineering and implantology: advances, challenges, and

prospects, Bioeng. Transl. Med. 7 (1) (2022), e10262, https://doi.org/10.1002/btm2.10262.
[66] H.Q. Wang, M. Batentschuk, A. Osvet, L. Pinna, C.J. Brabec, Rare-earth ion doped up-conversion materials for photovoltaic applications, Adv. Mater. 23 (22–23) (2011) 2675–2680, https://doi.org/10.1002/adma.201100511.
[67] B. McMahon, P. Mauer, C.P. McCoy, T.C. Lee, T. Gunnlaugsson, Selective imaging of damaged bone structure (microcracks) using a targeting supramolecular Eu(III) complex as a lanthanide luminescent contrast agent, J. Am. Chem. Soc. 131 (48) (2009) 17542–17543, https://doi.org/10.1021/ja908006r.
[68] Y. Wang, C. Jiang, W. He, K. Ai, X. Ren, L. Liu, M. Zhang, L. Lu, Targeted imaging of damaged bone in vivo with gemstone spectral computed tomography, ACS Nano 10 (4) (2016) 4164–4172, https://doi.org/10.1021/acsnano.5b07401.
[69] H. Nejadnik, D. Ye, O.D. Lenkov, J.S. Donig, J.E. Martin, R. Castillo, N. Derugin, B. Sennino, J. Rao, H. Daldrup-Link, Magnetic resonance imaging of stem cell apoptosis in arthritic joints with a caspase activatable contrast agent, ACS Nano 9 (2) (2015) 1150–1160, https://doi.org/10.1021/nn504494c.
[70] Q. Wang, L. Lv, Z. Ling, Y. Wang, Y. Liu, L. Li, G. Liu, L. Shen, J. Yan, Y. Wang, Long-circulating iodinated albumin-gadolinium nanoparticles as enhanced magnetic resonance and computed tomography imaging probes for osteosarcoma visualization, Anal. Chem. 87 (8) (2015) 4299–4304, https://doi.org/10.1021/ac504752a.
[71] S. Sarkar, N. Levi-Polyachenko, Conjugated polymer nano-systems for hyperthermia, imaging and drug delivery, Adv. Drug Deliv. Rev. 163 (2020) 40–64, https://doi.org/10.1016/j.addr.2020.01.002.
[72] S. Xiao, Y. Tang, Y. Lin, Z. Lv, L. Chen, Tracking osteoarthritis progress through cationic nanoprobe-enhanced photoacoustic imaging of cartilage, Acta Biomater. 109 (2020) 153–162, https://doi.org/10.1016/j.actbio.2020.04.001.
[73] L. Chen, Y. Ji, X. Hu, C. Cui, H. Liu, Y. Tang, B. Qi, Y. Niu, X. Hu, A. Yu, Q. Fan, Cationic poly-l-lysine-encapsulated melanin nanoparticles as efficient photoacoustic agents targeting to glycosaminoglycans for the early diagnosis of articular cartilage degeneration in osteoarthritis, Nanoscale 10 (28) (2018) 13471–13484, https://doi.org/10.1039/c8nr03791d.
[74] X. Zhou, N. Yan, E.J. Cornel, H. Cai, S. Xue, H. Xi, Z. Fan, S. He, J. Du, Bone-targeting polymer vesicles for simultaneous imaging and effective malignant bone tumor treatment, Biomaterials 269 (2021), 120345, https://doi.org/10.1016/j.biomaterials.2020.120345.
[75] Y. Lu, L. Li, Z. Lin, M. Li, X. Hu, Y. Zhang, M. Peng, H. Xia, G. Han, Enhancing osteosarcoma killing and CT imaging using ultrahigh drug loading and NIR-responsive bismuth Sulfide@Mesoporous silica nanoparticles, Adv. Healthc. Mater. 7 (19) (2018), e1800602, https://doi.org/10.1002/adhm.201800602.
[76] A. Singh, Y.H. Seo, C.K. Lim, J. Koh, W.D. Jang, I.C. Kwon, S. Kim, Biolighted nanotorch capable of systemic self-delivery and diagnostic imaging, ACS Nano 9 (10) (2015) 9906–9911, https://doi.org/10.1021/acsnano.5b03377.
[77] M.B. Greenblatt, J.N. Tsai, M.N. Wein, Bone turnover markers in the diagnosis and monitoring of metabolic bone disease, Clin. Chem. 63 (2) (2017) 464–474, https://doi.org/10.1373/clinchem.2016.259085.
[78] A. Santoro, J. Conde, M. Scotece, V. Abella, V. Lopez, J. Pino, R. Gomez, J. J. Gomez-Reino, O. Gualillo, Choosing the right chondrocyte cell line: focus on nitric oxide, J. Orthop. Res. 33 (12) (2015) 1784–1788, https://doi.org/10.1002/jor.22954.
[79] A. Mc Ardle, B. Flatley, S.R. Pennington, O. FitzGerald, Early biomarkers of joint damage in rheumatoid and psoriatic arthritis, Arthritis Res. Ther. 17 (2015) 141, https://doi.org/10.1186/s13075-015-0652-z.
[80] Y. Zhao, Y. Liu, X. Li, H. Wang, Y. Zhang, H. Ma, Q. Wei, Label-free ECL immunosensor for the early diagnosis of rheumatoid arthritis based on asymmetric heterogeneous polyaniline-gold nanomaterial, Sensor. Actuator. B Chem. 257 (2018) 354–361, https://doi.org/10.1016/j.snb.2017.10.184.
[81] X. Jia, C. Wang, Z. Rong, J. Li, K. Wang, Z. Qie, R. Xiao, S. Wang, Dual dye-loaded Au@Ag coupled to a lateral flow immunoassay for the accurate and sensitive detection of Mycoplasma pneumoniae infection, RSC Adv. 8 (38) (2018) 21243–21251, https://doi.org/10.1039/c8ra03323d.
[82] B. Veigas, A. Matias, T. Calmeiro, E. Fortunato, A.R. Fernandes, P.V. Baptista, Antibody modified gold nanoparticles for fast colorimetric screening of rheumatoid arthritis, Analyst 144 (11) (2019) 3613–3619, https://doi.org/10.1039/c9an00319c.
[83] S. Peng, Q. Zheng, X. Zhang, L. Dai, J. Zhu, Y. Pi, X. Hu, W. Cheng, C. Zhou, Y. Sha, Y. Ao, Detection of ADAMTS-4 activity using a fluorogenic peptide-conjugated Au nanoparticle probe in human knee synovial fluid, ACS Appl. Mater. Interfaces 5 (13) (2013) 6089–6096, https://doi.org/10.1021/am400854z.
[84] C.Y. Chiang, M.L. Hsieh, K.W. Huang, L.K. Chau, C.M. Chang, S.R. Lyu, Fiber-optic particle plasmon resonance sensor for detection of interleukin-1beta in synovial fluids, Biosens. Bioelectron. 26 (3) (2010) 1036–1042, https://doi.org/10.1016/j.bios.2010.08.047.
[85] E.Y. Hwang, J.H. Lee, D.W. Lim, Compartmentalized bimetal cluster-poly(aniline) hybrid nanostructures for multiplexed detection of autoantibodies in early diagnosis of rheumatoid arthritis, Sensor. Actuator. B Chem. 321 (2020), https://doi.org/10.1016/j.snb.2020.128482.
[86] K.A. Chu, W. Chen, C.Y. Hsu, Y.M. Hung, J.C. Wei, Increased risk of rheumatoid arthritis among patients with Mycoplasma pneumonia: a nationwide population-based cohort study in Taiwan, PLoS One 14 (1) (2019), e0210750, https://doi.org/10.1371/journal.pone.0210750.
[87] P. Jin, C. Wiraja, J. Zhao, J. Zhang, L. Zheng, C. Xu, Nitric oxide nanosensors for predicting the development of osteoarthritis in rat model, ACS Appl. Mater. Interfaces 9 (30) (2017) 25128–25137, https://doi.org/10.1021/acsami.7b06404.
[88] R. Villalonga, P. Diez, A. Sanchez, E. Aznar, R. Martinez-Manez, J.M. Pingarron, Enzyme-controlled sensing-actuating nanomachine based on Janus Au-mesoporous silica nanoparticles, Chemistry 19 (24) (2013) 7889–7894, https://doi.org/10.1002/chem.201300723.
[89] S. Marconi, M.A. Giambra, A. Montanaro, V. Miseikis, S. Soresi, S. Tirelli, P. Galli, F. Buchali, W. Templ, C. Coletti, V. Sorianello, M. Romagnoli, Photo thermal effect graphene detector featuring 105 Gbit s(-1) NRZ and 120 Gbit s(-1) PAM4 direct detection, Nat. Commun. 12 (1) (2021) 806, https://doi.org/10.1038/s41467-021-21137-z.
[90] M.G. Neuman, L.B. Cohen, R.M. Nanau, Hyaluronic acid as a non-invasive biomarker of liver fibrosis, Clin. Biochem. 49 (3) (2016) 302–315, https://doi.org/10.1016/j.clinbiochem.2015.07.019.
[91] F. Rivas, O.K. Zahid, H.L. Reesink, B.T. Peal, A.J. Nixon, P.L. DeAngelis, A. Skardal, E. Rahbar, A.R. Hall, Label-free analysis of physiological hyaluronan size distribution with a solid-state nanopore sensor, Nat. Commun. 9 (1) (2018) 1037, https://doi.org/10.1038/s41467-018-03439-x.
[92] F. Danhier, E. Ansorena, J.M. Silva, R. Coco, A. Le Breton, V. Preat, PLGA-based nanoparticles: an overview of biomedical applications, J. Contr. Release 161 (2) (2012) 505–522, https://doi.org/10.1016/j.jconrel.2012.01.043.
[93] J.K. Patra, G. Das, L.F. Fraceto, E.V.R. Campos, M.D.P. Rodriguez-Torres, L. S. Acosta-Torres, L.A. Diaz-Torres, R. Grillo, M.K. Swamy, S. Sharma, S. Habtemariam, H.S. Shin, Nano based drug delivery systems: recent developments and future prospects, J. Nanobiotechnol. 16 (1) (2018) 71, https://doi.org/10.1186/s12951-018-0392-8.
[94] Q. Hu, H. Li, L. Wang, H. Gu, C. Fan, DNA nanotechnology-enabled drug delivery systems, Chem. Rev. 119 (10) (2019) 6459–6506, https://doi.org/10.1021/acs.chemrev.7b00663.
[95] C. Simitzi, A. Ranella, E. Stratakis, Controlling the morphology and outgrowth of nerve and neuroglial cells: the effect of surface topography, Acta Biomater. 51 (2017) 21–52, https://doi.org/10.1016/j.actbio.2017.01.023.
[96] S.T. Yang, Y. Liu, Y.W. Wang, A. Cao, Biosafety and bioapplication of nanomaterials by designing protein-nanoparticle interactions, Small 9 (9–10) (2013) 1635–1653, https://doi.org/10.1002/smll.201201492.
[97] P. Maudens, C.A. Seemayer, C. Thauvin, C. Gabay, O. Jordan, E. Allemann, Nanocrystal-polymer particles: extended delivery carriers for osteoarthritis treatment, Small 14 (8) (2018), https://doi.org/10.1002/smll.201703108.
[98] W. Fan, J. Li, L. Yuan, J. Chen, Z. Wang, Y. Wang, C. Guo, X. Mo, Z. Yan, Intra-articular injection of kartogenin-conjugated polyurethane nanoparticles attenuates the progression of osteoarthritis, Drug Deliv. 25 (1) (2018) 1004–1012, https://doi.org/10.1080/10717544.2018.1461279.
[99] P. Maudens, C.A. Seemayer, F. Pfefferle, O. Jordan, E. Allemann, Nanocrystals of a potent p38 MAPK inhibitor embedded in microparticles: therapeutic effects in inflammatory and mechanistic murine models of osteoarthritis, J. Contr. Release 276 (2018) 102–112, https://doi.org/10.1016/j.jconrel.2018.03.007.
[100] P. Liu, L. Gu, L. Ren, J. Chen, T. Li, X. Wang, J. Yang, C. Chen, L. Sun, Intra-articular injection of etoricoxib-loaded PLGA-PEG-PLGA triblock copolymeric nanoparticles attenuates osteoarthritis progression, Am. J. Transl. Res. 11 (11) (2019) 6775–6789.
[101] A. Jain, S.K. Mishra, P.R. Vuddanda, S.K. Singh, R. Singh, S. Singh, Targeting of diacerein loaded lipid nanoparticles to intra-articular cartilage using chondroitin sulfate as homing carrier for treatment of osteoarthritis in rats, Nanomedicine 10 (5) (2014) 1031–1040, https://doi.org/10.1016/j.nano.2014.01.008.
[102] M. Bishnoi, A. Jain, P. Hurkat, S.K. Jain, Aceclofenac-loaded chondroitin sulfate conjugated SLNs for effective management of osteoarthritis, J. Drug Target. 22 (9) (2014) 805–812, https://doi.org/10.3109/1061186X.2014.928714.
[103] R.E. Whitmire, D.S. Wilson, A. Singh, M.E. Levenston, N. Murthy, A.J. Garcia, Self-assembling nanoparticles for intra-articular delivery of anti-inflammatory proteins, Biomaterials 33 (30) (2012) 7665–7675, https://doi.org/10.1016/j.biomaterials.2012.06.101.
[104] Y. Pi, X. Zhang, Z. Shao, F. Zhao, X. Hu, Y. Ao, Intra-articular delivery of anti-Hif-2 alpha siRNA by chondrocyte-homing nanoparticles to prevent cartilage degeneration in arthritic mice, Gene Ther. 22 (6) (2015) 439–448, https://doi.org/10.1038/gt.2015.16.
[105] H. Yan, X. Duan, H. Pan, A. Akk, L.J. Sandell, S.A. Wickline, M.F. Rai, C.T. N. Pham, Development of a peptide-siRNA nanocomplex targeting NF- kappaB for efficient cartilage delivery, Sci. Rep. 9 (1) (2019) 442, https://doi.org/10.1038/s41598-018-37018-3.
[106] S.H. Hsu, T.B. Huang, S.J. Cheng, S.Y. Weng, C.L. Tsai, C.S. Tseng, D.C. Chen, T. Y. Liu, K.Y. Fu, B.L. Yen, Chondrogenesis from human placenta-derived mesenchymal stem cells in three-dimensional scaffolds for cartilage tissue engineering, Tissue Eng. 17 (11–12) (2011) 1549–1560, https://doi.org/10.1089/ten.TEA.2010.0419.
[107] T. Yang, M. Tamaddon, L. Jiang, J. Wang, Z. Liu, Z. Liu, H. Meng, Y. Hu, J. Gao, X. Yang, Y. Zhao, Y. Wang, A. Wang, Q. Wu, C. Liu, J. Peng, X. Sun, Q. Xue, Bilayered scaffold with 3D printed stiff subchondral bony compartment to provide constant mechanical support for long-term cartilage regeneration, J. Orthop. Translat. 30 (2021) 112–121, https://doi.org/10.1016/j.jot.2021.09.001.
[108] L.D. Wright, K.D. McKeon-Fischer, Z. Cui, L.S. Nair, J.W. Freeman, PDLA/PLLA and PDLA/PCL nanofibers with a chitosan-based hydrogel in composite scaffolds for tissue engineered cartilage, J. Tissue Eng. Regen. Med. 8 (12) (2014) 946–954, https://doi.org/10.1002/term.1591.
[109] Z. Li, P. Liu, T. Yang, Y. Sun, Q. You, J. Li, Z. Wang, B. Han, Composite poly(l-lactic-acid)/silk fibroin scaffold prepared by electrospinning promotes chondrogenesis for cartilage tissue engineering, J. Biomater. Appl. 30 (10) (2016) 1552–1565, https://doi.org/10.1177/0885328216638587.

[110] E. Arslan, M. Sardan Ekiz, C. Eren Cimenci, N. Can, M.H. Gemci, H. Ozkan, M. O. Guler, A.B. Tekinay, Protective therapeutic effects of peptide nanofiber and hyaluronic acid hybrid membrane in in vivo osteoarthritis model, Acta Biomater. 73 (2018) 263–274, https://doi.org/10.1016/j.actbio.2018.04.015.
[111] M.L. Kang, J.Y. Ko, J.E. Kim, G.I. Im, Intra-articular delivery of kartogenin-conjugated chitosan nano/microparticles for cartilage regeneration, Biomaterials 35 (37) (2014) 9984–9994, https://doi.org/10.1016/j.biomaterials.2014.08.042.
[112] H. Zhao, T. Zhang, C. Xia, L. Shi, S. Wang, X. Zheng, T. Hu, B. Zhang, Berberine ameliorates cartilage degeneration in interleukin-1beta-stimulated rat chondrocytes and in a rat model of osteoarthritis via Akt signalling, J. Cell Mol. Med. 18 (2) (2014) 283–292, https://doi.org/10.1111/jcmm.12186.
[113] Y. Zhou, S.Q. Liu, H. Peng, L. Yu, B. He, Q. Zhao, In vivo anti-apoptosis activity of novel berberine-loaded chitosan nanoparticles effectively ameliorates osteoarthritis, Int. Immunopharm. 28 (1) (2015) 34–43, https://doi.org/10.1016/j.intimp.2015.05.014.
[114] S. Mitragotri, P.A. Burke, R. Langer, Overcoming the challenges in administering biopharmaceuticals: formulation and delivery strategies, Nat. Rev. Drug Discov. 13 (9) (2014) 655–672, https://doi.org/10.1038/nrd4363.
[115] R.M. Samarasinghe, R.K. Kanwar, J.R. Kanwar, The effect of oral administration of iron saturated-bovine lactoferrin encapsulated chitosan-nanocarriers on osteoarthritis, Biomaterials 35 (26) (2014) 7522–7534, https://doi.org/10.1016/j.biomaterials.2014.04.109.
[116] J.R. Kanwar, K.P. Palmano, X. Sun, R.K. Kanwar, R. Gupta, N. Haggarty, A. Rowan, S. Ram, G.W. Krissansen, Iron-saturated' lactoferrin is a potent natural adjuvant for augmenting cancer chemotherapy, Immunol. Cell Biol. 86 (3) (2008) 277–288, https://doi.org/10.1038/sj.icb.7100163.
[117] J. McMasters, S. Poh, J.B. Lin, A. Panitch, Delivery of anti-inflammatory peptides from hollow PEGylated poly(NIPAM) nanoparticles reduces inflammation in an ex vivo osteoarthritis model, J. Contr. Release 258 (2017) 161–170, https://doi.org/10.1016/j.jconrel.2017.05.008.
[118] M.J. Sandker, A. Petit, E.M. Redout, M. Siebelt, B. Muller, P. Bruin, R. Meyboom, T. Vermonden, W.E. Hennink, H. Weinans, In situ forming acyl-capped PCLA-PEG-PCLA triblock copolymer based hydrogels, Biomaterials 34 (32) (2013) 8002–8011, https://doi.org/10.1016/j.biomaterials.2013.07.046.
[119] Z. Zhang, J. Ni, L. Chen, L. Yu, J. Xu, J. Ding, Biodegradable and thermoreversible PCLA-PEG-PCLA hydrogel as a barrier for prevention of post-operative adhesion, Biomaterials 32 (21) (2011) 4725–4736, https://doi.org/10.1016/j.biomaterials.2011.03.046.
[120] A. Petit, M. Sandker, B. Muller, R. Meyboom, P. van Midwoud, P. Bruin, E. M. Redout, M. Versluijs-Helder, C.H. van der Lest, S.J. Buwalda, L.G. de Leede, T. Vermonden, R.J. Kok, H. Weinans, W.E. Hennink, Release behavior and intra-articular biocompatibility of celecoxib-loaded acetyl-capped PCLA-PEG-PCLA thermogels, Biomaterials 35 (27) (2014) 7919–7928, https://doi.org/10.1016/j.biomaterials.2014.05.064.
[121] B.C. Geiger, S. Wang, R.F. Padera Jr., A.J. Grodzinsky, P.T. Hammond, Cartilage-penetrating nanocarriers improve delivery and efficacy of growth factor treatment of osteoarthritis, Sci. Transl. Med. 10 (469) (2018), https://doi.org/10.1126/scitranslmed.aat8800.
[122] Y. Liang, X. Xu, L. Xu, I. Prasadam, L. Duan, Y. Xiao, J. Xia, Non-surgical osteoarthritis therapy, intra-articular drug delivery towards clinical applications, J. Drug Target. 29 (6) (2021) 609–616, https://doi.org/10.1080/1061186X.2020.1870231.
[123] R.H. Deng, B. Qiu, P.H. Zhou, Chitosan/hyaluronic acid/plasmid-DNA nanoparticles encoding interleukin-1 receptor antagonist attenuate inflammation in synoviocytes induced by interleukin-1 beta, J. Mater. Sci. Mater. Med. 29 (10) (2018) 155, https://doi.org/10.1007/s10856-018-6160-3.
[124] P.H. Zhou, B. Qiu, R.H. Deng, H.J. Li, X.F. Xu, X.F. Shang, Chondroprotective effects of hyaluronic acid-chitosan nanoparticles containing plasmid DNA encoding cytokine response modifier A in a rat knee osteoarthritis model, Cell. Physiol. Biochem. 47 (3) (2018) 1207–1216, https://doi.org/10.1159/000490217.
[125] X. Chen, Y. Liu, Y. Wen, Q. Yu, J. Liu, Y. Zhao, J. Liu, G. Ye, A photothermal-triggered nitric oxide nanogenerator combined with siRNA for precise therapy of osteoarthritis by suppressing macrophage inflammation, Nanoscale 11 (14) (2019) 6693–6709, https://doi.org/10.1039/c8nr10013f.
[126] S. Wang, X. Wei, X. Sun, C. Chen, J. Zhou, G. Zhang, H. Wu, B. Guo, L. Wei, A novel therapeutic strategy for cartilage diseases based on lipid nanoparticle-RNAi delivery system, Int. J. Nanomed. 13 (2018) 617–631, https://doi.org/10.2147/IJN.S142797.
[127] C. Sacchetti, R. Liu-Bryan, A. Magrini, N. Rosato, N. Bottini, M. Bottini, Polyethylene-glycol-modified single-walled carbon nanotubes for intra-articular delivery to chondrocytes, ACS Nano 8 (12) (2014) 12280–12291, https://doi.org/10.1021/nn504537b.
[128] G. Xu, Y. Zhao, Y. Geng, S. Cao, P. Pan, J. Wang, J. Chen, Nano-hybrid gradient scaffold for articular repair, Colloids Surf. B Biointerfaces 208 (2021), 112116, https://doi.org/10.1016/j.colsurfb.2021.112116.
[129] X. Xin, M. Hussain, J.J. Mao, Continuing differentiation of human mesenchymal stem cells and induced chondrogenic and osteogenic lineages in electrospun PLGA nanofiber scaffold, Biomaterials 28 (2) (2007) 316–325, https://doi.org/10.1016/j.biomaterials.2006.08.042.
[130] W. Chen, S. Chen, Y. Morsi, H. El-Hamshary, M. El-Newhy, C. Fan, X. Mo, Superabsorbent 3D scaffold based on electrospun nanofibers for cartilage tissue engineering, ACS Appl. Mater. Interfaces 8 (37) (2016) 24415–24425, https://doi.org/10.1021/acsami.6b06825.
[131] Y. Li, Y. Liu, X. Xun, W. Zhang, Y. Xu, D. Gu, Three-dimensional porous scaffolds with biomimetic microarchitecture and bioactivity for cartilage tissue engineering, ACS Appl. Mater. Interfaces 11 (40) (2019) 36359–36370, https://doi.org/10.1021/acsami.9b12206.
[132] J. Radhakrishnan, A. Manigandan, P. Chinnaswamy, A. Subramanian, S. Sethuraman, Gradient nano-engineered in situ forming composite hydrogel for osteochondral regeneration, Biomaterials 162 (2018) 82–98, https://doi.org/10.1016/j.biomaterials.2018.01.056.
[133] D. Shi, X. Xu, Y. Ye, K. Song, Y. Cheng, J. Di, Q. Hu, J. Li, H. Ju, Q. Jiang, Z. Gu, Photo-cross-linked scaffold with kartogenin-encapsulated nanoparticles for cartilage regeneration, ACS Nano 10 (1) (2016) 1292–1299, https://doi.org/10.1021/acsnano.5b06663.
[134] N.O. Chahine, N.M. Collette, C.B. Thomas, D.C. Genetos, G.G. Loots, Nanocomposite scaffold for chondrocyte growth and cartilage tissue engineering: effects of carbon nanotube surface functionalization, Tissue Eng. 20 (17–18) (2014) 2305–2315, https://doi.org/10.1089/ten.TEA.2013.0328.
[135] A.A.K. King, B. Matta-Domjan, M.J. Large, C. Matta, S.P. Ogilvie, N. Bardi, H. J. Byrne, A. Zakhidov, I. Jurewicz, E. Velliou, R. Lewis, R. La Ragione, A. B. Dalton, Pristine carbon nanotube scaffolds for the growth of chondrocytes, J. Mater. Chem. B 5 (41) (2017) 8178–8182, https://doi.org/10.1039/c7tb02065a.
[136] H. Shen, H. Lin, A.X. Sun, S. Song, B. Wang, Y. Yang, J. Dai, R.S. Tuan, Acceleration of chondrogenic differentiation of human mesenchymal stem cells by sustained growth factor release in 3D graphene oxide incorporated hydrogels, Acta Biomater. 105 (2020) 44–55, https://doi.org/10.1016/j.actbio.2020.01.048.
[137] M. Durymanov, T. Kamaletdinova, S.E. Lehmann, J. Reineke, Exploiting passive nanomedicine accumulation at sites of enhanced vascular permeability for non-cancerous applications, J. Contr. Release 261 (2017) 10–22, https://doi.org/10.1016/j.jconrel.2017.06.013.
[138] M. Qindeel, D. Khan, N. Ahmed, S. Khan, R. Asim Ur, Surfactant-free, self-assembled nanomicelles-based transdermal hydrogel for safe and targeted delivery of methotrexate against rheumatoid arthritis, ACS Nano 14 (4) (2020) 4662–4681, https://doi.org/10.1021/acsnano.0c00364.
[139] F. Yan, H. Li, Z. Zhong, M. Zhou, Y. Lin, C. Tang, C. Li, Co-delivery of prednisolone and curcumin in human serum albumin nanoparticles for effective treatment of rheumatoid arthritis, Int. J. Nanomed. 14 (2019) 9113–9125, https://doi.org/10.2147/IJN.S219413.
[140] B. Kapoor, M. Gulati, S.K. Singh, G.L. Khatik, R. Gupta, R. Kumar, R. Kumar, K. Gowthamarajan, S. Mahajan, S. Gupta, Fail-safe nano-formulation of prodrug of sulfapyridine: preparation and evaluation for treatment of rheumatoid arthritis, Mater. Sci. Eng. C Mater. Biol. Appl. 118 (2021), 111332, https://doi.org/10.1016/j.msec.2020.111332.
[141] J.Y. Park, S. Kwon, S.H. Kim, Y.J. Kang, D. Khang, Triamcinolone-gold nanoparticles repolarize synoviocytes and macrophages in an inflamed synovium, ACS Appl. Mater. Interfaces 12 (35) (2020) 38936–38949, https://doi.org/10.1021/acsami.0c09842.
[142] S.K. Kalangi, N.K. Swarnakar, R. Sathyavathi, D. Narayana Rao, S. Jain, P. Reddanna, Synthesis, characterization, and biodistribution of quantum dot-celecoxib conjugate in mouse paw edema model, Oxid. Med. Cell. Longev. 2018 (2018), 3090517, https://doi.org/10.1155/2018/3090517.
[143] Y. Yang, L. Guo, Z. Wang, P. Liu, X. Liu, J. Ding, W. Zhou, Targeted silver nanoparticles for rheumatoid arthritis therapy via macrophage apoptosis and Re-polarization, Biomaterials 264 (2021), 120390, https://doi.org/10.1016/j.biomaterials.2020.120390.
[144] M. Zhou, J. Hou, Z. Zhong, N. Hao, Y. Lin, C. Li, Targeted delivery of hyaluronic acid-coated solid lipid nanoparticles for rheumatoid arthritis therapy, Drug Deliv. 25 (1) (2018) 716–722, https://doi.org/10.1080/10717544.2018.1447050.
[145] S. Pandey, N. Rai, A. Mahtab, D. Mittal, F.J. Ahmad, N. Sandal, Y.R. Neupane, A. K. Verma, S. Talegaonkar, Hyaluronate-functionalized hydroxyapatite nanoparticles laden with methotrexate and teriflunomide for the treatment of rheumatoid arthritis, Int. J. Biol. Macromol. 171 (2021) 502–513, https://doi.org/10.1016/j.ijbiomac.2020.12.204.
[146] A. Mahtab, S.A. Rabbani, Y.R. Neupane, S. Pandey, A. Ahmad, M.A. Khan, N. Gupta, A. Madaan, M. Jaggi, N. Sandal, H. Rawat, M. Aqil, S. Talegaonkar, Facile functionalization of Teriflunomide-loaded naloliposomes with Chondroitin sulphate for the treatment of Rheumatoid arthritis, Carbohydr. Polym. 250 (2020), 116926, https://doi.org/10.1016/j.carbpol.2020.116926.
[147] C. Deng, Q. Zhang, P. He, B. Zhou, K. He, X. Sun, G. Lei, T. Gong, Z. Zhang, Targeted apoptosis of macrophages and osteoclasts in arthritic joints is effective against advanced inflammatory arthritis, Nat. Commun. 12 (1) (2021) 2174, https://doi.org/10.1038/s41467-021-22454-z.
[148] X.L. Xu, W.S. Li, X.J. Wang, Y.L. Du, X.Q. Kang, J.B. Hu, S.J. Li, X.Y. Ying, J. You, Y.Z. Du, Endogenous sialic acid-engineered micelles: a multifunctional platform for on-demand methotrexate delivery and bone repair of rheumatoid arthritis, Nanoscale 10 (6) (2018) 2923–2935, https://doi.org/10.1039/c7nr08430g.
[149] J. Lyu, L. Wang, X. Bai, X. Du, J. Wei, J. Wang, Y. Lin, Z. Chen, Z. Liu, J. Wu, Z. Zhong, Treatment of rheumatoid arthritis by serum albumin nanoparticles coated with mannose to target neutrophils, ACS Appl. Mater. Interfaces 13 (1) (2021) 266–276, https://doi.org/10.1021/acsami.0c19468.
[150] A.M. Aldayel, H.L. O'Mary, S.A. Valdes, X. Li, S.G. Thakkar, B.E. Mustafa, Z. Cui, Lipid nanoparticles with minimum burst release of TNF-alpha siRNA show strong activity against rheumatoid arthritis unresponsive to methotrexate, J. Contr. Release 283 (2018) 280–289, https://doi.org/10.1016/j.jconrel.2018.05.035.
[151] W. Duan, H. Li, Combination of NF-kB targeted siRNA and methotrexate in a hybrid nanocarrier towards the effective treatment in rheumatoid arthritis, J. Nanobiotechnol. 16 (1) (2018) 58, https://doi.org/10.1186/s12951-018-0382-x.

[152] C. Ma, B. Li, J. Zhang, Y. Sun, J. Li, H. Zhou, J. Shen, R. Gu, J. Qian, C. Fan, H. Zhang, K. Liu, Significantly improving the bioefficacy for rheumatoid arthritis with supramolecular nanoformulations, Adv. Mater. 33 (16) (2021), e2100098, https://doi.org/10.1002/adma.202100098.
[153] X. Sun, S. Dong, X. Li, K. Yu, F. Sun, R.J. Lee, Y. Li, L. Teng, Delivery of siRNA using folate receptor-targeted pH-sensitive polymeric nanoparticles for rheumatoid arthritis therapy, Nanomedicine 20 (2019), 102017, https://doi.org/10.1016/j.nano.2019.102017.
[154] G. Zhao, A. Liu, Y. Zhang, Z.Q. Zuo, Z.T. Cao, H.B. Zhang, C.F. Xu, J. Wang, Nanoparticle-delivered siRNA targeting Bruton's tyrosine kinase for rheumatoid arthritis therapy, Biomater. Sci. 7 (11) (2019) 4698–4707, https://doi.org/10.1039/c9bm01025d.
[155] S. Jain, T.H. Tran, M. Amiji, Macrophage repolarization with targeted alginate nanoparticles containing IL-10 plasmid DNA for the treatment of experimental arthritis, Biomaterials 61 (2015) 162–177, https://doi.org/10.1016/j.biomaterials.2015.05.028.
[156] Y. Deng, Y. Zhou, Q. Liang, C. Ge, J. Yang, B. Shan, Y. Liu, X. Zhou, L. Yin, Inflammation-instructed hierarchical delivery of IL-4/miR-21 orchestrates osteoimmune microenvironment toward the treatment of rheumatoid arthritis, Adv. Funct. Mater. 31 (33) (2021), https://doi.org/10.1002/adfm.202101033.
[157] S. Zhang, L. Wu, J. Cao, K. Wang, Y. Ge, W. Ma, X. Qi, S. Shen, Effect of magnetic nanoparticles size on rheumatoid arthritis targeting and photothermal therapy, Colloids Surf. B Biointerfaces 170 (2018) 224–232, https://doi.org/10.1016/j.colsurfb.2018.06.016.
[158] P.K. Pandey, R. Maheshwari, N. Raval, P. Gondaliya, K. Kalia, R.K. Tekade, Nanogold-core multifunctional dendrimer for pulsatile chemo-photothermal-and photodynamic-therapy of rheumatoid arthritis, J. Colloid Interface Sci. 544 (2019) 61–77, https://doi.org/10.1016/j.jcis.2019.02.073.
[159] X. Chen, X. Zhu, T. Xu, M. Xu, Y. Wen, Y. Liu, J. Liu, X. Qin, Targeted hexagonal Pd nanosheet combination therapy for rheumatoid arthritis via the photothermal controlled release of MTX, J. Mater. Chem. B 7 (1) (2019) 112–122, https://doi.org/10.1039/c8tb02302f.
[160] W. Pan, C. Dai, Y. Li, Y. Yin, L. Gong, J.O. Machuki, Y. Yang, S. Qiu, K. Guo, F. Gao, PRP-chitosan thermoresponsive hydrogel combined with black phosphorus nanosheets as injectable biomaterial for biotherapy and phototherapy treatment of rheumatoid arthritis, Biomaterials 239 (2020), 119851, https://doi.org/10.1016/j.biomaterials.2020.119851.
[161] X. Chen, X. Zhu, L. Ma, A. Lin, Y. Gong, G. Yuan, J. Liu, A core-shell structure QRu-PLGA-RES-DS NP nanocomposite with photothermal response-induced M2 macrophage polarization for rheumatoid arthritis therapy, Nanoscale 11 (39) (2019) 18209–18223, https://doi.org/10.1039/c9nr05922a.
[162] Q. Zhang, D. Dehaini, Y. Zhang, J. Zhou, X. Chen, L. Zhang, R.H. Fang, W. Gao, L. Zhang, Neutrophil membrane-coated nanoparticles inhibit synovial inflammation and alleviate joint damage in inflammatory arthritis, Nat. Nanotechnol. 13 (12) (2018) 1182–1190, https://doi.org/10.1038/s41565-018-0254-4.
[163] Y. Wei, Y. Nie, Z. Han, H. Huang, X. Liao, X. Wang, Z. Fan, Y. Zheng, Au@polydopamine nanoparticles/tocilizumab composite as efficient scavengers of oxygen free radicals for improving the treatment of rheumatoid arthritis, Mater. Sci. Eng. C Mater. Biol. Appl. 118 (2021), 111434, https://doi.org/10.1016/j.msec.2020.111434.
[164] M. Lorscheider, N. Tsapis, M. Ur-Rehman, F. Gaudin, I. Stolfa, S. Abreu, S. Mura, P. Chaminade, M. Espeli, E. Fattal, Dexamethasone palmitate nanoparticles: an efficient treatment for rheumatoid arthritis, J. Contr. Release 296 (2019) 179–189, https://doi.org/10.1016/j.jconrel.2019.01.015.
[165] M. Bashir, J. Ahmad, M. Asif, S.U. Khan, M. Irfan, Y.I. A, S. Asghar, I.U. Khan, M. S. Iqbal, A. Haseeb, S.H. Khalid, M. As Abourehab, Nanoemulgel, an innovative carrier for diflunisal topical delivery with profound anti-inflammatory effect: in vitro and in vivo evaluation, Int. J. Nanomed. 16 (2021) 1457–1472, https://doi.org/10.2147/IJN.S294653.
[166] N. Yin, X. Guo, R. Sun, H. Liu, L. Tang, J. Gou, T. Yin, H. He, Y. Zhang, X. Tang, Intra-articular injection of indomethacin-methotrexate in situ hydrogel for the synergistic treatment of rheumatoid arthritis, J. Mater. Chem. B 8 (5) (2020) 993–1007, https://doi.org/10.1039/c9tb01795j.
[167] Q. Wang, J. Jiang, W. Chen, H. Jiang, Z. Zhang, X. Sun, Targeted delivery of low-dose dexamethasone using PCL-PEG micelles for effective treatment of rheumatoid arthritis, J. Contr. Release 230 (2016) 64–72, https://doi.org/10.1016/j.jconrel.2016.03.035.
[168] R.N. Alolga, Y. Opoku-Damoah, D.A. Alagpulinsa, F.Q. Huang, G. Ma, M. Chavez Leon, C. Kudzai, X. Yin, Y. Ding, Metabolomic and transcriptomic analyses of the anti-rheumatoid arthritis potential of xylopic acid in a bioinspired lipoprotein nanoformulation, Biomaterials 268 (2021), 120482, https://doi.org/10.1016/j.biomaterials.2020.120482.
[169] R.R. Meka, S.H. Venkatesha, B. Acharya, K.D. Moudgil, Peptide-targeted liposomal delivery of dexamethasone for arthritis therapy, Nanomedicine 14 (11) (2019) 1455–1469, https://doi.org/10.2217/nnm-2018-0501.
[170] Q. Shen, X. Zhang, J. Qi, G. Shu, Y. Du, X. Ying, Sinomenine hydrochloride loaded thermosensitive liposomes combined with microwave hyperthermia for the treatment of rheumatoid arthritis, Int. J. Pharm. 576 (2020), 119001, https://doi.org/10.1016/j.ijpharm.2019.119001.
[171] Q. Wang, L. He, D. Fan, W. Liang, J. Fang, Improving the anti-inflammatory efficacy of dexamethasone in the treatment of rheumatoid arthritis with polymerized stealth liposomes as a delivery vehicle, J. Mater. Chem. B 8 (9) (2020) 1841–1851, https://doi.org/10.1039/c9tb02538c.
[172] H. Wu, Y. He, H. Wu, M. Zhou, Z. Xu, R. Xiong, F. Yan, H. Liu, Near-infrared fluorescence imaging-guided focused ultrasound-mediated therapy against Rheumatoid Arthritis by MTX-ICG-loaded iRGD-modified echogenic liposomes, Theranostics 10 (22) (2020) 10092–10105, https://doi.org/10.7150/thno.44865.
[173] H. An, Z. Song, P. Li, G. Wang, B. Ma, X. Wang, Development of biofabricated gold nanoparticles for the treatment of alleviated arthritis pain, Appl. Nanosci. 10 (2) (2019) 617–622, https://doi.org/10.1007/s13204-019-01135-w.
[174] F. Gao, Q. Yuan, P. Cai, L. Gao, L. Zhao, M. Liu, Y. Yao, Z. Chai, X. Gao, Au clusters treat rheumatoid arthritis with uniquely reversing cartilage/bone destruction, Adv. Sci. 6 (7) (2019), 1801671, https://doi.org/10.1002/advs.201801671.
[175] J. Kim, H.Y. Kim, S.Y. Song, S.H. Go, H.S. Sohn, S. Baik, M. Soh, K. Kim, D. Kim, H.C. Kim, N. Lee, B.S. Kim, T. Hyeon, Synergistic oxygen generation and reactive oxygen species scavenging by manganese ferrite/ceria Co-decorated nanoparticles for rheumatoid arthritis treatment, ACS Nano 13 (3) (2019) 3206–3217, https://doi.org/10.1021/acsnano.8b08785.
[176] H. Lee, M.Y. Lee, S.H. Bhang, B.S. Kim, Y.S. Kim, J.H. Ju, K.S. Kim, S.K. Hahn, Hyaluronate-gold nanoparticle/tocilizumab complex for the treatment of rheumatoid arthritis, ACS Nano 8 (5) (2014) 4790–4798, https://doi.org/10.1021/nn500685h.
[177] A.C. Lima, C.F. Campos, C. Cunha, A. Carvalho, R.L. Reis, H. Ferreira, N.M. Neves, Biofunctionalized liposomes to monitor rheumatoid arthritis regression stimulated by interleukin-23 neutralization, Adv. Healthc. Mater. 10 (2) (2021), e2001570, https://doi.org/10.1002/adhm.202001570.
[178] M. Yang, J. Ding, X. Feng, F. Chang, Y. Wang, Z. Gao, X. Zhuang, X. Chen, Scavenger receptor-mediated targeted treatment of collagen-induced arthritis by dextran sulfate-methotrexate prodrug, Theranostics 7 (1) (2017) 97–105, https://doi.org/10.7150/thno.16844.
[179] P. Li, X. Yang, Y. Yang, H. He, C.K. Chou, F. Chen, H. Pan, L. Liu, L. Cai, Y. Ma, X. Chen, Synergistic effect of all-trans-retinal and triptolide encapsulated in an inflammation-targeted nanoparticle on collagen-induced arthritis in mice, J. Contr. Release 319 (2020) 87–103, https://doi.org/10.1016/j.jconrel.2019.12.025.
[180] F. Yan, Z. Zhong, Y. Wang, Y. Feng, Z. Mei, H. Li, X. Chen, L. Cai, C. Li, Exosome-based biomimetic nanoparticles targeted to inflamed joints for enhanced treatment of rheumatoid arthritis, J. Nanobiotechnol. 18 (1) (2020) 115, https://doi.org/10.1186/s12951-020-00675-6.
[181] T. Gong, T. Tan, P. Zhang, H. Li, C. Deng, Y. Huang, T. Gong, Z. Zhang, Palmitic acid-modified bovine serum albumin nanoparticles target scavenger receptor-A on activated macrophages to treat rheumatoid arthritis, Biomaterials 258 (2020), 120296, https://doi.org/10.1016/j.biomaterials.2020.120296.
[182] F. Hao, R.J. Lee, L. Zhong, S. Dong, C. Yang, L. Teng, Q. Meng, J. Lu, J. Xie, L. Teng, Hybrid micelles containing methotrexate-conjugated polymer and co-loaded with microRNA-124 for rheumatoid arthritis therapy, Theranostics 9 (18) (2019) 5282–5297, https://doi.org/10.7150/thno.32268.
[183] L. Guo, Y. Chen, T. Wang, Y. Yuan, Y. Yang, X. Luo, S. Hu, J. Ding, W. Zhou, Rational design of metal-organic frameworks to deliver methotrexate for targeted rheumatoid arthritis therapy, J. Contr. Release 330 (2021) 119–131, https://doi.org/10.1016/j.jconrel.2020.10.069.
[184] G. Eelen, P. de Zeeuw, L. Treps, U. Harjes, B.W. Wong, P. Carmeliet, Endothelial cell metabolism, Physiol. Rev. 98 (1) (2018) 3–58, https://doi.org/10.1152/physrev.00001.2017.
[185] X.L. Xu, G.F. Shu, X.J. Wang, J. Qi, F.Y. Jin, Q.Y. Shen, X.Y. Ying, J.S. Ji, Y.Z. Du, Sialic acid-modified chitosan oligosaccharide-based biphasic calcium phosphate promote synergetic bone formation in rheumatoid arthritis therapy, J. Contr. Release 323 (2020) 578–590, https://doi.org/10.1016/j.jconrel.2020.04.047.
[186] Y. Wang, Z. Liu, T. Li, L. Chen, J. Lyu, C. Li, Y. Lin, N. Hao, M. Zhou, Z. Zhong, Enhanced therapeutic effect of RGD-modified polymeric micelles loaded with low-dose methotrexate and nimesulide on rheumatoid arthritis, Theranostics 9 (3) (2019) 708–720, https://doi.org/10.7150/thno.30418.
[187] J. Li, Y. Long, R. Guo, K. Ren, Z. Lu, M. Li, X. Wang, J. Li, Y. Wang, Z. Zhang, Q. He, Shield and sword nano-soldiers ameliorate rheumatoid arthritis by multi-stage manipulation of neutrophils, J. Contr. Release 335 (2021) 38–48, https://doi.org/10.1016/j.jconrel.2021.05.008.
[188] J. Li, L. Chen, X. Xu, Y. Fan, X. Xue, M. Shen, X. Shi, Targeted combination of antioxidative and anti-inflammatory therapy of rheumatoid arthritis using multifunctional dendrimer-entrapped gold nanoparticles as a platform, Small 16 (49) (2020), e2005661, https://doi.org/10.1002/smll.202005661.
[189] P. Song, C. Yang, J.S. Thomsen, F. Dagnaes-Hansen, M. Jakobsen, A. Bruel, B. Deleuran, J. Kjems, Lipidoid-siRNA nanoparticle-mediated IL-1beta gene silencing for systemic arthritis therapy in a mouse model, Mol. Ther. 27 (8) (2019) 1424–1435, https://doi.org/10.1016/j.ymthe.2019.05.002.
[190] N. Yin, X. Tan, H. Liu, F. He, N. Ding, J. Gou, T. Yin, H. He, Y. Zhang, X. Tang, A novel indomethacin/methotrexate/MMP-9 siRNA in situ hydrogel with dual effects of anti-inflammatory activity and reversal of cartilage disruption for the synergistic treatment of rheumatoid arthritis, Nanoscale 12 (15) (2020) 8546–8562, https://doi.org/10.1039/d0nr00454e.
[191] Q. Wang, H. Jiang, Y. Li, W. Chen, H. Li, K. Peng, Z. Zhang, X. Sun, Targeting NF-kB signaling with polymeric hybrid micelles that co-deliver siRNA and dexamethasone for arthritis therapy, Biomaterials 122 (2017) 10–22, https://doi.org/10.1016/j.biomaterials.2017.01.008.
[192] S. Jin, H. Chen, Y. Li, H. Zhong, W. Sun, J. Wang, T. Zhang, J. Ma, S. Yan, J. Zhang, Q. Tian, X. Yang, J. Wang, Maresin 1 improves the Treg/Th17 imbalance in rheumatoid arthritis through miR-21, Ann. Rheum. Dis. 77 (11) (2018) 1644–1652, https://doi.org/10.1136/annrheumdis-2018-213511.
[193] Y. Dong, W. Cao, J. Cao, Treatment of rheumatoid arthritis by phototherapy: advances and perspectives, Nanoscale 13 (35) (2021) 14591–14608, https://doi.org/10.1039/d1nr03623h.

[194] C.W. Chiang, Y.C. Hsiao, P.R. Jheng, C.H. Chen, Y.B. Manga, R. Lekha, K.M. Chao, Y.C. Ho, E.Y. Chuang, Strontium ranelate-laden near-infrared photothermal-inspired methylcellulose hydrogel for arthritis treatment, Mater. Sci. Eng. C Mater. Biol. Appl. 123 (2021), 111980, https://doi.org/10.1016/j.msec.2021.111980.
[195] Y. Lu, L. Li, Z. Lin, L. Wang, L. Lin, M. Li, Y. Zhang, Q. Yin, Q. Li, H. Xia, A new treatment modality for rheumatoid arthritis: combined photothermal and photodynamic therapy using Cu7.2 S4 nanoparticles, Adv. Healthc. Mater. 7 (14) (2018), e1800013, https://doi.org/10.1002/adhm.201800013.
[196] R. Huang, C. Zhang, Y. Bu, Z. Li, X. Zheng, S. Qiu, J.O. Machuki, L. Zhang, Y. Yang, K. Guo, F. Gao, A multifunctional nano-therapeutic platform based on octahedral yolk-shell Au NR@CuS: photothermal/photodynamic and targeted drug delivery tri-combined therapy for rheumatoid arthritis, Biomaterials 277 (2021), 121088, https://doi.org/10.1016/j.biomaterials.2021.121088.
[197] V. Eswaraiah, Q. Zeng, Y. Long, Z. Liu, Black phosphorus nanosheets: synthesis, characterization and applications, Small 12 (26) (2016) 3480–3502, https://doi.org/10.1002/smll.201600032.
[198] R.H. Fang, A.V. Kroll, W. Gao, L. Zhang, Cell membrane coating nanotechnology, Adv. Mater. 30 (23) (2018), e1706759, https://doi.org/10.1002/adma.201706759.
[199] J. Li, X. Zhen, Y. Lyu, Y. Jiang, J. Huang, K. Pu, Cell membrane coated semiconducting polymer nanoparticles for enhanced multimodal cancer phototheranostics, ACS Nano 12 (8) (2018) 8520–8530, https://doi.org/10.1021/acsnano.8b04066.
[200] S.E. Headland, H.R. Jones, L.V. Norling, A. Kim, P.R. Souza, E. Corsiero, C.D. Gil, A. Nerviani, F. Dell'Accio, C. Pitzalis, S.M. Oliani, L.Y. Jan, M. Perretti, Neutrophil-derived microvesicles enter cartilage and protect the joint in inflammatory arthritis, Sci. Transl. Med. 7 (315) (2015), https://doi.org/10.1126/scitranslmed.aac5608.
[201] L.M. Topping, B.L. Thomas, H.I. Rhys, J.L. Tremoleda, M. Foster, M. Seed, M. B. Voisin, C. Vinci, H.L. Law, M. Perretti, L.V. Norling, H.S. Azevedo, A. Nissim, Targeting extracellular vesicles to the arthritic joint using a damaged cartilage-specific antibody, Front. Immunol. 11 (2020) 10, https://doi.org/10.3389/fimmu.2020.00010.
[202] R. Li, Y. He, Y. Zhu, L. Jiang, S. Zhang, J. Qin, Q. Wu, W. Dai, S. Shen, Z. Pang, J. Wang, Route to rheumatoid arthritis by macrophage-derived microvesicle-coated nanoparticles, Nano Lett. 19 (1) (2019) 124–134, https://doi.org/10.1021/acs.nanolett.8b03439.
[203] Y. Shi, F. Xie, P. Rao, H. Qian, R. Chen, H. Chen, D. Li, D. Mu, L. Zhang, P. Lv, G. Shi, L. Zheng, G. Liu, TRAIL-expressing cell membrane nanovesicles as an anti-inflammatory platform for rheumatoid arthritis therapy, J. Contr. Release 320 (2020) 304–313, https://doi.org/10.1016/j.jconrel.2020.01.054.
[204] J. Yeo, Y.M. Lee, J. Lee, D. Park, K. Kim, J. Kim, J. Park, W.J. Kim, Nitric oxide-scavenging nanogel for treating rheumatoid arthritis, Nano Lett. 19 (10) (2019) 6716–6724, https://doi.org/10.1021/acs.nanolett.9b00496.
[205] T. Kim, J. Suh, W.J. Kim, Polymeric aggregate-embodied hybrid nitric-oxide-scavenging and sequential drug-releasing hydrogel for combinatorial treatment of rheumatoid arthritis, Adv. Mater. 33 (34) (2021), e2008793, https://doi.org/10.1002/adma.202008793.
[206] N. Feng, M. Yang, X. Feng, Y. Wang, F. Chang, J. Ding, Reduction-responsive polypeptide nanogel for intracellular drug delivery in relieving collagen-induced arthritis, ACS Biomater. Sci. Eng. 4 (12) (2018) 4154–4162, https://doi.org/10.1021/acsbiomaterials.8b00738.
[207] I. Kalashnikova, S.J. Chung, M. Nafiujjaman, M.L. Hill, M.E. Siziba, C.H. Contag, T. Kim, Ceria-based nanotheranostic agent for rheumatoid arthritis, Theranostics 10 (26) (2020) 11863–11880, https://doi.org/10.7150/thno.49069.
[208] Y. Cai, T. Gao, S. Fu, P. Sun, Development of zoledronic acid functionalized hydroxyapatite loaded polymeric nanoparticles for the treatment of osteoporosis, Exp. Ther. Med. 16 (2) (2018) 704–710, https://doi.org/10.3892/etm.2018.6263.
[209] D. Narayanan, A. Anitha, R. Jayakumar, K.P. Chennazhi, In vitro and in vivo evaluation of osteoporosis therapeutic peptide PTH 1-34 loaded pegylated chitosan nanoparticles, Mol. Pharm. 10 (11) (2013) 4159–4167, https://doi.org/10.1021/mp400184v.
[210] J.C. Fricain, S. Schlaubitz, C. Le Visage, I. Arnault, S.M. Derkaoui, R. Siadous, S. Catros, C. Lalande, R. Bareille, M. Renard, T. Fabre, S. Cornet, M. Durand, A. Leonard, N. Sahraoui, D. Letourneur, J. Amedee, A nano-hydroxyapatite-pullulan/dextran polysaccharide composite macroporous material for bone tissue engineering, Biomaterials 34 (12) (2013) 2947–2959, https://doi.org/10.1016/j.biomaterials.2013.01.049.
[211] C. Dou, J. Li, J. He, F. Luo, T. Yu, Q. Dai, Y. Chen, J. Xu, X. Yang, S. Dong, Bone-targeted pH-responsive cerium nanoparticles for anabolic therapy in osteoporosis, Bioact. Mater. 6 (12) (2021) 4697–4706, https://doi.org/10.1016/j.bioactmat.2021.04.038.
[212] T.K. Ryu, R.H. Kang, K.Y. Jeong, D.R. Jun, J.M. Koh, D. Kim, S.K. Bae, S.W. Choi, Bone-targeted delivery of nanodiamond-based drug carriers conjugated with alendronate for potential osteoporosis treatment, J. Contr. Release 232 (2016) 152–160, https://doi.org/10.1016/j.jconrel.2016.04.025.
[213] Y. Sun, X. Ye, M. Cai, X. Liu, J. Xiao, C. Zhang, Y. Wang, L. Yang, J. Liu, S. Li, C. Kang, B. Zhang, Q. Zhang, Z. Wang, A. Hong, X. Wang, Osteoblast-targeting-peptide modified nanoparticle for siRNA/microRNA delivery, ACS Nano 10 (6) (2016) 5759–5768, https://doi.org/10.1021/acsnano.5b07828.
[214] S. Li, Y. Liu, T. Tian, T. Zhang, S. Lin, M. Zhou, X. Zhang, Y. Lin, X. Cai, Bioswitchable delivery of microRNA by framework nucleic acids: application to bone regeneration, Small 17 (47) (2021), e2104359, https://doi.org/10.1002/smll.202104359.
[215] D. Sezlev Bilecen, H. Uludag, V. Hasirci, Development of PEI-RANK siRNA complex loaded PLGA nanocapsules for the treatment of osteoporosis, Tissue Eng. 25 (1–2) (2019) 34–43, https://doi.org/10.1089/ten.TEA.2017.0476.
[216] L. Lipp, D. Sharma, A. Banerjee, J. Singh, Controlled delivery of salmon calcitonin using thermosensitive triblock copolymer depot for treatment of osteoporosis, ACS Omega 4 (1) (2019) 1157–1166, https://doi.org/10.1021/acsomega.8b02781.
[217] Y. Liu, X. Chen, S. Li, Q. Guo, J. Xie, L. Yu, X. Xu, C. Ding, J. Li, J. Ding, Calcitonin-loaded thermosensitive hydrogel for long-term antiosteopenia therapy, ACS Appl. Mater. Interfaces 9 (28) (2017) 23428–23440, https://doi.org/10.1021/acsami.7b05740.
[218] N.H. Lee, M.S. Kang, T.H. Kim, D.S. Yoon, N. Mandakhbayar, S.B. Jo, H.S. Kim, J. C. Knowles, J.H. Lee, H.W. Kim, Dual actions of osteoclastic-inhibition and osteogenic-stimulation through strontium-releasing bioactive nanoscale cement imply biomaterial-enabled osteoporosis therapy, Biomaterials 276 (2021), 121025, https://doi.org/10.1016/j.biomaterials.2021.121025.
[219] H. Quan, Y. He, J. Sun, W. Yang, W. Luo, C. Dou, F. Kang, C. Zhao, J. He, X. Yang, S. Dong, H. Jiang, Chemical self-assembly of multifunctional hydroxyapatite with a coral-like nanostructure for osteoporotic bone reconstruction, ACS Appl. Mater. Interfaces 10 (30) (2018) 25547–25560, https://doi.org/10.1021/acsami.8b09879.
[220] M. Li, S. Fu, Z. Cai, D. Li, L. Liu, D. Deng, R. Jin, H. Ai, Dual regulation of osteoclastogenesis and osteogenesis for osteoporosis therapy by iron oxide hydroxyapatite core/shell nanocomposites, Regen. Biomater. 8 (5) (2021), https://doi.org/10.1093/rb/rbab027.
[221] V.N. Mochalin, O. Shenderova, D. Ho, Y. Gogotsi, The properties and applications of nanodiamonds, Nat. Nanotechnol. 7 (1) (2011) 11–23, https://doi.org/10.1038/nnano.2011.209.
[222] H. Yin, R.L. Kanasty, A.A. Eltoukhy, A.J. Vegas, J.R. Dorkin, D.G. Anderson, Non-viral vectors for gene-based therapy, Nat. Rev. Genet. 15 (8) (2014) 541–555, https://doi.org/10.1038/nrg3763.
[223] S. Li, Y. Liu, T. Zhang, S. Lin, S. Shi, J. He, Y. Xie, X. Cai, T. Tian, Y. Lin, A tetrahedral framework DNA-based bioswitchable miRNA inhibitor delivery system: application to skin anti-aging, Adv. Mater. (2022), e2204287, https://doi.org/10.1002/adma.202204287.
[224] J. Liu, L. Dang, D. Li, C. Liang, X. He, H. Wu, A. Qian, Z. Yang, D.W. Au, M. W. Chiang, B.T. Zhang, Q. Han, K.K. Yue, H. Zhang, C. Lv, X. Pan, J. Xu, Z. Bian, P. Shang, W. Tan, Z. Liang, B. Guo, A. Lu, G. Zhang, A delivery system specifically approaching bone resorption surfaces to facilitate therapeutic modulation of microRNAs in osteoclasts, Biomaterials 52 (2015) 148–160, https://doi.org/10.1016/j.biomaterials.2015.02.007.
[225] Y. Gao, X. Chen, T. Tian, T. Zhang, S. Gao, X. Zhang, Y. Yao, Y. Lin, X. Cai, A lysosome-activated tetrahedral nanobox for encapsulated siRNA delivery, Adv. Mater. (2022), e2201731, https://doi.org/10.1002/adma.202201731.
[226] G. Zhang, B. Guo, H. Wu, T. Tang, B.T. Zhang, L. Zheng, Y. He, Z. Yang, X. Pan, H. Chow, K. To, Y. Li, D. Li, X. Wang, Y. Wang, K. Lee, Z. Hou, N. Dong, G. Li, K. Leung, L. Hung, F. He, L. Zhang, L. Qin, A delivery system targeting bone formation surfaces to facilitate RNAi-based anabolic therapy, Nat. Med. 18 (2) (2012) 307–314, https://doi.org/10.1038/nm.2617.
[227] C. Liang, B. Guo, H. Wu, N. Shao, D. Li, J. Liu, L. Dang, C. Wang, H. Li, S. Li, W. K. Lau, Y. Cao, Z. Yang, C. Lu, X. He, D.W. Au, X. Pan, B.T. Zhang, C. Lu, H. Zhang, K. Yue, A. Qian, P. Shang, J. Xu, L. Xiao, Z. Bian, W. Tan, Z. Liang, F. He, L. Zhang, A. Lu, G. Zhang, Aptamer-functionalized lipid nanoparticles targeting osteoblasts as a novel RNA interference-based bone anabolic strategy, Nat. Med. 21 (3) (2015) 288–294, https://doi.org/10.1038/nm.3791.
[228] Y. Dang, J. Guan, Nanoparticle-based drug delivery systems for cancer therapy, Smart Mater. Med. 1 (2020) 10–19, https://doi.org/10.1016/j.smaim.2020.04.001.
[229] J. Zhang, Y. Miao, W. Ni, H. Xiao, J. Zhang, Cancer cell membrane coated silica nanoparticles loaded with ICG for tumour specific photothermal therapy of osteosarcoma, Artif. Cell Nanomed. Biotechnol. 47 (1) (2019) 2298–2305, https://doi.org/10.1080/21691401.2019.1622554.
[230] X. Li, L. Wang, L. Wang, J. Yu, G. Lu, W. Zhao, C. Miao, C. Zou, J. Wu, Overcoming therapeutic failure in osteosarcoma via Apatinib-encapsulated hydrophobic poly(ester amide) nanoparticles, Biomater. Sci. 8 (21) (2020) 5888–5899, https://doi.org/10.1039/d0bm01296c.
[231] X. Wen, Q. Wang, T. Dai, J. Shao, X. Wu, Z. Jiang, J.A. Jacob, C. Jiang, Identification of possible reductants in the aqueous leaf extract of mangrove plant Rhizophora apiculata for the fabrication and cytotoxicity of silver nanoparticles against human osteosarcoma MG-63 cells, Mater. Sci. Eng. C Mater. Biol. Appl. 116 (2020), 111252, https://doi.org/10.1016/j.msec.2020.111252.
[232] L. Zhao, D. Bi, X. Qi, Y. Guo, F. Yue, X. Wang, M. Han, Polydopamine-based surface modification of paclitaxel nanoparticles for osteosarcoma targeted therapy, Nanotechnology 30 (25) (2019), 255101, https://doi.org/10.1088/1361-6528/ab055f.
[233] E. Gazzano, I. Buondonno, A. Marengo, B. Rolando, K. Chegaev, J. Kopecka, S. Saponara, M. Sorge, C.M. Hattinger, A. Gasco, R. Fruttero, M. Brancaccio, M. Serra, B. Stella, E. Fattal, S. Arpicco, C. Riganti, Hyaluronated liposomes containing H2S-releasing doxorubicin are effective against P-glycoprotein-positive/doxorubicin-resistant osteosarcoma cells and xenografts, Cancer Lett. 456 (2019) 29–39, https://doi.org/10.1016/j.canlet.2019.04.029.
[234] Y. Yan, X. Gao, S. Zhang, Y. Wang, Z. Zhou, J. Xiao, Q. Zhang, Y. Cheng, A carboxyl-terminated dendrimer enables osteolytic lesion targeting and photothermal ablation of malignant bone tumors, ACS Appl. Mater. Interfaces 11 (1) (2019) 160–168, https://doi.org/10.1021/acsami.8b15827.

[235] M. Martinez-Carmona, D. Lozano, M. Colilla, M. Vallet-Regi, Lectin-conjugated pH-responsive mesoporous silica nanoparticles for targeted bone cancer treatment, Acta Biomater. 65 (2018) 393–404, https://doi.org/10.1016/j.actbio.2017.11.007.
[236] S. Gurunathan, M. Jeyaraj, M.H. Kang, J.H. Kim, Tangeretin-assisted platinum nanoparticles enhance the apoptotic properties of doxorubicin: combination therapy for osteosarcoma treatment, Nanomaterials 9 (8) (2019), https://doi.org/10.3390/nano9081089.
[237] S. Li, Y. Xiong, X. Zhang, Poloxamer surface modified trimethyl chitosan nanoparticles for the effective delivery of methotrexate in osteosarcoma, Biomed. Pharmacother. 90 (2017) 872–879, https://doi.org/10.1016/j.biopha.2017.04.004.
[238] X. Ke, W. Lin, X. Li, H. Wang, X. Xiao, Z. Guo, Synergistic dual-modified liposome improves targeting and therapeutic efficacy of bone metastasis from breast cancer, Drug Deliv. 24 (1) (2017) 1680–1689, https://doi.org/10.1080/10717544.2017.1396384.
[239] K.M. Au, A. Satterlee, Y. Min, X. Tian, Y.S. Kim, J.M. Caster, L. Zhang, T. Zhang, L. Huang, A.Z. Wang, Folate-targeted pH-responsive calcium zoledronate nanoscale metal-organic frameworks: turning a bone antiresorptive agent into an anticancer therapeutic, Biomaterials 82 (2016) 178–193, https://doi.org/10.1016/j.biomaterials.2015.12.018.
[240] T. Liu, S. Romanova, S. Wang, M.A. Hyun, C. Zhang, S.M. Cohen, R.K. Singh, T. K. Bronich, Alendronate-modified polymeric micelles for the treatment of breast cancer bone metastasis, Mol. Pharm. 16 (7) (2019) 2872–2883, https://doi.org/10.1021/acs.molpharmaceut.8b01343.
[241] C. Li, Y. Zhang, G. Chen, F. Hu, K. Zhao, Q. Wang, Engineered multifunctional nanomedicine for simultaneous stereotactic chemotherapy and inhibited osteolysis in an orthotopic model of bone metastasis, Adv. Mater. 29 (13) (2017), https://doi.org/10.1002/adma.201605754.
[242] S. Jie, X. Guo, Z. Ouyang, Tumor ablation using novel photothermal NaxWO3 nanoparticles against breast cancer osteolytic bone metastasis, Int. J. Nanomed. 14 (2019) 7353–7362, https://doi.org/10.2147/IJN.S217974.
[243] S.B. Bai, D.Z. Liu, Y. Cheng, H. Cui, M. Liu, M.X. Cui, B.L. Zhang, Q.B. Mei, S. Y. Zhou, Osteoclasts and tumor cells dual targeting nanoparticle to treat bone metastases of lung cancer, Nanomedicine 21 (2019), 102054, https://doi.org/10.1016/j.nano.2019.102054.
[244] S.H. Chen, T.I. Liu, C.L. Chuang, H.H. Chen, W.H. Chiang, H.C. Chiu, Alendronate/folic acid-decorated polymeric nanoparticles for hierarchically targetable chemotherapy against bone metastatic breast cancer, J. Mater. Chem. B 8 (17) (2020) 3789–3800, https://doi.org/10.1039/d0tb00046a.
[245] G. Tiram, E. Segal, A. Krivitsky, R. Shreberk-Hassidim, S. Ferber, P. Ofek, T. Udagawa, L. Edry, N. Shomron, M. Roniger, B. Kerem, Y. Shaked, S. Aviel-Ronen, I. Barshack, M. Calderon, R. Haag, R. Satchi-Fainaro, Identification of dormancy-associated MicroRNAs for the design of osteosarcoma-targeted dendritic polyglycerol nanopolyplexes, ACS Nano 10 (2) (2016) 2028–2045, https://doi.org/10.1021/acsnano.5b06189.
[246] A. Alhaddad, M.P. Adam, J. Botsoa, G. Dantelle, S. Perruchas, T. Gacoin, C. Mansuy, S. Lavielle, C. Malvy, F. Treussart, J.R. Bertrand, Nanodiamond as a vector for siRNA delivery to Ewing sarcoma cells, Small 7 (21) (2011) 3087–3095, https://doi.org/10.1002/smll.201101193.
[247] C. Liang, F. Li, L. Wang, Z.K. Zhang, C. Wang, B. He, J. Li, Z. Chen, A.B. Shaikh, J. Liu, X. Wu, S. Peng, L. Dang, B. Guo, X. He, D.W.T. Au, C. Lu, H. Zhu, B. T. Zhang, A. Lu, G. Zhang, Tumor cell-targeted delivery of CRISPR/Cas9 by aptamer-functionalized lipopolymer for therapeutic genome editing of VEGFA in osteosarcoma, Biomaterials 147 (2017) 68–85, https://doi.org/10.1016/j.biomaterials.2017.09.015.
[248] C. Xu, B. Ma, J. Peng, L. Gao, Y. Xu, Z. Huan, J. Chang, Tricalcium silicate/graphene oxide bone cement with photothermal properties for tumor ablation, J. Mater. Chem. B 7 (17) (2019) 2808–2818, https://doi.org/10.1039/c9tb00246d.
[249] W. Dang, B. Ma, B. Li, Z. Huan, N. Ma, H. Zhu, J. Chang, Y. Xiao, C. Wu, 3D printing of metal-organic framework nanosheets-structured scaffolds with tumor therapy and bone construction, Biofabrication 12 (2) (2020), 025005, https://doi.org/10.1088/1758-5090/ab5ae3.
[250] F. Yang, J. Lu, Q. Ke, X. Peng, Y. Guo, X. Xie, Magnetic mesoporous calcium silicate/chitosan porous scaffolds for enhanced bone regeneration and photothermal-chemotherapy of osteosarcoma, Sci. Rep. 8 (1) (2018) 7345, https://doi.org/10.1038/s41598-018-25595-2.
[251] W. Dang, T. Li, B. Li, H. Ma, D. Zhai, X. Wang, J. Chang, Y. Xiao, J. Wang, C. Wu, A bifunctional scaffold with CuFeSe2 nanocrystals for tumor therapy and bone reconstruction, Biomaterials 160 (2018) 92–106, https://doi.org/10.1016/j.biomaterials.2017.11.020.
[252] S. Ghosh, S. Ghosh, S.K. Jana, N. Pramanik, Biomedical application of doxorubicin coated hydroxyapatite-poly(lactide-co-glycolide) nanocomposite for controlling osteosarcoma therapeutics, J. Nanosci. Nanotechnol. 20 (7) (2020) 3994–4004, https://doi.org/10.1166/jnn.2020.17689.
[253] Q. Yin, L. Tang, K. Cai, R. Tong, R. Sternberg, X. Yang, L.W. Dobrucki, L.B. Borst, D. Kamstock, Z. Song, W.G. Helferich, J. Cheng, T.M. Fan, Pamidronate functionalized nanoconjugates for targeted therapy of focal skeletal malignant osteolysis, Proc. Natl. Acad. Sci. U. S. A. 113 (32) (2016) E4601–E4609, https://doi.org/10.1073/pnas.1603316113.
[254] Z. Fang, Y. Sun, H. Xiao, P. Li, M. Liu, F. Ding, W. Kan, R. Miao, Targeted osteosarcoma chemotherapy using RGD peptide-installed doxorubicin-loaded biodegradable polymeric micelle, Biomed. Pharmacother. 85 (2017) 160–168, https://doi.org/10.1016/j.biopha.2016.11.132.
[255] M. Hameed, S. Panicker, S.H. Abdallah, A.A. Khan, C. Han, M.M. Chehimi, A. A. Mohamed, Protein-coated aryl modified gold nanoparticles for cellular uptake study by osteosarcoma cancer cells, Langmuir 36 (40) (2020) 11765–11775, https://doi.org/10.1021/acs.langmuir.0c01443.
[256] X. Wang, Z. Ye, S. Lin, L. Wei, L. Xiao, Nanozyme-triggered cascade reactions from cup-shaped nanomotors promote active cellular targeting, Research 2022 (2022), 9831012, https://doi.org/10.34133/2022/9831012.
[257] W. Gu, T. Zhang, J. Gao, Y. Wang, D. Li, Z. Zhao, B. Jiang, Z. Dong, H. Liu, Albumin-bioinspired iridium oxide nanoplatform with high photothermal conversion efficiency for synergistic chemo-photothermal of osteosarcoma, Drug Deliv. 26 (1) (2019) 918–927, https://doi.org/10.1080/10717544.2019.1662513.
[258] Y. Wang, Q. Huang, X. He, H. Chen, Y. Zou, Y. Li, K. Lin, X. Cai, J. Xiao, Q. Zhang, Y. Cheng, Multifunctional melanin-like nanoparticles for bone-targeted chemo-photothermal therapy of malignant bone tumors and osteolysis, Biomaterials 183 (2018) 10–19, https://doi.org/10.1016/j.biomaterials.2018.08.033.
[259] W. Sun, K. Ge, Y. Jin, Y. Han, H. Zhang, G. Zhou, X. Yang, D. Liu, H. Liu, X. J. Liang, J. Zhang, Bone-targeted nanoplatform combining zoledronate and photothermal therapy to treat breast cancer bone metastasis, ACS Nano 13 (7) (2019) 7556–7567, https://doi.org/10.1021/acsnano.9b00097.
[260] H. Qiao, Z. Cui, S. Yang, D. Ji, Y. Wang, Y. Yang, X. Han, Q. Fan, A. Qin, T. Wang, X.P. He, W. Bu, T. Tang, Targeting osteocytes to attenuate early breast cancer bone metastasis by theranostic upconversion nanoparticles with responsive plumbagin release, ACS Nano 11 (7) (2017) 7259–7273, https://doi.org/10.1021/acsnano.7b03197.
[261] J. Zhu, Q. Huo, M. Xu, F. Yang, Y. Li, H. Shi, Y. Niu, Y. Liu, Bortezomib-catechol conjugated prodrug micelles: combining bone targeting and aryl boronate-based pH-responsive drug release for cancer bone-metastasis therapy, Nanoscale 10 (38) (2018) 18387–18397, https://doi.org/10.1039/c8nr03899f.
[262] M.H. Ross, A.K. Esser, G.C. Fox, A.H. Schmieder, X. Yang, G. Hu, D. Pan, X. Su, Y. Xu, D.V. Novack, T. Walsh, G.A. Colditz, G.H. Lukaszewicz, E. Cordell, J. Novack, J.A.J. Fitzpatrick, D.L. Waning, K.S. Mohammad, T.A. Guise, G. M. Lanza, K.N. Weilbaecher, Bone-induced expression of integrin beta 3 enables targeted nanotherapy of breast cancer metastases, Cancer Res. 77 (22) (2017) 6299–6312, https://doi.org/10.1158/0008-5472.CAN-17-1225.
[263] M. Wang, X. Cai, J. Yang, C. Wang, L. Tong, J. Xiao, L. Li, A targeted and pH-responsive bortezomib nanomedicine in the treatment of metastatic bone tumors, ACS Appl. Mater. Interfaces 10 (48) (2018) 41003–41011, https://doi.org/10.1021/acsami.8b07527.
[264] J. Vanderburgh, J.L. Hill, M.K. Gupta, K.A. Kwakwa, S.K. Wang, K. Moyer, S. K. Bedingfield, A.R. Merkel, R. d'Arcy, S.A. Guelcher, J.A. Rhoades, C.L. Duvall, Tuning ligand density to optimize pharmacokinetics of targeted nanoparticles for dual protection against tumor-induced bone destruction, ACS Nano 14 (1) (2020) 311–327, https://doi.org/10.1021/acsnano.9b04571.
[265] L. Xiong, J. Bi, Y. Tang, S.Z. Qiao, Magnetic core-shell silica nanoparticles with large radial mesopores for siRNA delivery, Small 12 (34) (2016) 4735–4742, https://doi.org/10.1002/smll.201600531.
[266] F. Haghiralsadat, G. Amoabediny, S. Naderinezhad, B. Zandieh-Doulabi, T. Forouzanfar, M.N. Helder, Codelivery of doxorubicin and JIP1 siRNA with novel EphA2-targeted PEGylated cationic nanoliposomes to overcome osteosarcoma multidrug resistance, Int. J. Nanomed. 13 (2018) 3853–3866, https://doi.org/10.2147/IJN.S150017.
[267] K. Sun, J. Wang, J. Zhang, M. Hua, C. Liu, T. Chen, Dextran-g-PEI nanoparticles as a carrier for co-delivery of adriamycin and plasmid into osteosarcoma cells, Int. J. Biol. Macromol. 49 (2) (2011) 173–180, https://doi.org/10.1016/j.ijbiomac.2011.04.007.
[268] M.L. Tan, D.E. Dunstan, A.M. Friedhuber, P.F. Choong, C.R. Dass, A nanoparticulate system that enhances the efficacy of the tumoricide Dz13 when administered proximal to the lesion site, J. Contr. Release 144 (2) (2010) 196–202, https://doi.org/10.1016/j.jconrel.2010.01.011.
[269] Z. Sun, H. Xie, S. Tang, X.F. Yu, Z. Guo, J. Shao, H. Zhang, H. Huang, H. Wang, P. K. Chu, Ultrasmall black phosphorus quantum dots: synthesis and use as photothermal agents, Angew Chem. Int. Ed. Engl. 54 (39) (2015) 11526–11530, https://doi.org/10.1002/anie.201506154.
[270] B. Yang, J. Yin, Y. Chen, S. Pan, H. Yao, Y. Gao, J. Shi, 2D-Black-Phosphorus-Reinforced 3D-printed scaffolds:A stepwise countermeasure for osteosarcoma, Adv. Mater. 30 (10) (2018), https://doi.org/10.1002/adma.201705611.
[271] C. Zhao, A. Shen, L. Zhang, K. Lin, X. Wang, Borocarbonitrides nanosheets engineered 3D-printed scaffolds for integrated strategy of osteosarcoma therapy and bone regeneration, Chem. Eng. J. 401 (2020), https://doi.org/10.1016/j.cej.2020.125989.
[272] H. Wang, X. Zeng, L. Pang, H. Wang, B. Lin, Z. Deng, E.L.X. Qi, N. Miao, D. Wang, P. Huang, H. Hu, J. Li, Integrative treatment of anti-tumor/bone repair by combination of MoS2 nanosheets with 3D printed bioactive borosilicate glass scaffolds, Chem. Eng. J. 396 (2020), https://doi.org/10.1016/j.cej.2020.125081.
[273] H. Ma, C. Jiang, D. Zhai, Y. Luo, Y. Chen, F. Lv, Z. Yi, Y. Deng, J. Wang, J. Chang, C. Wu, A bifunctional biomaterial with photothermal effect for tumor therapy and bone regeneration, Adv. Funct. Mater. 26 (8) (2016) 1197–1208, https://doi.org/10.1002/adfm.201504142.
[274] Y. Lu, L. Li, M. Li, Z. Lin, L. Wang, Y. Zhang, Q. Yin, H. Xia, G. Han, Zero-dimensional carbon dots enhance bone regeneration, osteosarcoma ablation, and clinical bacterial eradication, Bioconjugate Chem. 29 (9) (2018) 2982–2993, https://doi.org/10.1021/acs.bioconjchem.8b00400.
[275] S. Pan, J. Yin, L. Yu, C. Zhang, Y. Zhu, Y. Gao, Y. Chen, 2D MXene-integrated 3D-printing scaffolds for augmented osteosarcoma phototherapy and accelerated

tissue reconstruction, Adv. Sci. 7 (2) (2020), 1901511, https://doi.org/10.1002/advs.201901511.
[276] P.-P. Zhao, Y.-W. Ge, X.-L. Liu, Q.-F. Ke, J.-W. Zhang, Z.-A. Zhu, Y.-P. Guo, Ordered arrangement of hydrated GdPO4 nanorods in magnetic chitosan matrix promotes tumor photothermal therapy and bone regeneration against breast cancer bone metastases, Chem. Eng. J. 381 (2020), https://doi.org/10.1016/j.cej.2019.122694.
[277] J.W. Lu, F. Yang, Q.F. Ke, X.T. Xie, Y.P. Guo, Magnetic nanoparticles modified-porous scaffolds for bone regeneration and photothermal therapy against tumors, Nanomedicine 14 (3) (2018) 811–822, https://doi.org/10.1016/j.nano.2017.12.025.
[278] A. Premkumar, D.A. Kolin, K.X. Farley, J.M. Wilson, A.S. McLawhorn, M.B. Cross, P.K. Sculco, Projected economic burden of periprosthetic joint infection of the hip and knee in the United States, J. Arthroplasty 36 (5) (2021) 1484–1489, https://doi.org/10.1016/j.arth.2020.12.005.
[279] Y. Liu, Z. Zheng, J.N. Zara, C. Hsu, D.E. Soofer, K.S. Lee, R.K. Siu, L.S. Miller, X. Zhang, D. Carpenter, C. Wang, K. Ting, C. Soo, The antimicrobial and osteoinductive properties of silver nanoparticle/poly (DL-lactic-co-glycolic acid)-coated stainless steel, Biomaterials 33 (34) (2012) 8745–8756, https://doi.org/10.1016/j.biomaterials.2012.08.010.
[280] Y. Yang, K. Zheng, R. Liang, A. Mainka, N. Taccardi, J.A. Roether, R. Detsch, W. H. Goldmann, S. Virtanen, A.R. Boccaccini, Cu-releasing bioactive glass/polycaprolactone coating on Mg with antibacterial and anticorrosive properties for bone tissue engineering, Biomed. Mater. 13 (1) (2017), 015001, https://doi.org/10.1088/1748-605X/aa87f2.
[281] I. Izquierdo-Barba, J.M. Garcia-Martin, R. Alvarez, A. Palmero, J. Esteban, C. Perez-Jorge, D. Arcos, M. Vallet-Regi, Nanocolumnar coatings with selective behavior towards osteoblast and Staphylococcus aureus proliferation, Acta Biomater. 15 (2015) 20–28, https://doi.org/10.1016/j.actbio.2014.12.023.
[282] G. Zhang, X. Zhang, Y. Yang, R. Chi, J. Shi, R. Hang, X. Huang, X. Yao, P.K. Chu, X. Zhang, Dual light-induced in situ antibacterial activities of biocompatibleTiO2/MoS2/PDA/RGD nanorod arrays on titanium, Biomater. Sci. 8 (1) (2020) 391–404, https://doi.org/10.1039/c9bm01507h.
[283] Y. Yu, Q. Ran, X. Shen, H. Zheng, K. Cai, Enzyme responsive titanium substrates with antibacterial property and osteo/angio-genic differentiation potentials, Colloids Surf. B Biointerfaces 185 (2020), 110592, https://doi.org/10.1016/j.colsurfb.2019.110592.
[284] A. Dwivedi, A. Mazumder, N. Nasongkla, Layer-by-layer nanocoating of antibacterial niosome on orthopedic implant, Int. J. Pharm. 547 (1–2) (2018) 235–243, https://doi.org/10.1016/j.ijpharm.2018.05.075.
[285] A. Karakecili, B. Topuz, S. Korpayev, M. Erdek, Metal-organic frameworks for on-demand pH controlled delivery of vancomycin from chitosan scaffolds, Mater. Sci. Eng. C Mater. Biol. Appl. 105 (2019), 110098, https://doi.org/10.1016/j.msec.2019.110098.
[286] D. Zhang, W. Liu, X.D. Wu, X. He, X. Lin, H. Wang, J. Li, J. Jiang, W. Huang, Efficacy of novel nano-hydroxyapatite/polyurethane composite scaffolds with silver phosphate particles in chronic osteomyelitis, J. Mater. Sci. Mater. Med. 30 (6) (2019) 59, https://doi.org/10.1007/s10856-019-6261-7.
[287] Y. Miao, X. Shi, Q. Li, L. Hao, L. Liu, X. Liu, Y. Chen, Y. Wang, Engineering natural matrices with black phosphorus nanosheets to generate multi-functional therapeutic nanocomposite hydrogels, Biomater. Sci. 7 (10) (2019) 4046–4059, https://doi.org/10.1039/c9bm01072f.
[288] D. Placente, J.M. Ruso, M. Baldini, J.A. Laiuppa, J.M. Sieben, G.E. Santillan, P. V. Messina, Self-fluorescent antibiotic MoOx-hydroxyapatite: a nano-theranostic platform for bone infection therapies, Nanoscale 11 (37) (2019) 17277–17292, https://doi.org/10.1039/c9nr01236b.
[289] A. Gao, R. Hang, X. Huang, L. Zhao, X. Zhang, L. Wang, B. Tang, S. Ma, P.K. Chu, The effects of titania nanotubes with embedded silver oxide nanoparticles on bacteria and osteoblasts, Biomaterials 35 (13) (2014) 4223–4235, https://doi.org/10.1016/j.biomaterials.2014.01.058.
[290] X. Shen, Y. Zhang, P. Ma, L. Sutrisno, Z. Luo, Y. Hu, Y. Yu, B. Tao, C. Li, K. Cai, Fabrication of magnesium/zinc-metal organic framework on titanium implants to inhibit bacterial infection and promote bone regeneration, Biomaterials 212 (2019) 1–16, https://doi.org/10.1016/j.biomaterials.2019.05.008.
[291] Z. Yuan, B. Tao, Y. He, J. Liu, C. Lin, X. Shen, Y. Ding, Y. Yu, C. Mu, P. Liu, K. Cai, Biocompatible MoS2/PDA-RGD coating on titanium implant with antibacterial property via intrinsic ROS-independent oxidative stress and NIR irradiation, Biomaterials 217 (2019), 119290, https://doi.org/10.1016/j.biomaterials.2019.119290.
[292] B. Tao, Y. Deng, L. Song, W. Ma, Y. Qian, C. Lin, Z. Yuan, L. Lu, M. Chen, X. Yang, K. Cai, BMP2-loaded titania nanotubes coating with pH-responsive multilayers for bacterial infections inhibition and osteogenic activity improvement, Colloids Surf. B Biointerfaces 177 (2019) 242–252, https://doi.org/10.1016/j.colsurfb.2019.02.014.
[293] K. Su, L. Tan, X. Liu, Z. Cui, Y. Zheng, B. Li, Y. Han, Z. Li, S. Zhu, Y. Liang, X. Feng, X. Wang, S. Wu, Rapid photo-sonotherapy for clinical treatment of bacterial infected bone implants by creating oxygen deficiency using sulfur doping, ACS Nano 14 (2) (2020) 2077–2089, https://doi.org/10.1021/acsnano.9b08686.
[294] Z. Yuan, B. Tao, Y. He, C. Mu, G. Liu, J. Zhang, Q. Liao, P. Liu, K. Cai, Remote eradication of biofilm on titanium implant via near-infrared light triggered photothermal/photodynamic therapy strategy, Biomaterials 223 (2019), 119479, https://doi.org/10.1016/j.biomaterials.2019.119479.
[295] L. Hong, X. Liu, L. Tan, Z. Cui, X. Yang, Y. Liang, Z. Li, S. Zhu, Y. Zheng, K.W. K. Yeung, D. Jing, D. Zheng, X. Wang, S. Wu, Rapid biofilm elimination on bone implants using near-infrared-activated inorganic semiconductor heterostructures, Adv. Healthc. Mater. 8 (19) (2019), e1900835, https://doi.org/10.1002/adhm.201900835.
[296] Y. Wu, Q. Liao, L. Wu, Y. Luo, W. Zhang, M. Guan, H. Pan, L. Tong, P.K. Chu, H. Wang, ZnL2-BPs integrated bone scaffold under sequential photothermal mediation: a win-win strategy delivering antibacterial therapy and fostering osteogenesis thereafter, ACS Nano (2021), https://doi.org/10.1021/acsnano.1c06062.
[297] L. Tong, Q. Liao, Y. Zhao, H. Huang, A. Gao, W. Zhang, X. Gao, W. Wei, M. Guan, P.K. Chu, H. Wang, Near-infrared light control of bone regeneration with biodegradable photothermal osteoimplant, Biomaterials 193 (2019) 1–11, https://doi.org/10.1016/j.biomaterials.2018.12.008.
[298] W. Zhou, Z. Jia, P. Xiong, J. Yan, M. Li, Y. Cheng, Y. Zheng, Novel pH-responsive tobramycin-embedded micelles in nanostructured multilayer-coatings of chitosan/heparin with efficient and sustained antibacterial properties, Mater. Sci. Eng. C Mater. Biol. Appl. 90 (2018) 693–705, https://doi.org/10.1016/j.msec.2018.04.069.
[299] W.Z. Bailong Tao, Chuanchuan Lin, Yuan Zhang, He Ye, Lu Lu, Maowen Chen, Yao Ding, Yulu Yang, Zengzilu Xia, Kaiyong Cai, Surface modification of titanium implants by ZIF-8@Levo/LBL coating for inhibition of bacterial-associated infection and enhancement of in vivo osseointegration, Chem. Eng. J. 390 (124621) (2020).
[300] Y. Yang, B. Tao, Y. Gong, R. Chen, W. Yang, C. Lin, M. Chen, L. Qin, Y. Jia, K. Cai, Functionalization of Ti substrate with pH-responsive naringin-ZnO nanoparticles for the reconstruction of large bony after osteosarcoma resection, J. Biomed. Mater. Res. 108 (11) (2020) 2190–2205, https://doi.org/10.1002/jbm.a.36977.
[301] L. Sutrisno, Y. Hu, X. Shen, M. Li, Z. Luo, L. Dai, S. Wang, J.L. Zhong, K. Cai, Fabrication of hyaluronidase-responsive biocompatible multilayers on BMP2 loaded titanium nanotube for the bacterial infection prevention, Mater. Sci. Eng. C Mater. Biol. Appl. 89 (2018) 95–105, https://doi.org/10.1016/j.msec.2018.03.024.
[302] J. Min, K.Y. Choi, E.C. Dreaden, R.F. Padera, R.D. Braatz, M. Spector, P. T. Hammond, Designer dual therapy nanolayered implant coatings eradicate biofilms and accelerate bone tissue repair, ACS Nano 10 (4) (2016) 4441–4450, https://doi.org/10.1021/acsnano.6b00087.
[303] X. Feng, L. Ma, J. Lei, Q. Ouyang, Y. Zeng, Y. Luo, X. Zhang, Y. Song, G. Li, L. Tan, X. Liu, C. Yang, Piezo-augmented sonosensitizer with strong ultrasound-propelling ability for efficient treatment of osteomyelitis, ACS Nano 16 (2) (2022) 2546–2557, https://doi.org/10.1021/acsnano.1c09189.
[304] Y. Yu, L. Tan, Z. Li, X. Liu, Y. Zheng, X. Feng, Y. Liang, Z. Cui, S. Zhu, S. Wu, Single-atom catalysis for efficient sonodynamic therapy of methicillin-resistant Staphylococcus aureus-infected osteomyelitis, ACS Nano 15 (6) (2021) 10628–10639, https://doi.org/10.1021/acsnano.1c03424.
[305] J.J. Seo, N. Mandakhbayar, M.S. Kang, J.Y. Yoon, N.H. Lee, J. Ahn, H.H. Lee, J. H. Lee, H.W. Kim, Antibacterial, proangiogenic, and osteopromotive nanoglass paste coordinates regenerative process following bacterial infection in hard tissue, Biomaterials 268 (2021), 120593, https://doi.org/10.1016/j.biomaterials.2020.120593.
[306] N. David, R. Nallaiyan, Biologically anchored chitosan/gelatin-SrHAP scaffold fabricated on Titanium against chronic osteomyelitis infection, Int. J. Biol. Macromol. 110 (2018) 206–214, https://doi.org/10.1016/j.ijbiomac.2017.11.174.
[307] H. Lin, C. Yang, Y. Luo, M. Ge, H. Shen, X. Zhang, J. Shi, Biomimetic nanomedicine-triggered in situ vaccination for innate and adaptive immunity activations for bacterial osteomyelitis treatment, ACS Nano (2022), https://doi.org/10.1021/acsnano.1c11132.
[308] K.T. Peng, C.F. Chen, I.M. Chu, Y.M. Li, W.H. Hsu, R.W. Hsu, P.J. Chang, Treatment of osteomyelitis with teicoplanin-encapsulated biodegradable thermosensitive hydrogel nanoparticles, Biomaterials 31 (19) (2010) 5227–5236, https://doi.org/10.1016/j.biomaterials.2010.03.027.
[309] J. Chen, A. Ashames, M.A. Buabeid, K.M. Fahelelbom, M. Ijaz, G. Murtaza, Nanocomposites drug delivery systems for the healing of bone fractures, Int. J. Pharm. 585 (2020), 119477, https://doi.org/10.1016/j.ijpharm.2020.119477.
[310] F. Kang, Q. Yi, P. Gu, Y. Dong, Z. Zhang, L. Zhang, Y. Bai, Controlled growth factor delivery system with osteogenic-angiogenic coupling effect for bone regeneration, J. Orthop. Translat. 31 (2021) 110–125, https://doi.org/10.1016/j.jot.2021.11.004.
[311] W. Yao, Y.E. Lay, A. Kot, R. Liu, H. Zhang, H. Chen, K. Lam, N.E. Lane, Improved mobilization of exogenous mesenchymal stem cells to bone for fracture healing and sex difference, Stem Cell. 34 (10) (2016) 2587–2600, https://doi.org/10.1002/stem.2433.
[312] C. Li, Q. Wang, X. Gu, Y. Kang, Y. Zhang, Y. Hu, T. Li, H. Jin, G. Deng, Q. Wang, Porous Se@SiO2 nanocomposite promotes migration and osteogenic differentiation of rat bone marrow mesenchymal stem cell to accelerate bone fracture healing in a rat model, Int. J. Nanomed. 14 (2019) 3845–3860, https://doi.org/10.2147/IJN.S202741.
[313] Y. Wang, M.R. Newman, M. Ackun-Farmmer, M.P. Baranello, T.J. Sheu, J. E. Puzas, D.S.W. Benoit, Fracture-targeted delivery of beta-catenin agonists via peptide-functionalized nanoparticles augments fracture healing, ACS Nano 11 (9) (2017) 9445–9458, https://doi.org/10.1021/acsnano.7b05103.
[314] Y. Liu, Z. Jia, M.P. Akhter, X. Gao, X. Wang, X. Wang, G. Zhao, X. Wei, Y. Zhou, X. Wang, C.W. Hartman, E.V. Fehringer, L. Cui, D. Wang, Bone-targeting liposome formulation of Salvianic acid A accelerates the healing of delayed fracture Union in Mice, Nanomedicine 14 (7) (2018) 2271–2282, https://doi.org/10.1016/j.nano.2018.07.011.
[315] M. Ma, Actuating smart, Nat. Nanotechnol. 14 (11) (2019) 1003–1004, https://doi.org/10.1038/s41565-019-0569-9.

[316] N. Guo, L. Zhang, J. Wang, S. Wang, Y. Zou, X. Wang, Novel fabrication of morphology tailored nanostructures with Gelatin/Chitosan Co-polymeric bio-composited hydrogel system to accelerate bone fracture healing and hard tissue nursing care management, Process Biochem. 90 (2020) 177–183, https://doi.org/10.1016/j.procbio.2019.11.016.
[317] S.A.A. Ghavimi, E.S. Lungren, T.J. Faulkner, M.A. Josselet, Y. Wu, Y. Sun, F. M. Pfeiffer, C.L. Goldstein, C. Wan, B.D. Ulery, Inductive co-crosslinking of cellulose nanocrystal/chitosan hydrogels for the treatment of vertebral compression fractures, Int. J. Biol. Macromol. 130 (2019) 88–98, https://doi.org/10.1016/j.ijbiomac.2019.02.086.
[318] K. Kawamoto, H. Miyaji, E. Nishida, S. Miyata, A. Kato, A. Tateyama, T. Furihata, K. Shitomi, T. Iwanaga, T. Sugaya, Characterization and evaluation of graphene oxide scaffold for periodontal wound healing of class II furcation defects in dog, Int. J. Nanomed. 13 (2018) 2365–2376, https://doi.org/10.2147/IJN.S163206.
[319] M. Xu, D. Zhai, L. Xia, H. Li, S. Chen, B. Fang, J. Chang, C. Wu, Hierarchical bioceramic scaffolds with 3D-plotted macropores and mussel-inspired surface nanolayers for stimulating osteogenesis, Nanoscale 8 (28) (2016) 13790–13803, https://doi.org/10.1039/c6nr01952h.
[320] J.Y. Park, C. Yang, I.H. Jung, H.C. Lim, J.S. Lee, U.W. Jung, Y.K. Seo, J.K. Park, S. H. Choi, Regeneration of rabbit calvarial defects using cells-implanted nano-hydroxyapatite coated silk scaffolds, Biomater. Res. 19 (2015) 7, https://doi.org/10.1186/s40824-015-0027-1.
[321] X. Gao, J. Song, P. Ji, X. Zhang, X. Li, X. Xu, M. Wang, S. Zhang, Y. Deng, F. Deng, S. Wei, Polydopamine-templated hydroxyapatite reinforced polycaprolactone composite nanofibers with enhanced cytocompatibility and osteogenesis for bone tissue engineering, ACS Appl. Mater. Interfaces 8 (5) (2016) 3499–3515, https://doi.org/10.1021/acsami.5b12413.
[322] J. Li, F. Kang, X. Gong, Y. Bai, J. Dai, C. Zhao, C. Dou, Z. Cao, M. Liang, R. Dong, H. Jiang, X. Yang, S. Dong, Ceria nanoparticles enhance endochondral ossification-based critical-sized bone defect regeneration by promoting the hypertrophic differentiation of BMSCs via DHX15 activation, Faseb. J. 33 (5) (2019) 6378–6389, https://doi.org/10.1096/fj.201802187R.
[323] D. Li, X. Xie, Z. Yang, C. Wang, Z. Wei, P. Kang, Enhanced bone defect repairing effects in glucocorticoid-induced osteonecrosis of the femoral head using a porous nano-lithium-hydroxyapatite/gelatin microsphere/erythropoietin composite scaffold, Biomater. Sci. 6 (3) (2018) 519–537, https://doi.org/10.1039/c7bm00975e.
[324] W. Zhang, Q. Chang, L. Xu, G. Li, G. Yang, X. Ding, X. Wang, D. Cui, X. Jiang, Graphene oxide-copper nanocomposite-coated porous CaP scaffold for vascularized bone regeneration via activation of hif-1 alpha, Adv. Healthc. Mater. 5 (11) (2016) 1299–1309, https://doi.org/10.1002/adhm.201500824.
[325] R. Arun Kumar, A. Sivashanmugam, S. Deepthi, J.D. Bumgardner, S.V. Nair, R. Jayakumar, Nano-fibrin stabilized CaSO4 crystals incorporated injectable chitin composite hydrogel for enhanced angiogenesis & osteogenesis, Carbohydr. Polym. 140 (2016) 144–153, https://doi.org/10.1016/j.carbpol.2015.11.074.
[326] T. Tian, W. Xie, W. Gao, G. Wang, L. Zeng, G. Miao, B. Lei, Z. Lin, X. Chen, Micro-nano bioactive glass particles incorporated porous scaffold for promoting osteogenesis and angiogenesis in vitro, Front. Chem. 7 (2019) 186, https://doi.org/10.3389/fchem.2019.00186.
[327] Q. Yao, Y. Liu, B. Selvaratnam, R.T. Koodali, H. Sun, Mesoporous silicate nanoparticles/3D nanofibrous scaffold-mediated dual-drug delivery for bone tissue engineering, J. Contr. Release 279 (2018) 69–78, https://doi.org/10.1016/j.jconrel.2018.04.011.
[328] Y. Karabey-Akyurek, A.G. Gurcay, O. Gurcan, O.F. Turkoglu, S. Yabanoglu-Ciftci, H. Eroglu, M.F. Sargon, E. Bilensoy, L. Oner, Localized delivery of methylprednisolone sodium succinate with polymeric nanoparticles in experimental injured spinal cord model, Pharmaceut. Dev. Technol. 22 (8) (2017) 972–981, https://doi.org/10.3109/10837450.2016.1143002.
[329] A. Gaudin, M. Yemisci, H. Eroglu, S. Lepetre-Mouelhi, O.F. Turkoglu, B. Donmez-Demir, S. Caban, M.F. Sargon, S. Garcia-Argote, G. Pieters, O. Loreau, B. Rousseau, O. Tagit, N. Hildebrandt, Y. Le Dantec, J. Mougin, S. Valetti, H. Chacun, V. Nicolas, D. Desmaele, K. Andrieux, Y. Capan, T. Dalkara, P. Couvreur, Squalenoyl adenosine nanoparticles provide neuroprotection after stroke and spinal cord injury, Nat. Nanotechnol. 9 (12) (2014) 1054–1062, https://doi.org/10.1038/nnano.2014.274.
[330] J. Li, Y. Yao, Y. Wang, J. Xu, D. Zhao, M. Liu, S. Shi, Y. Lin, Modulation of the crosstalk between Schwann cells and macrophages for nerve regeneration: a therapeutic strategy based on a multifunctional tetrahedral framework nucleic acids system, Adv. Mater. (2022), e2202513, https://doi.org/10.1002/adma.202202513.
[331] Q. Wang, J. Yan, J. Yang, B. Li, Nanomaterials promise better bone repair, Mater. Today 19 (8) (2016) 451–463, https://doi.org/10.1016/j.mattod.2015.12.003.
[332] A.L. Armstead, C.B. Arena, B. Li, Exploring the potential role of tungsten carbide cobalt (WC-Co) nanoparticle internalization in observed toxicity toward lung epithelial cells in vitro, Toxicol. Appl. Pharmacol. 278 (1) (2014) 1–8, https://doi.org/10.1016/j.taap.2014.04.008.
[333] I.D. Bianco, M.R. Ceballos, C. Casado, V.G. Dabbene, C. Rizzi, R.K. Mizutamari, Formulation, quality control and safety issues of nanocarriers used for cancer treatment, Curr. Pharmaceut. Des. 23 (35) (2017) 5413–5425, https://doi.org/10.2174/1381612823666170608082815.
[334] P. Couvreur, Nanoparticles in drug delivery: past, present and future, Adv. Drug Deliv. Rev. 65 (1) (2013) 21–23, https://doi.org/10.1016/j.addr.2012.04.010.
[335] A.J.T. Stefan Wilhelm, Dai Qin, Seiichi Ohta, Julie Audet, Harold F. Dvorak, Warren C.W. Chan, Analysis of nanoparticle delivery to tumours, Nat. Rev. Mater. 16014 (1) (2016).
[336] O. Lavi, M.M. Gottesman, D. Levy, The dynamics of drug resistance: a mathematical perspective, Drug Resist. Updates 15 (1–2) (2012) 90–97, https://doi.org/10.1016/j.drup.2012.01.003.
[337] A. Shastri, L.M. McGregor, Y. Liu, V. Harris, H. Nan, M. Mujica, Y. Vasquez, A. Bhattacharya, Y. Ma, M. Aizenberg, O. Kuksenok, A.C. Balazs, J. Aizenberg, X. He, An aptamer-functionalized chemomechanically modulated biomolecule catch-and-release system, Nat. Chem. 7 (5) (2015) 447–454, https://doi.org/10.1038/nchem.2203.
[338] S. Brown, J. Pistiner, I.M. Adjei, B. Sharma, Nanoparticle properties for delivery to cartilage: the implications of disease state, synovial fluid, and off-target uptake, Mol. Pharm. 16 (2) (2019) 469–479, https://doi.org/10.1021/acs.molpharmaceut.7b00484.
[339] P.Y. Teo, W. Cheng, J.L. Hedrick, Y.Y. Yang, Co-delivery of drugs and plasmid DNA for cancer therapy, Adv. Drug Deliv. Rev. 98 (2016) 41–63, https://doi.org/10.1016/j.addr.2015.10.014.